Universitat
de les Illes Balears

DOCTORAL THESIS
2019

GENERATION AND SUPPLY OPTIMISATION OF A POWER PLANT AND DHC NETWORK

Nicolás Pérez de la Mora

Universitat
de les Illes Balears

DOCTORAL THESIS
2019

Doctoral Programme of Physics

GENERATION AND SUPPLY OPTIMISATION OF A POWER PLANT AND DHC NETWORK

Nicolás Pérez de la Mora

Thesis Supervisor: Víctor Martínez Moll

Thesis tutor: Eduard Cesari Aliberch

Doctor by the Universitat de les Illes Balears

Acknowledgement

Firstly, I would like to express my sincere gratitude to my supervisor Prof. Víctor Martinez Moll for the support during this long trip which has been my PhD. I would like to thank him for his patience and for staying involved with the thesis from the begging till the end, despite its ups and downs.

Besides my supervisor, I would like to thank Politecnico di Torino, especially to Prof. Maurizio Repetto and to Dr. Paolo Lazzeroni for their help and support during my secondment in Torino, for turning those months into a highly profitable time, for sharing with me their immense knowledge and for our collaboration since the moment we met.

My sincere thanks also goes to the SHINE program, in particular to the coordinator Prof. Ulrike Jordan and the work package leader Prof. Chris Bales, for providing me the opportunity to work in research, to be part of an outstanding training network and to be funded with Marie Curie scholarship. Without their precious support it would have impossible to conduct this research and to learn as much as I have in this period.

Thanks are also due to the European Union for funding SHINE project through FP7 Marie-Curie Innovative Training Network and the fellowship at Sampol (317085), and the OPTi project which funding is received from the Horizon 2020 Research and Innovation Programme under grant number 649796 for their financial support that I otherwise would not have been able to develop my scientific discoveries.

I am very grateful to my colleagues in Sampol, in particular to the energy department, which has always been a great support and source of knowledge. I show my gratitude to Ignacio Molera, Frederic Decuyper and Juan Antonio Vicens for guiding me from theoretical to real engineering and for helping me applying the ideas of this PhD to real life. I would especially like to thank the working team in Parc Bit, particularly to Mateu Creus and Toni Van Schilt, for welcoming me into it, for their encouragement, multiple ideas, and

for always finding time for me all along this project. Without all of you this thesis dissertation would just be another piece of paper with formulas and variables on it.

I also want to take the chance to thank all those who have been there not to help but to create problems and undermine my work. This PhD thesis would have never reach its quality without you, because *your hate only makes me stronger*.

After so many years of schooling in different universities and countries, I want to thank my colleagues, class mates, and friends that I have met on the road for being part of this process, for letting me your notes, for sharing good and bad times, and for such good memories.

Last but not least, and more in a personal note, I would like to express my deepest gratitude to my family, friends and significant other. This dissertation would not have been finished without their warm love, continued patience and endless support. Thank you for listening, even though, sometimes, you did not really understand what I was talking about.

Thank you all for being part of this!

Summary

This PhD focuses on the operation optimisation of a hybrid power plant which covers the demand of a district heating and cooling network (DHC). This thesis also pursues optimal supply strategies which are a promising and inexpensive way to improve energy efficiency and to reduce expenditure in district network energy supply.

To achieve this, this thesis must develop an electricity price for the Spanish market and a thermal demand forecasting tool which works together with an energy simulator. The simulator determines generation strategies by optimising the production mix that minimises the energy cost and maximises the renewable energy fraction. This leads to an optimisation of the power plant's operation and integration of the solar field.

Parc Bit is the power plant under study and is in Palma of Majorca, Spain. The power plant can generate heating, cooling and electricity. Thus, the power plant obtains revenue by injecting electricity into the grid and supplying thermal energy to the DHC. To maximise the plant's revenue, it is necessary to develop algorithms that can provide energy generation strategies to meet generation and demand curves.

An energy management system is developed to provide the power plant manager with optimal generation strategies. The tool is developed jointly with Politecnico di Torino and can optimise a multi-energy node power plant at different time horizons.

This simulator requires information such as thermal and electric demand to fulfil, climatic conditions, power plant configuration, and machine behavior at different generation points. As a result, the tool provides the schedule of the generation machines, primary energy consumption, and total revenue for the time horizon under consideration.

A two-cores forecasting tool was developed based on the ARIMAX and neural networks models to obtain the future electricity prices of the Spanish

wholesale energy market and the DHC's thermal demand. Those values are fed to the optimisation tool to determine future generation strategies.

A solar generation forecaster is developed enabling solar generation to be fed to the optimiser. Therefore, the solar fraction can be maximised by avoiding overlaps with the CHP's thermal generation schedule.

Heat losses in the DHC distribution are considered to be part of the thermal load to be fulfilled by the power plant. Therefore, this thesis upgrades the network to acquire reliable information from the energy consumers. The acquired information helps the network operator to optimise supply temperature. Moreover, the possibility of modifying the supply temperature allows generators to provide energy more efficiently. Generators provide energy more efficiently when conditions are more relaxed. In addition, these strategies aim to reduce heat losses by modifying the supply temperature within its working boundaries. Through supply temperature adjustment and network's thermal mass harnessing the network can be used as energy storage.

Resumen

El presente doctorado se centra en la optimización de la operación de una planta hibrida que cubre la demanda de una red de distrito de frio y calor (DHC). Esta tesis busca estrategias de suministro energético óptimo, las cuales son una forma económica y prometedora de aumentar la eficiencia energética y reducir los costes de suministro en redes de distrito.

Para alcanzar estos objetivos la tesis ha desarrollado heramientas de predicción de precio eléctrico del mercado Español y de demanda térmica que se integrarán en un simulador energético. El simulador determina estrategias de generación optimizando el mix energético que minimice los costes de energía y maximice la fracción de energía renovable. Esto conduce a la optimización de la operación en la planta de cogeneración y a la integración del campo solar.

La planta en la que se aplica el estudio se denomina Parc Bit y está ubicada en Mallorca, España. La planta puede generar calor, frío y electricidad. Por lo tanto, la planta obtiene beneficios por la venta de electricidad a la red y por el suministro energético a la red de distrito. Para maximizar estos beneficios es necesario el desarrollo de algoritmos que proporcionen estrategias de generación que se ajusten a las curvas de demanda.

El responsable de la planta obtiene estrategias de generación óptimas obtenidas a través del sistema de gestión energético desarrollado. Esta herramienta se ha desarrollado en colaboración con el Politécnico de Torino y es capaz de optimizar plantas multi energía en diferentes horizontes temporales.

El simulador necesita información como la demanda térmica y eléctrica, las condiciones climáticas, la configuración de la planta y el funcionamiento de los generadores a diferentes cargas. Como resultado la herramienta proporciona el programa de generación, consumos de energía primaria y el beneficio total para el horizonte temporal considerado.

Se desarrolla una herramienta de predicción de precios eléctricos de mer-

cado y demanda térmica en la red de distrito basada en dos modelos: ARIMAX y redes neuronales. Esta información se integra en la herramienta de optimización para determinar futuras estrategias de generación.

Adicionalmente, se desarrolla un predictor de energía solar que se integra con el optimizador. De esta forma se maximiza la fracción solar evitando coincidencias innecesarias con la generación térmica de los motores de cogeneración.

Las pérdidas térmicas en la red de distrito son consideradas parte de la demanda a suministrar por la planta de generación. Por ello, durante esta tesis se mejora el sistema de comunicación de la red para poder adquirir información de los consumidores térmicos de manera fidedigna. La información adquirida facilita al operador la optimización de la temperatura a suministrar en la red de distrito. Además, la posibilidad de modificar la temperatura de suministro permite a los generadores generar energía de una manera más eficiente. Los generadores energéticos mejoran su eficiencia cuando las condiciones de operación son menos restrictivas. Por otra parte, estas estrategias persiguen reducir las pérdidas energéticas modificando la temperatura de suministro dentro de sus límites. Utilizando conjuntamente la masa térmica de la red de distrito y el ajuste de temperatura de suministro, la red distribución puede ser utilizada como almacenamiento energético.

Resum

El present doctorat es focalitza en l'optimització de l'operació d'una planta híbrida que cobreix la demanda d'una xarxa de districte de fred i calor (DHC). Aquesta tesi busca estratègies de subministrament energètic òptim, les quals són una forma econòmica i prometedora d'augmentar l'eficiència energètica i reduir els costos de subministrament de xarxes de districte.

Per assolir els objectius, aquesta tesi ha desenvolupat eines de predicció del preu elèctric del mercat Espanyol i la demanda tèrmica les quals s'han integrat en un simulador energètic. El simulador permet definir estratègies de generació optimitzant el mix energètic per tal d'aconseguir minimitzar els costos d'energia i maximitzar la fracció d'energia renovable. El resultat és una optimització de l'operació de la planta de cogeneració i la integració del camp solar.

La planta objecte d'estudi és Parc Bit, ubicada a Mallorca, Espanya. La planta pot generar calor, fred i electricitat. Així doncs, la planta obté beneficis de la venta d'electricitat a la xarxa i del subministrament energètic a la xarxa de districte. Per maximitzar aquests beneficis és necessari el desenvolupament d'algoritmes que proporcionin estratègies de generació que s'ajustin a les corbes de demanda.

S'ha desenvolupat un sistema de gestió energètica que proporciona al responsable de la planta estratègies de generació òptima. Aquesta eina s'ha desenvolupat amb la col·laboració del Politècnic de Torino i és capaç d'optimitzar plantes multi energia en diferents horitzons temporals.

El simulador necessita informació de la demanda tèrmica y elèctrica, les condicions climàtiques, la configuració de la planta i el funcionament dels generadors a diferents càrregues. El resultat de l'eina proporciona la programació de generació, els consums d'energia primària i els beneficis totals per l'horitzó temporal considerat.

S'ha desenvolupat una eina de predicció de preus elèctrics de mercat i la

demanda tèrmica de la xarxa de districte basada en dos models: ARIMAX i xarxes neuronals. Aquesta informació s'ha integrat en l'eina d'optimització per determinar futures estratègies de generació.

Addicionalment, es desenvolupa un predictor d'energia solar que s'integra a l'optimitzador. D'aquesta manera es maximitza la fracció solar evitant coincidències innecessàries amb la generació tèrmica dels motors de cogeneració.

Les pèrdues tèrmiques en la xarxa de districte són considerades part de la demanda a subministrar per la planta de generació. Per això, l'objectiu d'aquesta tesi és millorar el sistema de comunicació de la xarxa per poder adquirir informació dels consumidors tèrmics de manera fiable. La informació adquirida facilita a l'operador l'optimització de la temperatura de subministrament. A més, la possibilitat de modificar la temperatura de subministrament permet als generadors, generar energia d'una manera més eficient. Els generadors energètics milloren la seva eficiència quan les condicions d'operació són menys restrictives. Per una altra banda, aquestes estratègies busquen reduir les pèrdues energètiques modificant la temperatura de subministrament dins els seus límits. Utilitzant conjuntament l'ajustament de temperatura de subministrament i la massa tèrmica de la xarxa de districte, la xarxa pot ser utilitzada com emmagatzemant energètic.

Contents

List of Figures

List of Tables

Glossary

ACF autocorrelation function. 66, 68, 144, 151

ANN artificial neural networks. 28, 29, 53, 54, 55, 64, 67, 68, 145

ARIMA auto regressive integrated moving average. 53, 66

ARIMAX auto regressive integrated moving average with explanatory variable. 28, 29, 54, 64, 66, 67, 126, 131, 145, 146, 147, 148, 149, 151, 152, 153

CCHP combined cooling, heating and power. 24, 31, 32

CHP combined heat and power. 24, 28, 31, 32, 37, 44, 50, 51, 56, 59, 70, 72, 73, 76, 92, 94, 95, 100, 107, 109, 110, 111, 121, 123, 125, 126, 129, 158, 159, 160

COP coefficient of performance. 76, 77, 78, 96, 97, 112

DB data base. 28, 64, 65, 141, 143

DC district cooling systems. 33, 34, 59, 85, 86, 101, 102, 103

DH district heating systems. 33, 34, 46, 50, 86, 101, 102, 103, 158

DHC district heating and cooling. 24, 26, 27, 28, 30, 32, 33, 34, 35, 36, 37, 46, 47, 48, 70, 81, 83, 84, 85, 86, 87, 88, 89, 90, 91, 101, 106, 112, 113, 115, 119, 120, 121, 123, 153, 158, 159

EMS energy management system. 26, 28, 29, 30, 48, 56, 57, 58, 64, 93, 95, 96, 127, 157, 158, 159, 160

ESCO energy service company. 47, 48

EU European Union. 22, 31, 46

FP7 7th frame program. 22

GARCH generalized autoregressive conditional heteroskedasticity. 53

HL Heat Loss. 30

KPI key performance indicators. 114, 115

LCOE levelized cost of energy. 114, 115, 120

MADPE mean absolute daily percentage error. 69, 150, 152, 153

MAE Mean Absolute Error. 68, 69, 126, 146, 147, 148, 150, 152, 154, 155

MAPE mean absolute percentage error. 69, 126, 146, 150, 152, 154, 155

MILP mixed integer linear programming. 52, 62, 63, 64, 102

NARX nonlinear autoRegressive models with exogenous neural network. 54, 66, 67, 131, 145, 146, 147, 148, 149, 151, 152, 153

NWP numerical weather predictions. 52, 134, 142, 149

O&M operation and maintenance. 39, 44, 49, 73, 74, 75, 92, 95, 158

OMIE operador mercado iberico español. 37, 126, 141

PACF partial autocorrelation function. 66, 68, 144, 151

POLITO Politecnico di Torino. 24, 28, 30, 56

RES renewable energy system. 28, 33, 149, 159

SAMPOL SAMPOL ingeniería y obras. 22, 24, 26, 56, 64, 65, 70, 141, 158, 160

SCADA supervisory control and data acquisition system. 51, 121, 123, 143, 158

SCIP solving constraint integer programs. 30

SHINE solar heat integration network. 22, 23

SQL structured query language. 28, 65, 141

UIB University of Balearic Islands. 22, 24, 47, 70, 81, 121

VFD variable frequency drives. 71, 83

WHB waste heat boiler. 73

Nomenclature

Name	Symbol	Units
Area of solar collector	A	m^2
Annual amplitude of the surface soil temperature	A_0	°C
Solar collector first order parameter	a_1	$\mathrm{W\,m^{-2}\,K^{-1}}$
Solar collector second order parameter	a_2	$\mathrm{W\,m^{-2}\,K^{-2}}$
Boiler	B	–
Chiller	C	–
Specific heat capacity of metal	c_{pm}	$\mathrm{J\,kg^{-1}K^{-1}}$
Specific heat capacity of water	c_{pw}	$\mathrm{J\,kg^{-1}K^{-1}}$
Damping depth	d	m
Energy wastes	D_h	kWh
Diameter internal of pipe	D_{in}	m
Diameter external of pipe	D_{out}	m
Energy cooling	E_c	kWh
Energy condensing	E_{cn}	kWh
Energy electric	E_e	kWh
Energy generated	EG	kWh
Energy heating	E_h	kWh
Energy input	E_{IN}	kWh
Energy stored in water tanks	E_{stored}	kWh
Solar irradiation	G	$\mathrm{W\,m^{-2}}$
Solar irradiation on a tilted surface	G_{0T}	$\mathrm{W\,m^{-2}}$
Mass flow of air	G_s	$\mathrm{kg\,s^{-1}}$
Solar constant	G_{SC}	$\mathrm{W\,m^{-2}}$
Specific Enthalpy	H	$\mathrm{J\,kg^{-1}}$
Irradiance	I	$\mathrm{W\,m^{-2}}$
Net incoming irradiance at the ground level	Ig_{in}	$\mathrm{W\,m^{-2}}$
Net incoming irradiance at the top of the atmosphere	$I_{in}TOA$	$\mathrm{W\,m^{-2}}$

Name	**Symbol**	**Units**
Ratio of electric consumption by mass flow	k_{ele}	$\mathrm{kWh\,m^{-3}}$
Ratio of heat loss	k_{ϕ}	$\mathrm{kW\,^{\circ}C}$
Length of the pipe	L	m
Mass flow of water	$\dot{m}$	$\mathrm{m^3\,h^{-1}}$
Cloudiness index	N_f	$-$
Condensing power	P_{cn}	kW
Electric power of fan	P_{efan}	kW
Pumping system electric power	$P_{ele,p}$	kW
Power produced by generator	P_{Gen}	kW
Solar thermal power	P_{sh}	kW
Power produced by slack generator	P_{Slack}	kW
Power wasted	P_{wasted}	kW
Ambient temperature	T_a	$^{\circ}$C
Collector mean temperature	T_c	$^{\circ}$C
Temperature of supply, temperature of flow	T_f	$^{\circ}$C
Temperature of water generation	T_g	$^{\circ}$C
Thermal mass	TM	$\mathrm{kJ\,K^{-1}}$
Temperature of return	T_r	$^{\circ}$C
Temperature of soil	T_{soil}	$^{\circ}$C
U-value, overall heat transfer coefficient	U	$\mathrm{W\,m^{-2}K^{-1}}$
Heating demand	U_h	$\mathrm{kW_h}$
Forecasted Value	V_f	$-$
Real Value	V_r	$-$
Volume of stored water	V_{stored}	$\mathrm{m^3}$
Depth	z	m
Increase of temperature, DeltaT	ΔT	K
Efficiency of generator	η	$-$
Optical efficiency solar collector	η_0	$-$
Incidence angle	Θ_z	$^{\circ}$
Soil heat conductivity coefficient	λ_s	$\mathrm{W\,m^{-1}\,K^{-1}}$
Density of material	ρ_m	$\mathrm{kg\,m^{-3}}$
Density of water	ρ_w	$\mathrm{kg\,m^{-3}}$
Binary variable	σ	$-$
Cost of diesel	σ_{diesel}	$\mathrm{€\,kWh^{-1}}$
Cost of biomass	σ_{bio}	$\mathrm{€\,kWh^{-1}}$
Heat loss	ϕ	kW

Chapter 1

Introduction

1.1 Framework

This thesis work is part of the solar heat integration network (SHINE) project, which is a PhD programme supported by the European Union (EU) through the Marie-Curie scholarship at the 7th frame program (FP7), under grant number 317085. The research work was developed within SAMPOL ingeniería y obras (SAMPOL), industrial partner in the SHINE project. The student was assisted by the University of Balearic Islands (UIB), another partner in the SHINE project. The topic of this industrial PhD focuses on the optimisation of a pilot power plant operated by SAMPOL.

1.1.1 SHINE Project

SHINE is an international PhD education program and network for solar thermal engineering and the follow-up to SolNet. It is coordinated by the Institute of Thermal Engineering at the University of Kassel, Germany. This provides the opportunity for manifold networking activities between PhD and Master's students in the solar thermal field.

The EU project SHINE is a PhD scholarship education program that offers 13 PhD projects with a focus on large solar heating systems for district heating networks and industrial processes as well as novel components such as sorption heat stores and concentrated collectors. A map of partners is presented on Figure 1.1. The total budget for the SHINE project is 3.46M€ and it took place from October 2013 to April 2018. Besides research, the network offers a set of specialized PhD courses on solar thermal engineering.

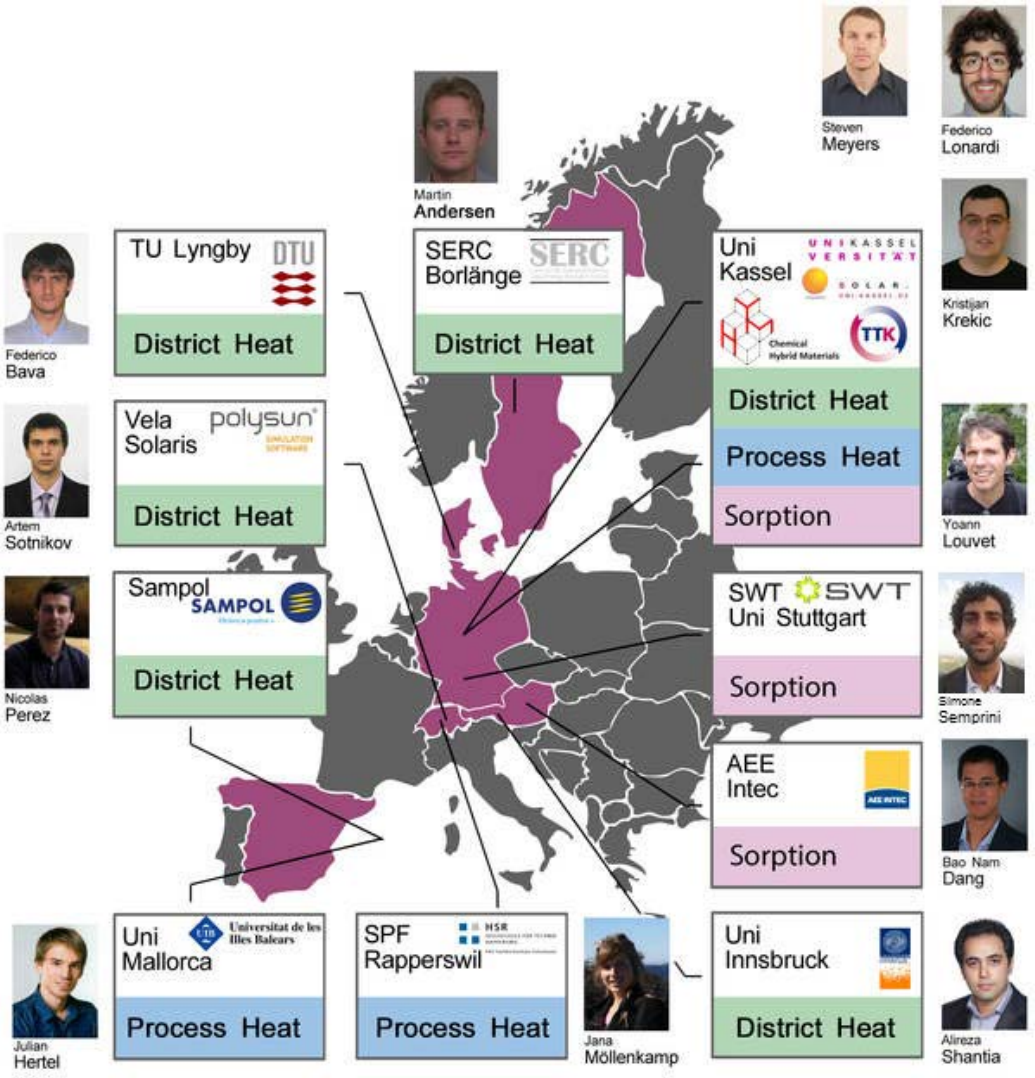

Figure 1.1: Map of SHINE partners

The SHINE project will include detailed experiments with innovative materials, components, systems, system integration analysis, and numerical optimisation and chemical investigations of storage materials. A close cooperation with industry will ensure fast utilization of the results. The SHINE network gathers a critical mass of PhD students at the European level and offers them a specialised and structured PhD course programme on large solar heating systems [1]. The SHINE project is divided into three work packages:

- WP1 - Solar District Heating
- WP2 - Solar Heat for Processes
- WP3 - Sorption Processes

This thesis addresses the topic studied in WP1.

1.1.2 Collaborating Institutions

As this PhD project and its research is conducted in an industrial company and supervised by a public university, this PhD is considered to be an industrial PhD. The institutions involved are the company SAMPOL and the UIB in Mallorca, Spain. During the research, the student enjoyed 4 months at the host institution Politecnico di Torino (POLITO), Italy to improve his knowledge on optimisation and modelling.

1.1.3 Pilot Plant

Parc Bit is a demonstration power plant located in Majorca. The power plant is a combined cooling, heating and power (CCHP) plant that provides electricity, heating and chilled water to the Parc Bit innovation center and to the UIB facilities through a district heating and cooling (DHC) network. The hot water is generated by combined heat and power (CHP) engines, a biomass boiler, solar thermal panels, and a fuel boiler. The cooling energy is generated by three conventional electric chillers and two absorption chillers. The absorption and the screw electric chiller are cooled down by water and both use the same cooling towers. The compressor electric chiller is cooled down with a dry cooler that uses surrounding air. Energy can be stored in hot water and cold water tanks for heating and cooling storage.

The district network was built in 2000 and used three branches to connect the tri-generation plant to Parc Bit office buildings. In 2002, the network was extended by connecting another branch to the university facilities, including the student house and the sports centre. The whole network comprises four branches of pre-isolated steel pipes. Each branch has two pairs of pipes: flow and return for heating and cooling. The total length of a single direction of the DHC is 4.6km.

Parc Bit's electric distribution system comprises an electric substation of 66/15kV, and the distribution is performed at 15kV. This distribution system provides electricity on multiple branches. One branch connects to the innovation Parc of the Balearic Islands, an urban waste plant and a school. Two other branches connect to Son Espases hospital. The system feeds electricity to six large customers at medium voltage, 137 small customers at low voltage, and to five electric vehicle charging stations in the Parc Bit parking lot.
The distribution in Parc Bit is performed at 15kV for medium voltage and at 400V in low voltage. The medium voltage and low voltage distribution comprises 5km and 6km of underground cable. The distribution system has one transforming center at 66/15kV and 15 transforming centres at 15/0.4kV. The energy consumption depends on the customer. The distribution system operator has a base load of about 90MWh/day which increases up to 150MWh/day in the summer season, the maximum power demand reaches 15MW. The annual consumption on the distribution system is around 40GWh. The different customers have different profiles, but most of them are seasonal and increase demand during summer. The distribution system also comprises an energy generation power plant connected to the line that feeds the innovation Parc (branch #1). The electric generation side consists of 2 CHP diesel generators of 1.36MW each, and a 7kWp photovoltaic array. The generation power plant also has electric consumption for pumping inside the power plant and the DHC, cooling through electrical chillers of about 650kW, and one electric vehicle charging and discharging point.

Figure 1.2: Frontal view of Parc Bit power plant

1.2 Problem Approach

In the southern European countries, solar thermal energy is harnessed a few months per year for heating. Therefore, solar cooling is a suitable option to increase the yield of thermo-solar fields that support tri-generation power plants. In these kinds of facilities, solar heating, and cooling integration does not significantly increase the complexity of the district network management strategies. These strategies depend on the decision-making system which aims to adjust the thermal and electric production curves to the forecasted consumption to lower the costs and maximise the benefits.

Energy generation is tied to energy consumption. Thus, the lack of information about the load or energy generation costs may lead to sub-optimally managed networks and energy waste. To achieve a fitting of energy between the load and generation, information is needed about the power plant as well as the district network and its distribution cost, primary energy cost, energy consumption estimation, and accurate energy price forecast.

Creating an energy management system (EMS) and including forecasted information into the model aims to assist the power plant manager to improve the generation strategies, maximise benefits by reducing production costs, and optimise the energy distribution through the DHC network.

1.3 Aim

SAMPOL aims to advance its analytic maturity with the help of this PhD project. A four-stages data analytic maturity is proposed in [2]. In Figure 1.3 an adaptation from the model is depicted. Thus, the aim of the project is to develop an EMS tool that can guide the plant manager through the decision-making process while operating the plant. This is achieved implementing more efficient generation strategies, optimising energy generation, and obtaining a higher solar thermal fraction.

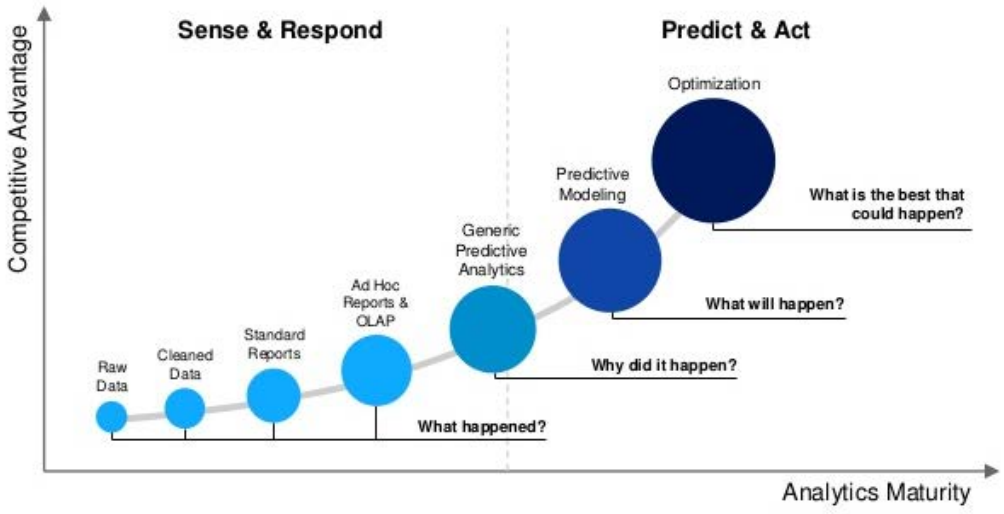

Figure 1.3: Big Data – From Descriptive to Prescriptive

Forecasting tools are included in a set of appropriated computer tools. These tools work together with thermal simulation software to estimate the energy generation strategies by determining the energy production mix that minimises the energy cost and optimises the electricity production. This leads to an optimisation of the plant operation and integration of the solar field. Several inputs are required to optimise the plant generation: heating and cooling demand, solar thermal generation, electric energy price, and the behavior of the generation systems as well as the district network and its heat losses under different operating conditions.

This PhD focuses on the operation optimisation of a hybrid power plant which covers the demand of a DHC and the maximisation of solar generation. To achieve this, this thesis must develop an electricity price for the Spanish market and a thermal demand forecasting tool which works together with an energy simulator. The simulator determines generation strategies by optimising the production mix that minimises the energy cost and maximises the renewable energy fraction. This leads to an optimization of the power plant's operation and integration of the solar field. Parc Bit is the power plant under study and is in Palma of Majorca, Spain. The power plant can generate heating, cooling and electricity. Thus, the power plant obtains revenue by injecting electricity into the grid and supplying thermal energy to the DHC. To maximise the plant's revenue, it is necessary to develop algo-

rithms that can provide energy generation strategies to meet generation and demand curves.

An EMS is developed to provide the power plant manager with optimal generation strategies. The tool is developed jointly with POLITO and can optimise a multi-energy node power plant at different time horizons.

This simulator requires information such as thermal and electric demand to fulfil, climatic conditions, power plant configuration, and machine behavior at different generation points. As a result, the tool provides the schedule of the generation machines, primary energy consumption, and total revenue for the time horizon under consideration.

A two-cores forecasting tool was developed based on the auto regressive integrated moving average with explanatory variable (ARIMAX) and artificial neural networks (ANN) models to obtain the future electricity prices of the Spanish wholesale energy market and the DHC's thermal demand. Those values are fed to the optimisation tool to determine future generation strategies.

Heat losses in the DHC distribution are considered to be part of the thermal load to be fulfilled by the power plant. A calculation tool is developed in order to accurately estimate the thermal losses in a four pipes DHC system under different working circumstances. In such a system, it is crucial to consider the influence between heating and cooling pipes and their working temperatures. The tool optimises the supply cost, taking into consideration the cost of generation for the thermal loss and the electricity cost of the pumps' circulation of the water in the network. A solar generation forecaster is developed, using the two forecasting cores (ARIMAX and ANN) to estimate the future solar thermal generation that can be expected at Parc Bit. Using the solar thermal forecaster enables the generation to be fed to the optimiser, included in the future generation schedule. Therefore, the solar fraction can be maximised by avoiding overlaps with the CHP's thermal generation schedule.

To clarify the general idea of the thesis, a graphical representation is presented in Figure 1.4. To summarise the aims, the following tasks must be carried out:

- Design of an structured query language (SQL) data base (DB)
- Development of an energy price forecaster
- Development of a renewable energy system (RES) forecaster

- Development of a demand forecaster
- Installation of dataloggers to register demand data
- Development of an EMS
- Design of generation strategies
- Scheduling and control of three-way valves for supply temperature

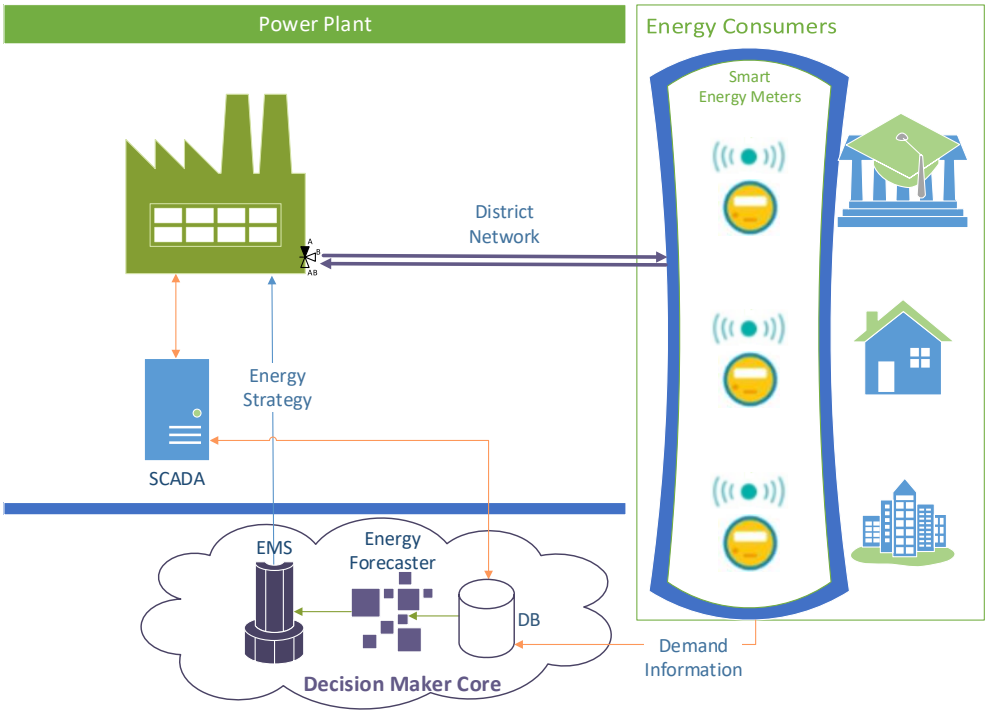

Figure 1.4: Graphical representation of thesis aims

1.4 Scope

Different computing tools are used in this thesis. The aim of the thesis is to develop an EMS which is composed of different tools.

This thesis covers the setting, configuration and usage of the forecasting tools. However, it does not cover the development of new forecasting models. The author configures and tests the best configurations but does not develop new methodology. The forecasting models used are off-the-shelf models included in Matlab and based on ANN and ARIMAX. In this work, these models are also compared and studied, although they are not developed.

This thesis will develop several parts of the power plant optimiser tool. Nevertheless, the solver used in the tool is developed by Gurobi, solving constraint integer programs (SCIP), or Matlab; this work only configures and uses the solver.

As part of the collaboration with POLITO, this thesis helps to develop several aspects of the EMS, namely XEMS13. The aspects of the EMS improved are:

- Development of the cooling node, specially the performance of cooling generators on partial loads and the impact of cooling output temperature
- Development of condensing node, including cooling towers, dry coolers and geothermal systems as heat sinks
- Usage of climatic data such as ambient temperature and relative humidity affecting condensing power calculations
- Inclusion of thermal mass of the DHC as thermal energy storage
- Calculation of Heat Loss (HL) in thermal energy distribution
- Development of optimal energy supply considering HL, electric pumping cost and supply temperature

Chapter 2

State of the Art

2.1 Background on Energy

Worldwide energy consumption is rapidly increasing. This has led to the consumption of more fossil fuels, whose price is increasing. This trend is also spurring the installation of renewable energy systems, often in combination with conventional generators [3].

The consumption of energy is increasing in general, but the demand for different forms of energy has also proliferated as working and life standards improve [4]. In developed countries, it is common to find simultaneous demand for electricity, heating, and cooling from the same customer. These three are the main forms of energy consumption in residential, public, and commercial buildings and their demand has been increasing in the last few years [5].

The separated generation of the three types of energy entails higher fuel consumptions. Consequently, it is necessary to find an effective solution for generating the energy required by EU targets. One of the adopted targets, known as 20-20-20, involves an increase of efficiency by 20%, reduction of greenhouse emissions by 20%, and the attainment of 20% of total energy generation as renewable sources [6].

One solution that has been commonly adopted to increase efficiency involves tri-generation power plants where different generators are combined in a single system that aims to achieve primary energy consumption savings [7, 8].

Tri-generation is an extension of a CHP system including cooling and

it is also known as CCHP [9, 8]. It is an effective way to improve energy efficiency throughout the year and to use unique source fuel to produce the threefold energy vector requested by the user [10, 11, 12]. Combined cooling, heating, and power plants are an efficient option to supply heating, cooling, and electricity to the network [13, 14]. These plants are essentially a CHP engine coupled with a heat-driven refrigeration system that produces cooling when requested. Therefore, the heat produced by the CHP, otherwise known as cogenerated heat, can also be used for regular heating demand.

Usually CCHP plants use electric chillers as auxiliary cooling generators to supply peak cooling demands when the CHP is not engaged [15]. Combined cooling, heating, and power plants are a widely used configuration for decentralised systems where the end user is close to the energy generation point and can be connected with a DHC network [16, 9, 17].

A hybrid system includes more than one type of primary energy into a single system to supply the demand. A polygeneration system can generate several types of energy. In hybrid polygeneration power plants, it is common to find tri-generation systems where the CCHP is the main generator but is backed up with some auxiliary generators. In such cases, electric chillers are used to improve cooling efficiency [15]. In the same way, heating auxiliary systems are often based on renewable energy sources such as biomass or solar thermal [18]. These hybrid systems are usually more efficient, but it is also more difficult to manage them properly.

Out of the three different forms of energy presented, cooling is the newest commodity requested by energy consumers. Nevertheless, cooling demand is foreseen to increase more than ten times by 2050 and be larger than heating demand by 2100 [19]. Centralised cooling plants have been proven to be more environmentally friendly than individual smaller cooling units [20]. This has created the need for distributing and transporting cooling energy efficiently to the consumption points. This need can be fulfilled with an existing and mature technology, such as DHC.

In warm climates, cooling consumption can be as significant of a contributor to total demand as heating consumption [21]. In centralised systems, cooling is generated with absorption chillers or electric chillers. Both technologies require a heat sink to evacuate the excess heat from the condenser. This excess heat can be dissipated by being disposed to the following:

- water bodies such as lakes or rivers,
- the air or environment through cooling towers or dry coolers, or

- the underground using geothermal systems.

The dissipation of excess heat is limited to the saturation of the heat sink. The most critical situations appear during disposals to air. When cooling towers or dry coolers are used to eliminate excess heat from the condensing node, the efficiency of the heat sink directly depends on the ambient conditions: the wet bulb temperature for cooling towers and dry bulb temperature for dry coolers. Therefore, the mass flow of air going through the heat sink may reach the saturation state, where no more heat can be rejected.

To avoid critical situations during operation, the best solution is to use heat sinks that do not depend on ambient conditions, such as geothermal systems [22]. Nevertheless, these sinks may come with the risk of media saturation over time.

Whenever the heat sink encounters saturation, the cooling performance is affected because its generation requirements cannot be matched.

As cooling demand by residential, public, and commercial consumers coincides with high ambient temperatures, the probability of heat sink saturation increases. Therefore, heat sink saturation influences the generator's performance by decreasing its cooling output. Ambient conditions are a main factor to consider when operating a cooling system coupled to an ambient-dependent heat sink.

2.2 Background on DHC

Most existing networks are used to transport a heating fluid and are commonly known as district heating systems (DH). The first DH system was constructed by the US Naval Academy at Annapolis in 1853 [23]. Networks used to transport a cooling fluid are know as district cooling systems (DC). The first known DC was installed in Denver, Colorado (USA) in 1889. Currently, DC systems are well established in North America and are becoming more popular in Europe [24]. The combination of a DH and DC system is known as DHC [23].

District heating and cooling systems use a pipe network to connect the energy users in a neighborhood, area, or city. These users can then be served from a centralised power plant or distributed plants that provide heating and cooling [25].

A centralised generation system uses large generation units with greater efficiency and more advanced air pollution control methods. Moreover, a

central power plant allows collaboration with a variety of energy sources, easing the integration of RES [26].

In addition, energy storage may improve the performance of the whole system [27] and provide an effective way to decouple energy production and energy demand [28].

The development of DH and DC systems has gone through four generations. This development has improved factors such as supply temperature and energy integration [25].

The main difference between DH and DC is the delivery temperature. In DC systems, temperature is normally below 10°C [27]. The temperature drop between the supply and return in DC is much lower than in DH. This means that DC's pipe size must be much larger to carry the same energy, which requires more investment in DC networks [29].

As previously mentioned, DHC systems are an efficient way to supply thermal energy to the customers, but these systems must be planned carefully for proper performance. The planning phase needs to address features such as pipe layout, insulation, size, underground depth, soil conductivity, and operation strategy.

The district network may be designed using different topologies. Pipe layout is arranged in one of the following three forms: branched, looped, and branched-looped network. A branched network is simple but unreliable. Looped is more reliable but has higher investment costs. Branched-looped is a combination of both designs. Figure 2.1 is a graphical representation of the configurations [27].

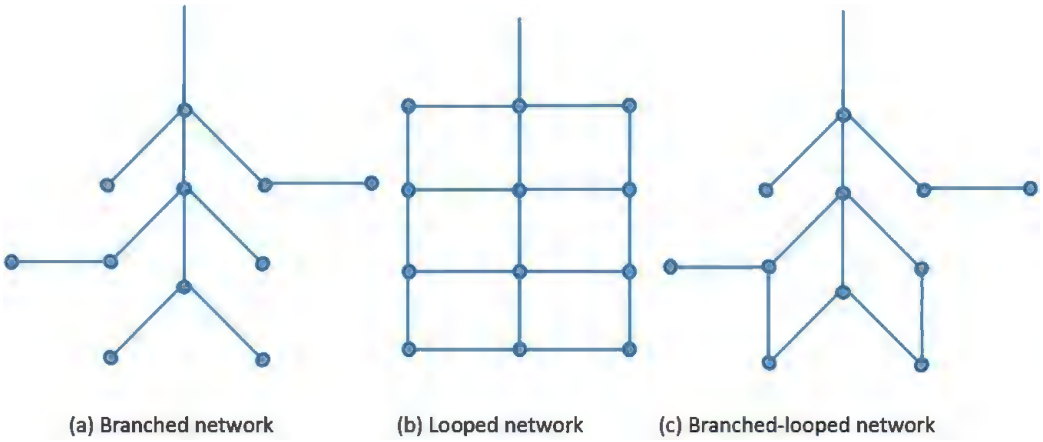

Figure 2.1: District networks configuration

Another factor that influences DHC performance is the piping. Pipe size, pumping consumption, and insulation thickness should be considered to achieve the shortest payback time [30]. The selection of a single or twin pipe is an important decision that can affect the initial investment and heat loss of the operation and the useful life of the installation. Using twin pipes instead of single pipes can result in significant energy savings with a minor increase in investment [31]. Equally important is the insulation used for the pipes, which plays an important role in the network's cost effectiveness [32].

One method to size the pipe section in a DHC considers the pressure loss per unit of length or target pressure loss of the network. This maximum target pressure loss is used to size the smallest pipe diameter in the network, and the remaining diameters are selected accordingly [30]. The selection criteria for target pressure loss values vary amongst European DHCs, and a review of them is depicted in [33].

In DHC network constructions, the location of the pipes varies among the following types: overhead, aboveground, and underground. Underground is the most common construction [34]. In such constructions, important design parameters include the soil around the pipe and the depth at which the pipe is placed. The soil composition and moisture are important for estimating the thermal transmittance that the network is subjected to. In large networks, the estimation of soil and its thermal conductivity is not easy because it varies with time and depends on the soil composition, structure, and moisture content [35].

Moreover, the depth of pipe burial has a direct impact on the soil's temperature around the pipe. The temperature undergoes cyclic variations on a daily and annual basis. The amplitude of such variations becomes damped with depth and is dependent on thermal conductivity [36]. The mean soil temperature at an infinite depth, where there are no temperature variations, is equal to the mean ambient temperature. Daily variations are negligible below 0.25m and may not be even observed at a depth of 1.0m [37].

An optimally operated DHC should consider the operation of pumps and supply strategies. The pumping system must be able to overcome the network flow resistance, including pressure losses in clients' heat exchangers. The study conducted by [33] indicates that operating strategies that employ variable flow and variable supply temperatures are beneficial in all cases.

Moreover, a slight change in the network's flow temperature can enhance the performance of the whole system: either through the improvement of the generation units' efficiency or the decrease of heat loss during distribution [38, 25, 39, 40]. Therefore, it is important to study and optimise the energy supply parameters to avoid poor delivery quality in the network [41]. Some studies approach the optimisation of DHC supply mainly from the design's point of view [42, 43]. Not much attention has been placed on the evaluation and study of energy supply strategies in DHC, despite their importance. The study in [44] proposes a new distribution concept based on mass flow control. [45] proposes an optimisation method for meshed grids, and [46, 47] present a model which takes into account the thermal inertia of the pipe. The studies carried on by [48, 49, 50, 51] have considered the thermal inertia of the DHC and buildings to be equal to transmission delay in terms of improving power plant performance through the inclusion of wind power generation. For example, in [51], the optimisation has been carried out by setting a fixed mass flow and defining a wide range for heating supply temperature (130°C - 50°C).

Nevertheless, the thermal mass of the fluid and pipe used to supply the energy on the DHC networks is neglected. Despite its significant potential, thermal load shifting in thermal networks is rarely implemented. This is mainly due to the absence of suitable smart meters and the lack of studies identifying thermal load shifting's benefits [52].

2.3 Background of Energy Markets

During the last decade, there was an increase in renewable energy power plants. This was motivated by subsidies that promoted the construction of green power plants [53] and the price increase of energy generated from fossil fuels. These factors and the policies adopted by many countries to integrate renewable energy into the energy generation mix rearranged the energy markets [54].

Energy generation is directly tied to the energy markets in which the power plant is playing an active role. Two energy markets must be considered for the power plant under consideration. The first one is the electric market. The power plant is connected to the grid where the energy is exchanged. The second is the thermal energy market where the energy prices are fixed for the customers who are demanding thermal energy in the DHC.

2.3.1 Electricity Market

The electric energy market referred to in this work is the Spanish energy market organized by operador mercado iberico español (OMIE). The power plant feeds energy into the grid generated from the CHP and may consume electricity from the grid. The energy cost in this market varies hourly. The variation of this market is linked with the energy mix at every hour.

The integration of energy generated by green power plants into the electric power system is a priority. This means that this power is fed into the system in preferential order within the energy mix. The volatility and variability of the renewable resource makes the integration in the grid difficult. In the Spanish energy market or pool, the aggregated electricity power production is balanced with the demand hourly. The electricity is traded in different markets: the daily market and the six regulation intraday market. In the daily market, the producers release their bids at 12:00 for next day's hourly generation. The intraday markets take place at 17:00 for intraday market 1, at 21:00 for intraday market 2, at 01:00 for intraday market 3, at 04:00 for intraday market 4, at 08:00 for intraday 5, and at 12:00 for intraday market 6. The generators can release their bids that cover each hour from a few hours after auction time till the end of the auctioned day, as long as that bid modifies a previous bid placed in the daily market [55]. Figure 2.2 provides a graphical explanation of the bid system.

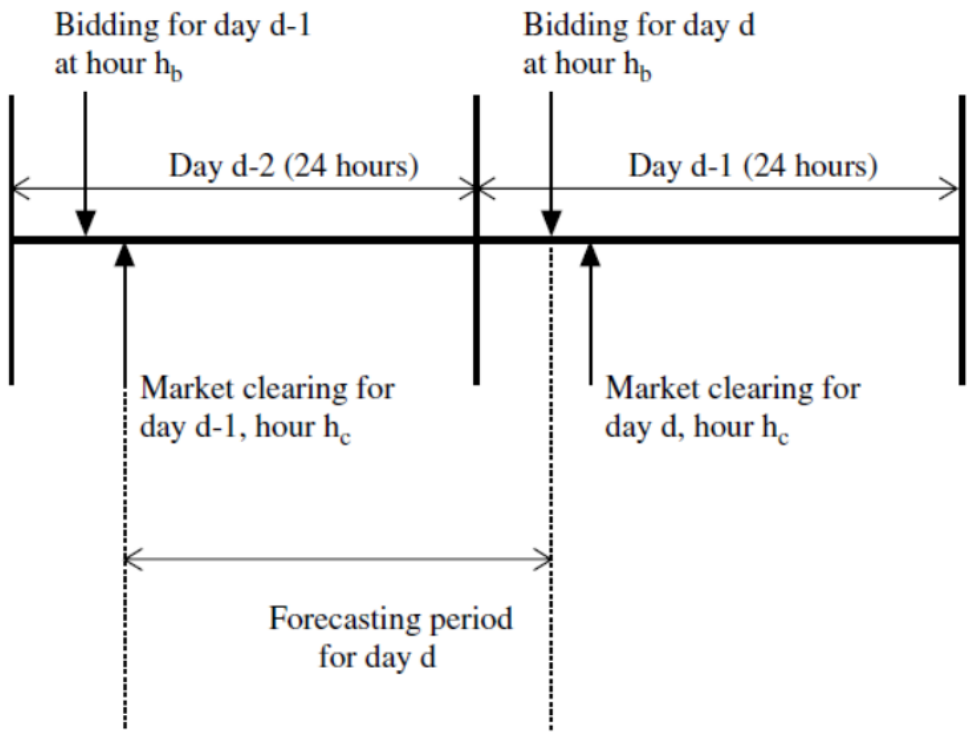

Figure 2.2: Electric energy market

The energy mix is the result of a counter clockwise auction: the highest price to purchase energy matches the cheapest offers. This process goes on until the cost of energy offered is the same as the price for purchasing from the demand. The lower and upper boundaries in the auction are 0€/MWh and 180€/MWh, where 40€/MWh is the annual average value. The repayment for all the accepted generators in an hour will be the same and equal to the last and highest accepted bid in the auction. To always ensure the acceptance of renewable energy into the generation mix, the green energies place their bids at the legal minimum of 0€/MWh and their return will be calculated as the sum of the final auction price times the generated energy plus the generation subsidy stipulated by the government. On the other hand, if the energy generation is different from what was offered in the auction, the grid operator may penalise the generator by charging the cost of the difference in energy.

Therefore, the energy mix in the auction is linked to its price. The en-

ergy mix in Spain is shared among different technologies. It is visibly divided between new installations based on renewable technologies and existing installations that are based on fossil fuels. The power installed and the energy mix of the different technologies in 2016 can be seen in Table 2.1 [56]. Biomass, biogas, geothermal, and marine hydraulic technologies are included under 'Other renewable'. Currently, the total annual energy consumption is 262.8TWh, and the maximum demanded power was $40,489$MW in 2016. The demand from renewable energy sources covered 41.1% of the total energy consumption. This generation is unsteady and changes with time, which directly affects the energy market price.

One major drawback for technologies supplying electricity from volatile resources is the non-continuous availability of the resource. Solar energy depends critically on the variability of irradiance [57]. Typically, cloud cover causes rapid changes in irradiance during the day [58] which brings along generation fluctuations in the same way that wind energy generation depends on the variation of wind speed and direction [59]. This dependence on weather conditions may lead to inaccurate bids from the generators in the energy auction and therefore penalties from the grid operator [60].

To understand the variability of the energy market, it is necessary to understand the variability of the green energy technologies since they have direct implications on the economic operation of the power system. These energy variations cause fluctuations in the hourly energy prices. These variations influence as many energy generators as consumers. Therefore, the renewable energy contribution must be known before energy prices can be forecast, which allows for energy scheduling at both ends [21, 61, 62]. In this section, the main factors affecting the energy price and their causes are described and evaluated.

2.3.1.1 Wind Generation

Wind power is a promising technology that has reached market competitiveness in the Spanish market without the help of subsidies. As depicted in Table 2.1, the installed power is equal to 23.02GW, which corresponds to 21.9% of the total energy mix. Figure 2.3 depicts the wind installation distribution in Spain. The map demonstrates the location and size of the installation in a colour-size map. The maximum installed power by law is 50MW. Wind energy is completely dependent on wind speed, but when the re- source is available, the generation is considered to be free. Therefore, the

Table 2.1: Spanish Energy Mix on 2016

Technology	**Energy** [GWh]	[%]	**Power** [MWh]	[%]
Hydro power	39,053	14.9%	20,354	19.3%
Wind power	48,927	18.6%	23,020	21.9%
Photovoltaic	7,979	3.0%	4,669	4.4%
Solar thermal	5,102	1.9%	2,300	2.2%
Other renewable	3,451	1.3%	748	0.7%
CHP	25,878	9.8%	6,714	6.4%
Nuclear	55,546	21.1%	7,573	7.2%
Coal	37,038	14.1%	10,004	9.5%
Fuel oil/Gas	6,748	2.6%	2,490	2.4%
Combined cycle	29,787	11.3%	26,670	25.3%
Waste	3,324	1.3%	754	0.7%
Total	262,852		105,307	

energy producer places energy bids on the market, ensuring that the energy will be accepted and matched. As the only expense wind power incurs is operation and maintenance (O&M), the strategy for bidding usually attempts to cover such costs, which generally are under 5€/MWh. That a significant part of the energy share is wind dependent has a significant impact on the energy grid and market prices. Wind is a highly variable resource; wind power varies from a minimum of 250MW to a maximum of 17.3GW and reaches peaks of production that may imply over 67% of the total injected power into the grid. Wind power does not necessarily follow the seasons but does have tendencies over the year. In 2016, wind power was the second energy producer in the Spanish energy mix at 18.6% of the total market. The impact of wind power due its variations is reduced with help of energy forecasters. The main forecasting difficulty is the error in wind speed estimation and the lack of information on wind farm layouts. This disables the use of wind direction to estimate power decreases due to shadowing between turbines.

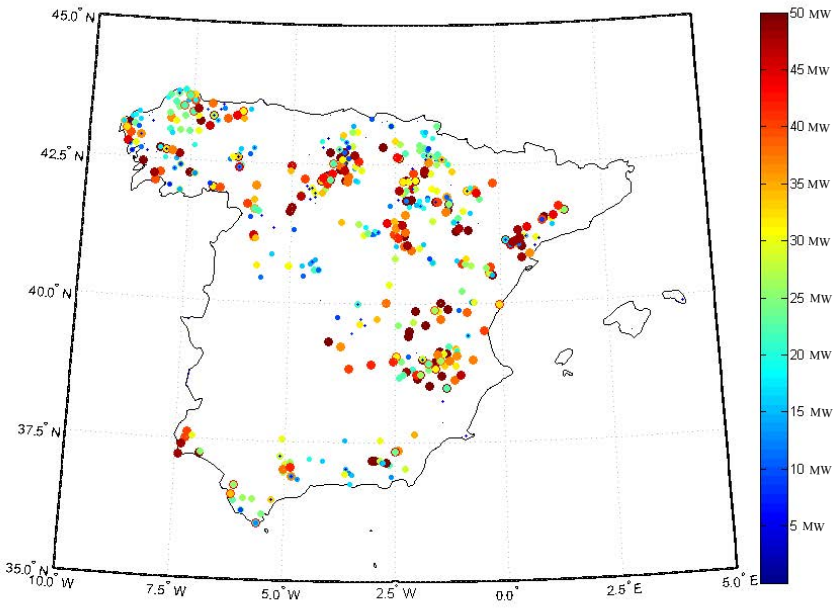

Figure 2.3: Map of wind installations in Spain by power

2.3.1.2 Solar Generation

Solar power is a common technology in Spain due to the high amount of irradiation in the country. Moreover, Spain led worldwide solar power development and installation in the previous decade. As depicted in Table 2.1, the installed total solar power is equal to 6.97GW, which corresponds to 6.6% of the total energy mix. These figures come from the sum of photovoltaic and solar thermal installations. Figure 2.4 depicts the solar installation distribution in Spain for both photovoltaic and thermal. The map indicates the location and size of the installation in a colour-size map. The maximum installed power by law is 50MW. In Figure 2.4, solar thermal installations are easily identifiable as they are usually over 40MW. Solar energy is completely dependent on solar irradiation, but when the resource is available, the generation is free. In the same way as wind producers, solar producers place energy bids on the market to ensure the energy will be accepted and matched. Their strategy for bidding usually involves the minimum energy market price, which is 0€/MWh. Similarly to wind energy, the dependence

on climate brings uncertainty to energy market, which can be attenuated with energy forecasting. The importance for forecasting energy generation lies in the marked difference in generation between stations that change from a peak of 7.5MW in winter to a $5,600$MW peak in summer and achieve a maximum of 25% of the total power injected into the grid. It is also important to understand that the solar electricity generation in Spain includes two technologies that can produce electricity:

- Photovoltaic. Ground mounted or in trackers. $4,669$MW
- Solar thermal power. Based on concentrating solar power. $2,300$MW

It is important to consider that the solar electricity generation from photovoltaic is only dependent on the solar irradiation on the panel surface. On the other hand, solar thermal plants generate electricity through a process that is dependent on solar irradiation and temperature. Additionally, some of these power plants come with an energy storage.

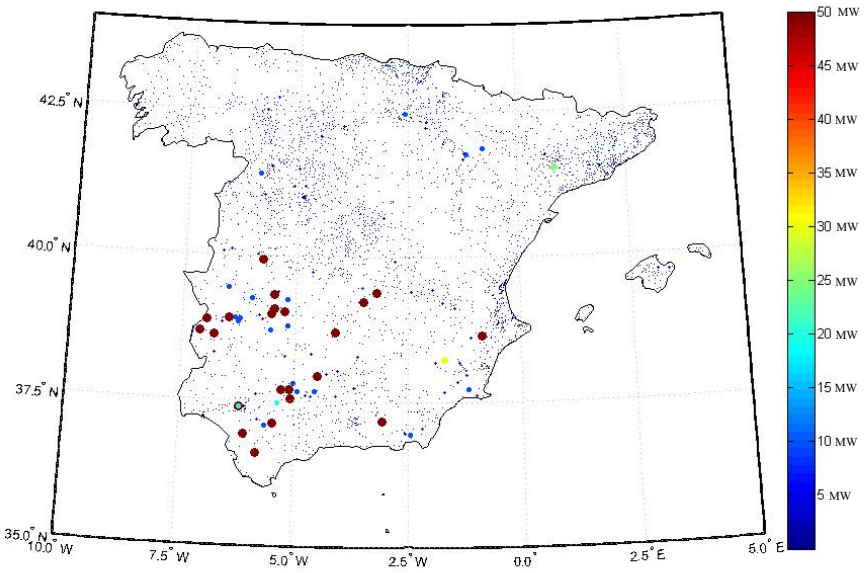

Figure 2.4: Map of solar installations in Spain by power

2.3.1.3 Nuclear Power

Nuclear generation is continuous over time. Nuclear power plants generate on its nominal power as long as they are running. This only changes when they start up and shut down to re-charge fuel. As the generators cannot be stopped (unless there is a critical situation), this technology bidding strategy is the legal minimum of 0€/MWh. Therefore, it is certain that the offer will be accepted and its energy will be consumed. In Spain, there are seven working nuclear power plants. All of them are slightly over 1.00GW of nominal power, and an extra power plant is currently out of duty at 466MW. The total working nuclear power is equal to 7.10GW, which generates 21.2% of the total annual demand.

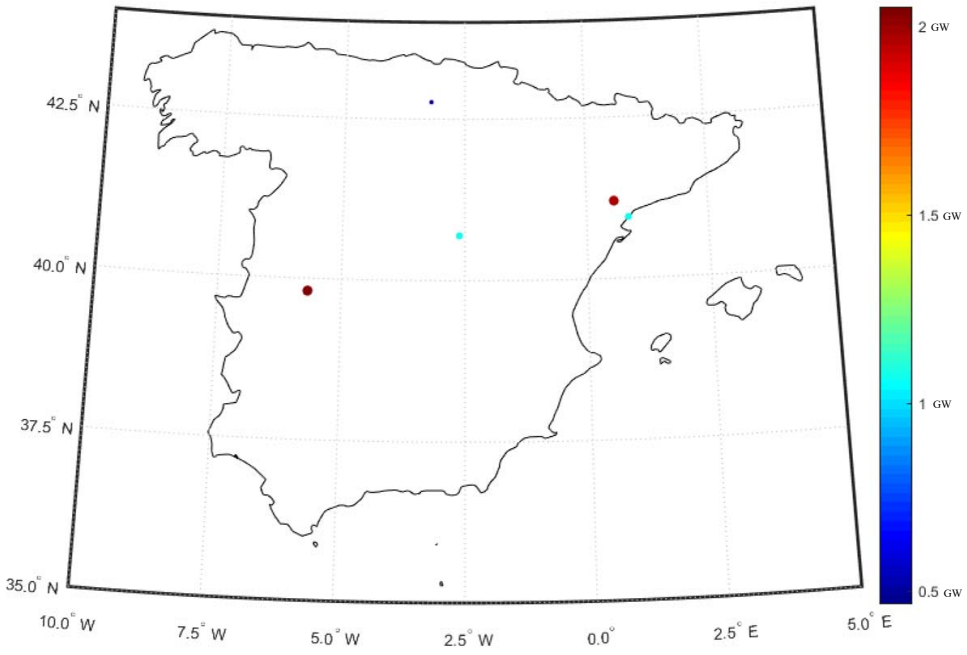

Figure 2.5: Map of nuclear installations in Spain by power

2.3.1.4 Hydro Power

The hydro power is divided in two groups. The first group comprises large hydro power plants that were constructed years ago. Their nominal power is

above 50MW, and the installation usually involves water storage and is fully manageable. These plants are equipped with backwards pumping, which enables the use of the pumps to charge the dam. This allows the stabilisation of the energy demand to act as a generator during high demand periods and as a consumer during low demand periods. The second group are smaller installations that are always below 50MW and lack dam or re-charging capacity. The generation of this group of installations is dependent on the water flow in the river where they are installed. Figure 2.6 depicts the hydro power installation distribution in Spain. The map shows the location and size of the installation in a colour-size map. The total hydro power from both groups is equal to 20.35GW and generates 14.9% of the total annual demand.

The generation strategies of the two groups are completely different. As the first group is regulable, they generate when the energy prices are higher to obtain higher profits. On the other hand, the second group offers energy bids to cover their O&M expenses as they would generate anyway.

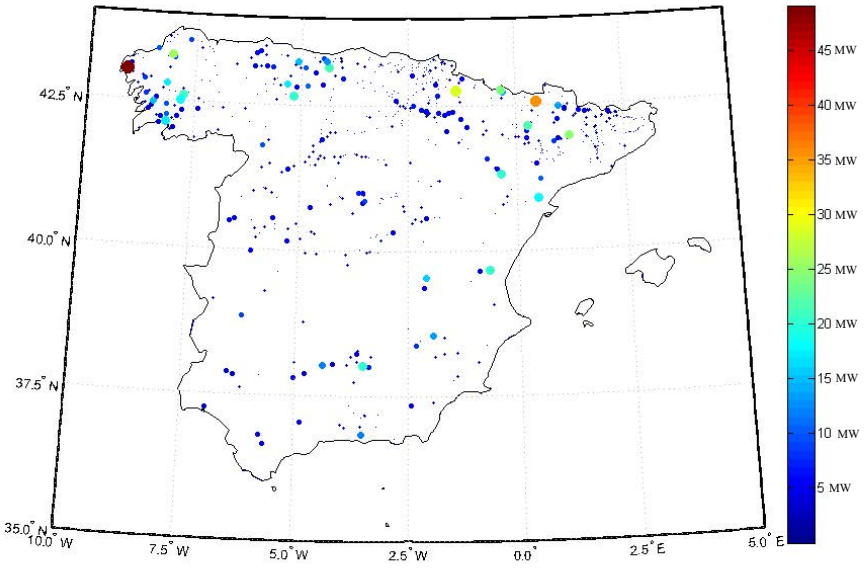

Figure 2.6: Map of hydro power installations in Spain by power

2.3.1.5 CHP

Combined heat and power refers to installations that transform fossil fuels into heat and power with high efficiency. These installations are tied to a thermal client to sell the thermal energy as the installations generate electricity. Therefore, their generation strategies depend on the client's thermal demand as the generation cost and the energy bid they place on the market may differ. Figure 2.7 depicts the CHP installation distribution in Spain. The map indicates the location and size of the installation in a colour-size map. The maximum installed power is 50MW by law. The currently installed CHP power is equal to 6.71GW and generates 6.4% of the total annual demand.

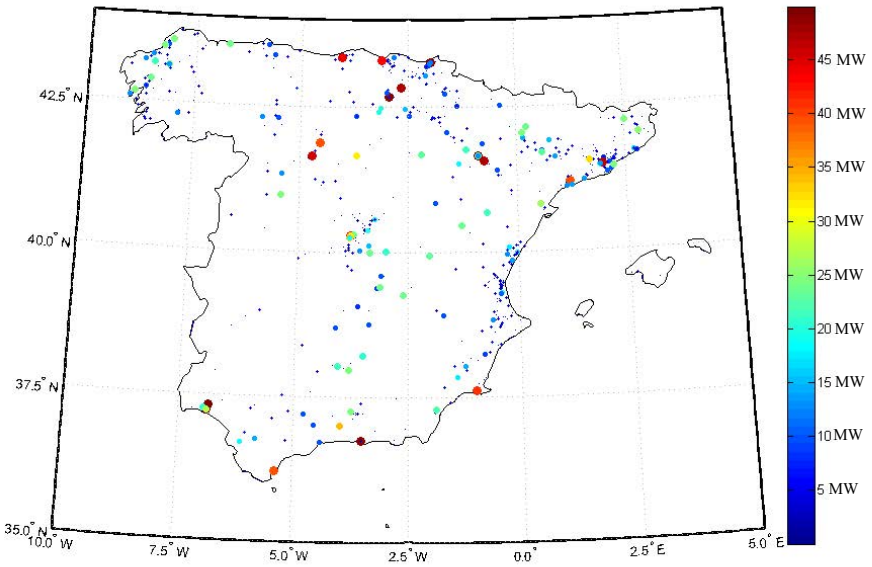

Figure 2.7: Map of CHP power installations in Spain by power

2.3.1.6 Conventional Power Plants

Conventional power plants refers to an installation which produces power using conventional generation techniques. These installations burn fuel to produce electricity through the movement of a generator. This category includes installations that burn fuel such as the following:

- Coal
- Fuel oil and gas
- Waste

The technologies included here in reference to Table 2.1 are the abovementioned fuels plus the combined cycle. Conventional power plants can generate energy at will because the primary energy used in the combustion is stored near the power plant. Therefore, the generation strategies followed depend on the energy market, and the generators generate when the energy prices are high enough to cover expenses and create benefit.

2.3.2 Heat Market

The effect of market forces on DH production is weaker than on electricity production because the heating network is smaller in scale and DH systems are often owned by a single entity. There are two basic types of heating markets [63]:

- Regulated: The energy price is government regulated.
- Deregulated: District heating competes freely with other heating options, and the DH's price is derived from the market.

Despite that nearly 40% of all primary energy in the EU are used for heating purposes, heating and cooling markets are not unified in a wholesale market or under common market rules [64]. It is difficult to estimate the figures or ratios of thermal energy supplied through DHC networks when compared with the total thermal demand. This is because of the numerous existing networks and the uncertainty of the total thermal energy that is consumed globally.

There is usually an agreement between the consumer and network manager on a fixed price or a price that is dependent on fuel cost. In the case of distribution with DHC networks, several customers acquire energy from a producer which generates the energy from a central power plant or several plants that are distributed along the network.

The costs of DH depend on three main factors [65]:

- The connection costs for customers

- The costs of a distribution network, which depend on the size of the DH network and its thermal loads
- The production costs of thermal energy

The heat is mainly produced by combustion of fuels such as coal, peat, fuel oil, natural gas, wood chips and pellets, and firewood. Electricity is also used for all heating demands at different temperature levels. Heat pumps and solar collectors generate small amounts of heat at a low temperature. When possible, heat is retrieved from industrial, power, and waste incineration processes and injected into the DHC network.

High and medium temperatures heat demands appear mainly within industry. Space heating and domestic hot water supply are the most common low temperature demands that appear in residential, commercial, public, and industrial buildings. The various heat supply methods provide different amounts of primary energy supply and carbon dioxide emissions [66].

The thermal energy market referred in this work is not an open market; instead, it refers to agreements between energy service company (ESCO) and the clients that fix a price for the energy and supply boundaries. The DHC network connects the power plant with the energy consumers. These consumers may demand heating or cooling. Furthermore, there is a difference between the original clients located in the Innovation Park Parc Bit in branches #1 to #3 and the clients added afterward at the UIB in branch #4. Every energy consumer has its own heat substation from where the energy is acquired. These substations must be supplied constantly with energy within the boundaries agreed on by contract. The constant supply of energy to all the consumers entails significant heat loss in the energy supply. The DHC network currently provides heating or cooling to 25 different clients. For district networks located in Mediterranean climates, particularly for this network, the cooling demand may be as important as the heating demand. One noteworthy feature of this district network is that some of the branches provide simultaneous heating and cooling to certain users. Nevertheless, most of the users are seasonal users that demand heat in winter and cooling summer. Moreover, according to the customer's energy profile, they can be split into three categories: office buildings, educational, and specific usages (such as residential, swimming pool, and IT room). These profiles are also differentiable between workdays and weekends. The supply of this energy demand will bring along the supply heat loss from the pipes used for its distribution, which will be added to the demand.

2.4 Background of Optimisation

The increased use of renewable technologies and the spread of different types of energy as commodities has increased the complexity of energy generation management. The appearance of hybrid generation systems with different technologies, fuels, and primary sources has multiplied the complexity of a problem that must be solved with computational algorithms. Similarly, the increase of customers demanding more than one type of energy has propelled the installation of hybrid generation systems. Therefore, it is necessary to develop a tool that can propose management strategies to control several technologies when they are combined or when several energy types are generated at the same site [67]. Polygeneration plants that use several generation technologies to match the same demand by using different fuels have different costs, efficiencies, and constraints. In these plants, the problems of managing the energy mix and keeping the overall generation cost at a minimum are complex. Several energy demands can be found on users connected to a DHC where the customers usually demand heating, cooling, and electricity. These demands are generally matched within the same power plant with a combination of generators [68, 69, 20].

This management problem is even worse in the case of generation from non-dispatchable energy sources as solar thermal, photovoltaic, or wind turbines [70]. The energy manager or power plant operator faces the complex problem of finding a suitable and optimum generation mix that takes into account the physical constraints on the generators. Besides, the operator must take into account the inertia, storage, and previous states of the generation machines if they are to operate smoothly, encounter reduced mechanical stress, and therefore avoid extra maintenance for the power plant.

From the ESCO point of view, it is very important to have precise knowledge of the cost of supplying the energy demand. Such cost comes mainly from the fuel consumption, DHC pumping, the power plant's self-consumption, and maintenance of the generators [21]. Once the primary energy costs and the benefits of the energy generation are known, the energy mix must be optimised by finding the most suitable schedule for the generation machines, which respects the technical constraints and boundaries.

From the environmental point of view, it is important to understand the different volumes of gases released to the atmosphere by the different generators at their different working points. Including such information in the tool aims to create environmental awareness while generating energy. It

also allows the power plant operator to take actions to conform the plant's operations to the new European directives regarding emissions and energy efficiency regulations regarding high efficiency generators [71]. An EMS aims to solve problems to the power plant operators in three different operation horizons:

- Daily optimisation schedules the power plant operation in a 24 hour time horizon. Demand and energy prices forecasts are used to optimise the future energy generation by minimising costs and maximising profit.
- Monthly optimisation schedules the power plant in the medium term. It is useful to define the maintenance of the generation equipment and to determine the volume of fuel that the power plant uses during that term to improve the logistics of primary energy purchase.
- Yearly optimisation schedules the power plant in the long run. It is useful to plan the O&M of the generators at the most convenient time in the year and estimate the power plant's profits.

To operate a hybrid polygeneration power plant in the most efficient way, the plant manager requires a set of generation strategies based on variable parameters such as the demand to fulfil, primary fuel costs, non-dispatchable energy generation, energy market prices, ambient conditions, and knowledge of the power plant and its generators' performance on the different working points. There are three common techniques to obtain the generation's strategies:

- Thermal follower
- Rule–based management
- Optimisation–based

2.4.1 Thermal Follower Strategy

The thermal follower principle assumes that is always important to supply the thermal demand of the user. The generation systems are ranked and ordered in terms of generation cost. Therefore, generators are successively turned on to fulfil the demand at a given time. Thus, the power plant manager needs to estimate the cost of generation for each generator beforehand. The thermal

follower principle is based on corrective control: a problem implies a response, such as a change in a power plant's prearranged generation order that was established by the energy manager (e.g., low supply temperature motivates engaging an extra generator to maintain the temperature). In the case of boilers or auxiliary systems, the generation costs are trivial to calculate if the efficiency along its power range is constant. This calculation relates to the primary energy cost, maintenance cost, and machine efficiency.

The calculation of cost of energy is no longer trivial when more than one type of energy is considered. This is the case of the CHP engines which can simultaneously generate thermal and electric energy at different efficiencies. These energies are sold at different prices. Moreover, electricity is sold in the wholesale energy market at a price that varies hourly.

Furthermore, the electric energy generation needs to be scheduled on the energy auction market 1-day ahead of its production to be acceptable by the grid operator. This means that since the rest of generators in the power plant depend on the CHP, the entire power plant's generation schedule must be defined 1-day ahead. Consequently, the power plant's schedule assumes that the forecasts or estimations are perfect. In many cases, these estimations are performed with the previous day's values for thermal demand and electric energy prices. Therefore, the generation's scheduling is not as optimum as it could be. Once the estimations are assumed, the operation of the CHP engine is scheduled. From this point on, the rest of the generators will be added to the generation in the prearranged order. A new generator is started when the power plant encounters difficulty in fulfilling user demand. This situation is indicated by a low temperature in the storage or buffer tanks. On the other hand, a high temperature in the DH and storage or buffer tanks implies extra heating generation in the power plant: when this happens, the costliest generator is switched off.

This means that the energy stored in the network and the storage tanks should be considered when scheduling generators to find the most cost-effective solution. However, this is very difficult to address with the thermal follower principle.

The decision-making process to create the generation strategies for the thermal follower principle also includes constraints such as maintenance and personnel.

A power plant operated using the thermal follower principle is significantly reliant on the knowledge of the power plant operator. The decision-making process that should be followed by the power plant manager also

includes the following constraints:

- Programmed maintenance of equipment
- Personnel availability
- Primary energy cost
- Approximate revenues for energy sale

Maintenance of the equipment is scheduled and is periodical in most cases. This periodicity may depend on the number of hours of utilization of a piece of equipment.

Generally, it is advisable to have an operator on site when the CHP engines are running. Nevertheless, whenever the CHP is not running, the power plant can work autonomously if it has a supervisory control and data acquisition system (SCADA). Understanding this fact, operator's availability is a constrain to operate the power plant.

2.4.2 Rule-based Generation Strategy

This generation technique is based on the experience of the generators and a detailed documentation of the possible generation situations that can occur at the power plant. The situations are documented, as are the follow-up actions. Power flows are managed according to a set of case-triggered rules built from heuristic knowledge.

It is important to notice that the development of a set of triggered rules is difficult because of the number of possibilities. Therefore, this technique is seldom used [72]. This technique is based on detective generation, which involves a set of conditions motivating an action.

2.4.3 Optimal Generation Strategy

To manage hybrid polygeneration systems, it is advisable to use an optimisation tool that can propose management strategies to the power plant operator. Such strategies decide the generation schedule of several technologies when they are combined, generating several types of energy at the same site [67]. This technique is based on preventive generation, which involves the estimation and optimisation of the outcome of a pre-scheduled action.

The wide variation in generator efficiency, working load, and ambient conditions as well as the inherent complexity of managing a hybrid polygeneration system creates a problem with several degrees of freedom when finding operating strategies [73]. An optimisation-based approach can have a significant impact on energy savings compared with the thermal follower approach and is a useful tool for power plant managers who are seeking energy efficiency [74].

To operate a hybrid polygeneration power plant in the most efficient way, the plant manager requires a set of generation strategies based on variable parameters such as demand to fulfil, primary fuel costs, non- dispatchable energy generation, energy market prices, ambient conditions, knowledge of the power plant, and its generators' performance at different working points.

Mathematical programming methods have been employed widely in optimal power plant operation. Mathematical models for optimisation usually lead to structured programming such as linear programming, mixed integer linear programming (MILP), non-linear programming and mixed integer non-linear programming. If the constraints and objective function are linear, the problem is linear. Otherwise, the problem is considered nonlinear. MILP and mixed integer non-linear programming involves both continuous and discrete variables which take place in many applications of engineering optimization [75]. This thesis chooses a linear model to find a unique optimal solution in a short time, and a MILP method is used to develop the optimisation tool due to the inherent existence of discrete and continuous variables in a power plant.

The information regarding climatic variables can be extracted from numerical weather predictions (NWP) to be used in optimising the power plant generation for future time intervals [17].

Primary fuel costs do not commonly vary within short optimisation periods, and their value can be obtained from the experience of the plant manager.

2.5 Background of Forecasting

The different energy vectors and prices are highly variable over time. Therefore, having reliable forecasts is critical for producers, consumers, and retailers. To optimally self-schedule production units, the operator needs accurate forecasts of prices before bidding time [76]. To optimally operate the

power plant, the manager needs accurate forecasts of energy demands before scheduling the production. Moreover, if the generation depends on renewable energies which depend on solar irradiation or wind, forecasts are necessary for scheduling production on the energy market.

Time series analysis is one way to approach such problems. This methodology of forecasting focuses on the historical behavior of a dependent variable. Therefore, time series models can be used to analyse and predict future movements based on the past behavior of the dependent variable. Several forecasting methods have been used in the energy field, and literature surveys are presented in [77, 78]. Time series-forecasting single models can be summarised as follows [79]:

- Stochastic models
- Regression models
- Artificial intelligence based models

Stochastic models are inspired by financial literature and are widely applied to forecast of energy-related indices and variables. There are several stochastic models which have been employed for modelling and forecasting: RandomWalk [80], Mean Reverting Processes [81], Brownian Motion Processes [82], Ornstein–Uhlenbeck Processes [82], Inverse Gaussian Process [83], and Jump Diffusion Processes [84].

Regression-type models are based on the relationship between the dependent variable and the number of exogenous variables that are known or can be estimated. The most common approaches that employ regression models are auto regressive integrated moving average (ARIMA) models [85, 86, 87] and generalized autoregressive conditional heteroskedasticity (GARCH)-family models [80, 88].

For more than half a century, ARIMA models have dominated many areas of time series forecasting. This regression model is fitted to time series data with forecasting purposes. It is composed by an autoregressive model (p), moving average model (q), and differencing degree (D). Mathematically, it can be expressed as ARIMA (p, D, q). In an ARIMA model, the future value of a variable is assumed to be a linear function of several past observations and random errors. Nevertheless, stationarity is a necessary condition for building an ARIMA model used for forecasting. A stationary time series is

characterised by statistical characteristics such as a mean and autocorrelation structure that is constant over time [89].

In recent times, artificially intelligent models have been extensively used to capture unknown or excessively complex structures in the time series. These models are growing in popularity. Examples of such models include ANNs, support vector regression, wavelets, and genetically evolved models. In the past, ANNs were used extensively for oil price forecasting. Currently, ANNs are used across the whole energy field. Since the late 1990s, ANNs have been used in the field of energy forecasting: different variables have been used as inputs to an ANN to predict generation values [90]. However, the design of ANN models that use specific sets of design constraints relies on expertise with similar applications and is subject to trial and error processes [91].

Artificial neural networks can model richer dynamics and approximate any continuous function of inputs. Evidence of the efficiency of these models can be found in [92, 93, 94]. Artificial neural networks have been found to outperform the regression models in terms of high resolutions [95, 96].

Furthermore, there is a substantial difficulty in training networks which may require a large amount of iterations before the network could converge [96].

nonlinear autoRegressive models with exogenous neural network (NARX) build recurrent neural networks by adding an autoregressive model with exogenous variables (ARX). The NARX model relates the current value of a time series to the current and past values of the exogenous series that influences the series of interest. Another common ANN approach which enables the discovery of the relationship between the inputs and the output data is the multi-layer perceptron network [95].

In a multi-layer perceptron, neurons are grouped in layers. Only forward connections exist, which creates a structure that can learn and model a phenomenon. To produce a forecast, a fixed number of past values are set as inputs. The output is the forecast of the future value in the time series [97]. In this thesis, the ANN model used is the NARX configuration, due its proven outperformance of the multi-layer perceptron [98].

In this thesis, two different kinds of models are selected due to their high performance in forecasting time series. Furthermore, due the proved improvement of the accuracy of the energy forecast, both models are supported with an explanatory variable [99]. The specific models used and improved by the explanatory variable are as follows:

- Based on regression models: ARIMAX [100, 96, 101]
- Based in artificial intelligence models: ANN [102, 103]

2.5.1 Explanatory Variable

Both forecasting models accept and are improved using a time series that is related to the one under forecast. This time series are referred to as explanatory or exogenous variables. The correlation between these two time series is studied by means of a Pearson or a R^2 correlation study. The results of either study ranges from [1, -1], where 1 is a direct and perfect correlation and -1 is a perfect and inverse correlation. Figure 2.8 depicts some examples.

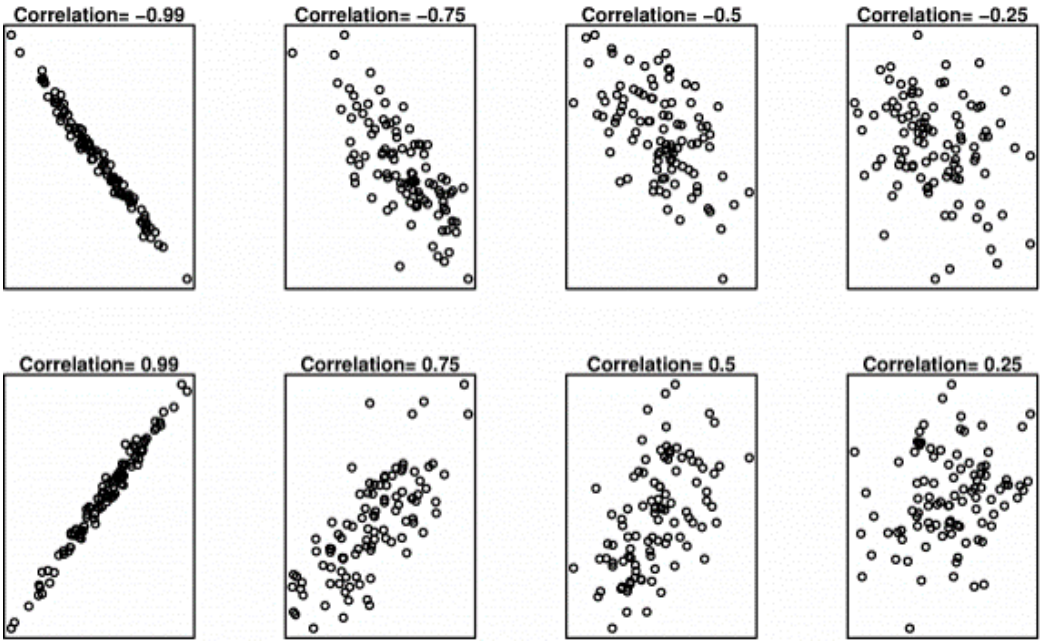

Figure 2.8: Examples of the correlation of two variables

The time series used as explanatory variables should have the following features:

- Have a direct or inverse relation with the main time series
- Same data granularity as the main time series
- Have as many future values as desired forecasted values

Chapter 3

Calculation Tools

3.1 Optimisation Tools

To manage hybrid polygeneration systems, it is advisable to use an optimisation tool that can devise management strategies for the power plant operator. Such strategies decide the generation schedule of several technologies when they are combined and generate several types of energy at the same site [67]. In this thesis, an EMS tool is proposed to optimise the generation of a hybrid polygeneration plant. The tool, XEMS13, has been developed in the energy department of POLITO and some parts have been developed in collaboration with the company SAMPOL. The tool can be categorised as a simulation tool, following the classification proposed by [10], where tools are categorised in terms of: dimensioning, simulation, research, and mini-grid design tools.

The tool aims to help the power plant operator to schedule generation, create operation and management strategies, maximise profit, and fulfil the customer's energy needs in the most efficient way. The optimisation carried out can either be economical, environmental, or both (multi-objective) by creating an objective function that pursues a minimum.

The optimisation tool is organised into three steps, according to the description provided in [61, 104, 105]. In the first step, the tool acquires the time profiles of the energy demand for the different energy vectors (heating, cooling, electricity,...), the time profiles of the energy prices (electricity, natural gas,...) and the time profile concerning the environmental conditions (outdoor temperature and humidity) and renewable generation (solar

thermal or photovoltaic). In the second step, the technical and operational characteristics of the different components (CHP, boilers, chillers,...) are defined within a library, and the connections between them are also set. Later, control variables and constraints are created according to the plant layout and the discretisation of the simulation's time horizon. Extensive explanation of the tool is provided in [62, 61, 106, 104, 70, 68]. A schema of the tool is depicted in Figure 3.1.

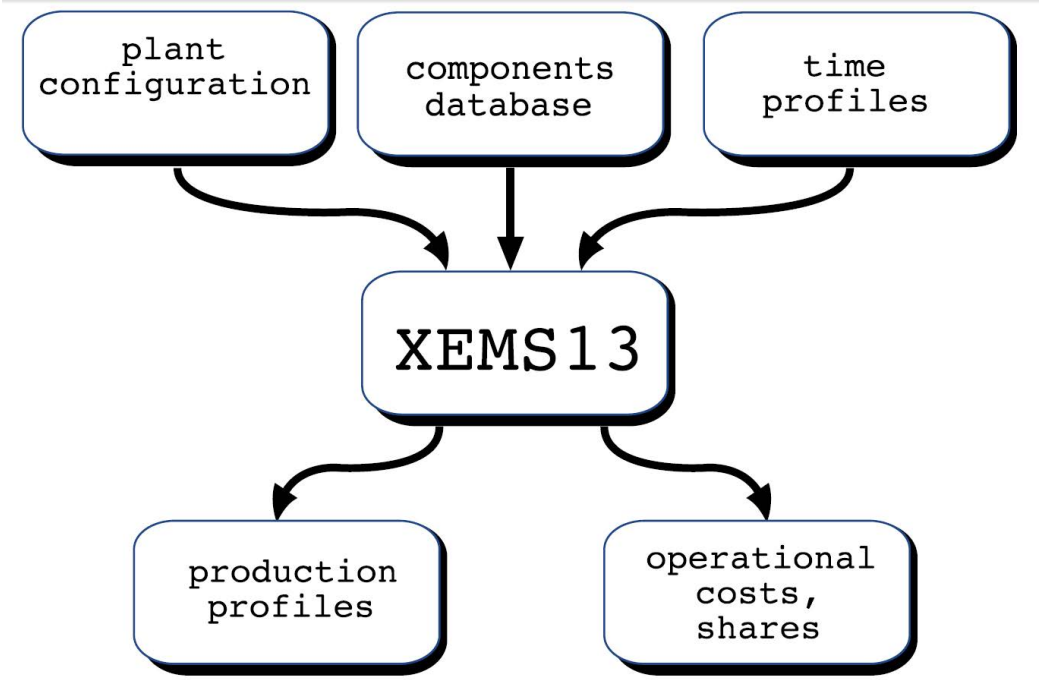

Figure 3.1: Schema of XEMS13 inputs and outputs

3.1.1 Pre-processing

At this stage, all the information is sorted out to be ready for calculations. The different types of energy are separated in energy vectors, where a load can be matched with the different energy mix of the generation machines. The EMS tool requires the introduction of the power plant's configuration, its components, the time profiles of loads, and prices before the tool can define a case study.

The following aspects are described in order: the different energy vectors, the available generators already defined in XEMS13, and the optimisation requirements.

3.1.1.1 Power Plant Configuration

The power plant is configured through a file (NetList) that contains all the components and the information required to perform a simulation. This information includes the solver type, the number of simulation steps, and information about fuel costs. The XEMS13 tool can consider different energy generators, demand profiles, several primary fuels with variable prices, non-dispatchable energy generation, and influence by external conditions. All this information is referred in this file and should be defined at this point. Some information is created with accessorised tools to generate information such as demand profiles, future energy prices, time-dependent boundaries, and processed climatic information. The EMS creates two different sets of equations from the components defined in this file and separated by energy vectors:

- **Balance Equations** for representing the balance of each energy vectors. These equations ensure feasible solutions when demand is covered by the generation at each time interval.
- **Constitutive Equations** for representing the relationship between the input and output power of a given component, as well as its operational limits and thermodynamic constraints.

In this file, the energy vectors are defined by adding generated components and demand. Therefore, for each of these vectors, a balance between demand and energy generation machines installed on the power plant is defined. In some cases, the generation must balance the loads. In other cases, intermediate energy conversions are defined to match the requirement of another energy vector: for instance, heat may not be used as is; it must be converted into cooling energy by an absorption chiller. The XEMS13 tool has already defined the following energy vectors as covering most of the existing loads in power plants:

- Electricity
- Heating

- Cooling
- Low-enthalpy heating
- Steam
- Condensing requirement

For a specific power plant's configuration, the user's demands always match in the balance equations by definition: the energy load must be equal to the energy generated at every time step. To avoid an infeasible solution, a slack generator is included in the equation in addition to the existing generators for that vector. This slack generator is fictitious and simply implies that the demand is impossible to fulfil at a given point with the provided power plant configuration. Purchasing energy from this slack generator must be the last option for the optimisation tool. To avoid the energy purchase from the slack generator, a high price is fixed for the external energy purchasing in XEMS13. The different slack generators defined in the tool and their features are as follows:

- Electric generator. It is permitted to purchase and sell energy with the external generator using variable prices.
- Heating generator. It is only possible to purchase energy from this generator at a fixed price.
- Cooling generator. It is only possible to purchase energy from this generator at a fixed price.

The heat waste is energy generated and released to the environment. Heating, for instance, can be understood as the non-cogeneration of the CHP fumes. Cooling can be understood as energy impulsed into the DC and wasted as heat losses along the distribution network.

Equation 3.1 an example of a balanced equation including different generators and the slack generator.

$$U_h = \sum_{n=1}^{N} P_{Gen(n)_t} + P_{Slack_t} - P_{wasted_t} \tag{3.1}$$

where $P_{Gen(n)_t}$ is the power produced by the n-th generator.

Figure 3.2 depicts an example of an energy vector that includes the relation of the generators (CHP, boiler and solar collectors), load, and storage within the heat vector.

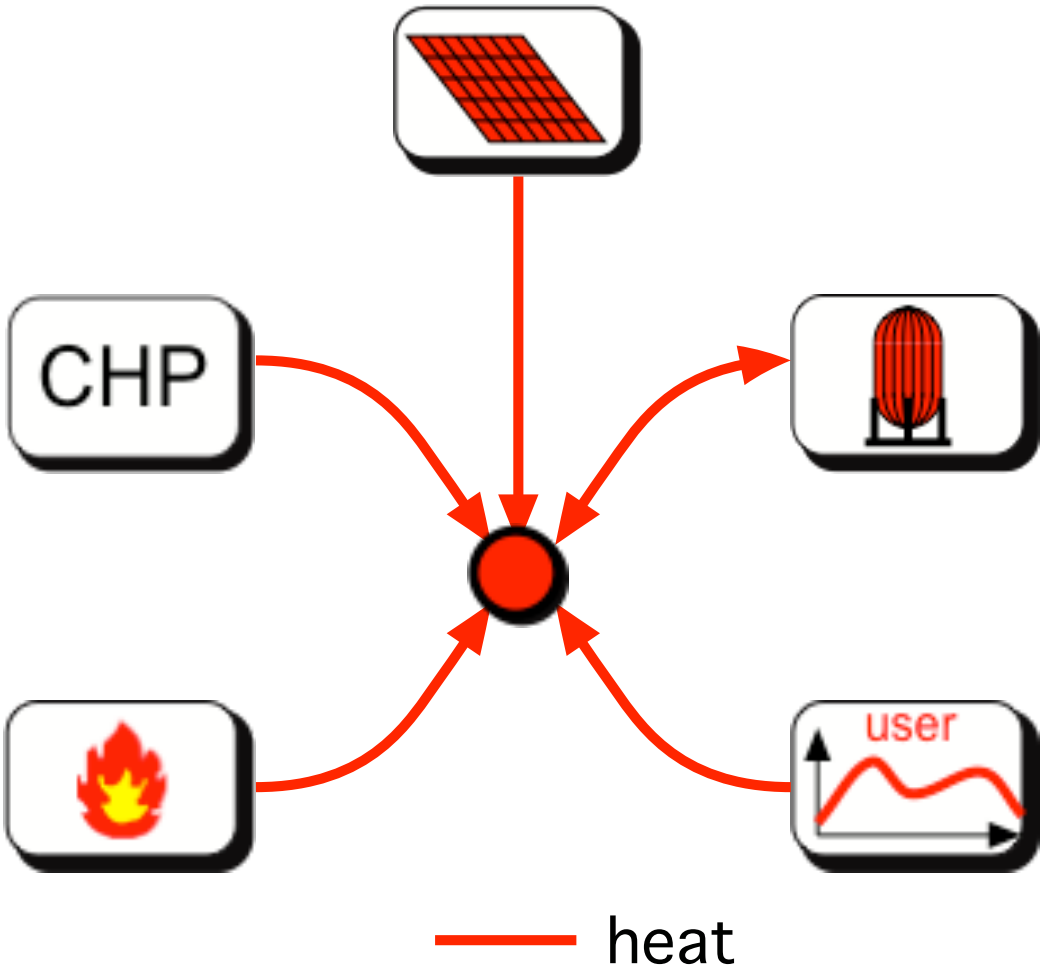

Figure 3.2: Schematic view of an energy vector configuration where heat power flows are considered

The defined energy vectors are not always energy demands from the user. Condensing vectors are mere requirements of the cooling generation systems; these requirements are operative vectors and not energy demands. Therefore, the condensing vector is required to limit the cooling vector. Thus, this vector does not include a slack generator.

Subsequently, the operating cost function is defined by considering the generation cost of each of the modules.

To create an objective function for optimisation, it is necessary to define the components and create the equations that relate generation and demand for the different types of energy vectors and their cost. The different fuels are defined in XEMS13 in terms of their low heating values and costs per unit of energy. The fuel costs are fixed for the whole optimisation period, except the cost of electricity which may be variable for each time step.

3.1.1.2 Components Definition

There are several components defined in XEMS13: these are most of the possibilities that can be found in a power plant. The components library defined in XEMS13 mainly comprises heating, cooling, and electricity generators, although it is possible to add any desired component. These components are listed and defined on an XML file, and most of them have a different structure since the acquisition of their data is done *ad hoc*.

The components are defined in a manner that considers their technical constraints, high and low boundaries, performances, energy consumption of primary energy, energy generation, and emissions. With this data, the definition of a component's constitutive equations can be created.

The thermodynamic constraints of the components are expressed within the constitutive equations. The steady state workings of the components are considered to neglect the implications of transient status. Possible technical constraints related to power ramp limits or minimum on or off time are considered. Common features defined in a XEMS13 defined component are as follows:

- Fuel used by the generator.
- P. Lvl: definition of the different power levels and working points of a generator.
- Primary energy consumption at a given power level.
- Energy generation at a given power level.
- E. Atm: emissions to the atmosphere of CO_x, NO_x, SO_x at a given power level.

- ESc: energy self consumption of the generator at a given power level.
- TON: minimum on time that the generator must remain working once turned on.
- TOFF: minimum shutdown time that the generator must remain stop once shut down.
- Maintenance cost per unit of generated energy.
- Priority: Position in which the generator is starting in relation with generators of equal characteristics.
- Collector area: Used in solar generation to define the aperture area of a collector.

In Table 3.1, the dispatchable energy generators from XEMS13 are defined and matched with the different features that are configurable in the tool.

Table 3.1: Constraints considered in some power components present in the XEMS13 library

Generator	**Fuel**	**P. Lvl**	**E. Atm**	**ESc**	**T. Cnst.**
CHP	✓	✓	✓	✓	✓
Boiler	✓	✓	✓	✓	✓
Absorption	✓	✓	-	✓	-
E. Chiller	✓	✓	-	✓	✓
C. Tower	-	✓	-	✓	-
Dry Cooler	-	✓	-	-	-
Geothermal	-	✓	-	-	-
Heat Pump	-	✓	-	-	-
Storage	-	-	-	✓	-

In the same way, Table 3.2 depicts the non-dispatchable energy generators from XEMS13 and matches them with the different features configurable in the tool.

Table 3.2: Data for non-dispatchable power components present in the XEMS13 library

Generator	Climatic info	Area	Efficiency
Solar th.	✓	✓	✓
Solar PV	✓	✓	✓
Geothermal	-	-	✓
Hydro gen.	-	-	✓

3.1.2 Processing

Since the optimisation problem is based on a MILP formulation, all the constraints that describe the plant layout and its operations need to be linear or must be linearised. For the generators, which usually can operate at different load factors with variable efficiency, this corresponds to the implementation of a piecewise linear approximation for the relationship between energy input and output [68, 70, 61].

Once all the variables, boundaries, equations, relations, and constraints are defined, they are related and merged within a unique objective function. This function can be either economic, environmental, or a mix of both, and the goal of the optimiser is to find a minimum value for the cost or environmental function when fulfilling the user-requested demand.

The XEMS13 tool uses a steady state power flow approach to solve the problem. The approach divides the horizon time considered in the optimisation into equal time steps where the boundary conditions are fixed and invariable. The transient status of the generators is not considered in the optimisation. The generation machine schedule and the final economic result of the considered period are given as a result once the optimisation is carried out.

The generators can work at different points within a working range and have different efficiencies at each point. As the optimiser is based on MILP, it is required to linearise any equation on their domain of definition by dividing it in intervals where the function is considered linear.

Once the problem is linearised and defined as a set of equations, boundaries, and constraints, a standard file MPS that condenses the information is created and delivered to a MILP solver such as SCIP [107], GUROBI [108], MatLab [109] solver, or another external solver that is able to solve the problem. The solver then returns the optimum solution along with the individual

values for the variables in the problem.

Finally, the tool finds the optimal scheduling for the different components of the plant using a solver for MILP formulation, which leads to minimum operational costs. The solution is processed, and the generation machines' schedule is provided in a spread sheet for use. These files present the balances for each energy vector. The EMS also provides an XML file that contains the Sankey diagram information and the final cost for the whole simulation period.

3.2 Forecasting Tools

This section describes the methodology followed to forecast energy variables such as price, thermal demand and energy generation. Accurate forecasts can be obtained using computational models such as ANN or ARIMAX. Both forecast model performances are improved by using an explanatory variable. This information needs to be acquired from different data sources and processed.

3.2.1 Data processing

This section briefly describes the process of data acquisition of the required information. There are several data sources used in this work; these sources and their uses are explained in further sections. However, the system operates similarly with all of them.

3.2.1.1 Data acquisition

Even though there are several sources of information used in this work, they can be divided in two kinds: from an existing DB or from disaggregated files. Information coming from a DB must have a connection point arranged with the DB manager. Once the connection point is agreed on and logging and permissions are sorted out, the recollection of data is simple. For the second case, where the information is scatted in different files or spread sheets, a filter of the information is requested . After filtering this information, it is arranged into a simple table file, including time and value for each variable. Once the information has gone through this process, the information on the files is ready to be included in the DB. To include this information on a central

DB, SAMPOL developed a code requesting this information. It covers two main functions:

- Monitor, retrieve and replicate the information of the existing DB
- Read and store the information located in the different files created on a designed folder

This code inputs the information on the central working DB and filters for possibly incorrect data.

3.2.1.2 Data Storage

After attaining the data from the source, this information is processed to avoid errors and stored in the central DB. Once the information is stored, an extra field of information is added on that pertains to the type of day: weekday, weekend, or holiday. The used DB is a SQL and is hosted in a virtual machine on SAMPOL's network, which makes it easier to access. Most of the data is acquired in hourly steps, but some variables could have greater granularity. If that is the case, the DB can provide averages for hourly values. The DB is also able to split the data according to different parameters if required.

3.2.1.3 Data Retrieving

Once the data is properly stored it is ready to be used. The data is obtained from the DB using Matlab and predefined queries stored in SQL procedures. These procedures are defined to retrieve an amount of data with significant information. These procedures can be configured with options such as

- data-granularity,
- type of day,
- starting and finishing date, and
- amount of values requested.

After the query requests the information, it is acquired in a suitable table where the first column is the time and it is ready to be used in Matlab.

3.2.2 Forecasting Models

This section describes the two forecasting models that are used in this thesis.

3.2.2.1 Time series correlations

To forecast next values of a time series it is necessary to understand which lags (also referred as delays) are important on that time series. [110] has proposed to use the autocorrelation function (ACF) and the partial autocorrelation function (PACF) of the sample data as the basic tools to identify the order of the ARIMA model [89]. Once the ACF and the PACF studies are carried out a threshold of correlation is used to determine appropriateness of the lags. This threshold is set in 0.7 for direct related lags and -0.7 for inverse related lags. Once these parameters are fixed, the most relevant lags are selected automatically with help of Matlab.

The selected lags can be used for both ARIMAX and NARX models.

3.2.2.2 ARIMAX

Matlab is used to configure the ARIMAX model and make it perform. This computational software has statistical software which eases the configuration and forecasting with this model.

The lags that were used as inputs in the configuration are extracted from ACF and PACF studies are variable and dependent on the case. The correlated lags can be distributed on the following:

- MA, stands for vector of non-seasonal moving average coefficients;
- SMA, stands for vector of seasonal moving average coefficients corresponding to an invertible polynomial;
- AR, stands for vector of non-seasonal auto-regressive coefficients;
- SAR, stands for vector of seasonal auto-regressive coefficients corresponding to a stable polynomial.

After careful consideration of the results from ACF and PACF studies, for the time series under study in this thesis, the seasonal coefficients are not considered relevant. Therefore, the used lags are distributed between MA and AR. To split the selected lags between MA and AR, the lags higher

than the forecasting horizon are placed as AR. The lags lower or equal to the forecasting horizon are placed as MA.

Another part of the model is the derivative part, D, which stands for integer indicating the degree of the non-seasonal differences in the time series. This variable is defined with natural numbers. For the time series used in this thesis the derivative part is either 0 or 1.

The data for the ARIMAX model is split as follows:

- training 95%;
- result comparison and testing 5%

3.2.2.3 NARX

Matlab is used to configure the NARX model and make it perform. This computational software has a specific toolbox for ANN, which eases the configuration of new networks to forecast. The following parameters are used:

- Training method
- Data split method
- Maximum epochs
- Minimum gradient
- Data split:
  - training
  - validation to avoid over fitting
  - result comparison and testing
- Number of neurons
- Activation function

The toolbox offers a list of training methods including: Levenberg-Marquardt, Bayesian Regularization, and Scaled conjugate gradient. After running several test, for the time series in this thesis, the most successful training method is Levenberg-Marquardt algorithm. The data split method used is random which gives better results when training the ANN. The data is split

as 70/15/15 which is the one used by default in Matlab toolbox and extensively used in forecasting applications. Maximum epochs and minimum gradient are values which stop the ANN whenever reached. To configure the minimum gradient a low value is given where the forecasts are considered accurate. The maximum epochs are configured to stop the ANN using the best achieved value. The more epochs allowed the better results obtained but the more computational time required, therefore, a time-accuracy balance is required.

The number of neurons is variable and dependent on the case. The neurons are located in input, hidden, and output layers. The amount of neurons on the input layer is equal to twice the time steps to forecast when an explanatory variable is used, otherwise, is one neuron for each time step. The amount of neurons on the hidden layer is equal to one for each time step to forecast. The amount of neurons on the output layer is one. There are several activation functions for the neurons to choose for on the hidden layer such as: linear, sigmoid, tangent, hyperbolic tangent.

The lags (or delays) used in the configuration of the ANN are extracted from ACF and PACF studies.

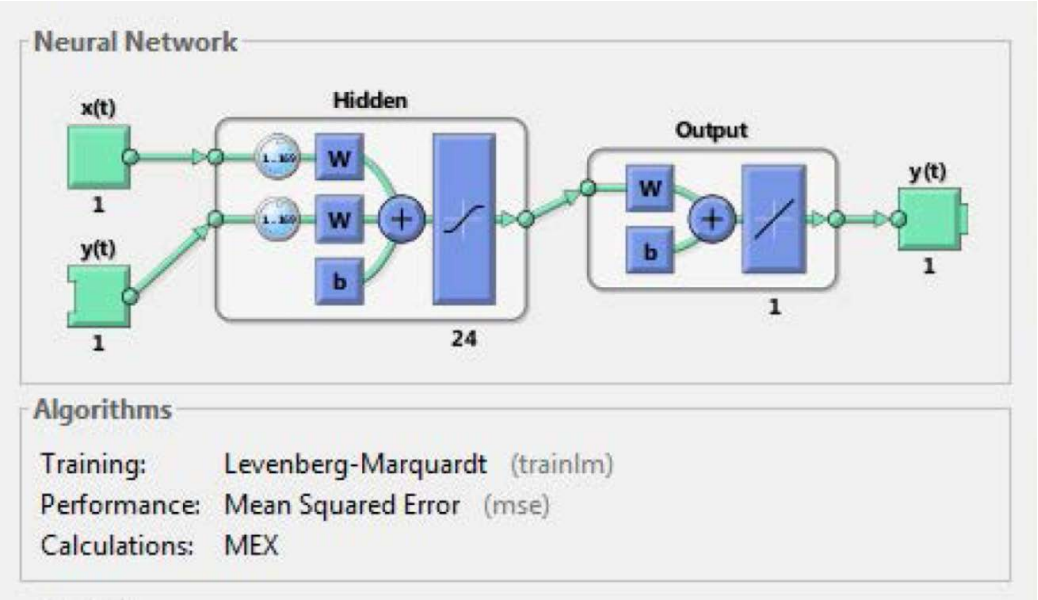

Figure 3.3: NARX configuration used in MatLab

3.2.3 Error Comparison

The following error metrics are used to evaluate the forecasting methods' performance. The first error metric is the Mean Absolute Error (MAE). This error metric depicts the deviation of the forecast from the real value as an absolute difference. This figure is useful to understand the accuracy of the forecast method. The error metric is expressed in Equation 3.2 in the forecasted unit.

The second selected metric is the mean absolute percentage error (MAPE). This error metric divides the absolute deviation by the real value. The error metric is expressed in Equation 3.3 as a percentage and is useful for understanding the impact of the error in further energy strategies.

The third selected metric is the mean absolute daily percentage error (MADPE). This error metric divides the absolute deviation by the real value of the day. The error metric is expressed in Equation 3.4 as a percentage and is useful to understand the impact of the error for forecasts where the values may be close to zero at some point, which may also be the case for solar generation.

In Equations MAE, MAPE, and MADPE $V_r(i)$ is the real value, and $V_f(i)$ is the forecasted value.

$$MAE = |V_r(i) - V_f(i)| \tag{3.2}$$

$$MAPE = \frac{|V_r(i) - V_f(i)|}{V_r(i)} \tag{3.3}$$

$$MADPE = \frac{\sum_{i=1}^{24} |V_r(i) - V_f(i)|}{\sum_{i=1}^{24} V_r(i)} \tag{3.4}$$

Chapter 4

Energy Management System

4.1 The Parc Bit Power Plant

The case study presented in this document is the Parc Bit power plant that is in the city of Palma of Majorca, Spain. The power plant provides heating and cooling through a DHC to the UIB and Parc Bit, the Balearic Islands Innovation Park. The district network was built in 2000 and connected the tri-generation plant to Parc Bit office buildings using three branches. In 2002, the network was extended by connecting another branch to the university facilities, including the student house and the sports centre. Currently, the network provides heating and cooling to 26 different customers. For district networks located in Mediterranean climates such as Spain, the cooling demand may be as important as the heating demand.

The whole network comprises four branches of pre-isolated steel pipes. Each branch has two pairs of pipes: flow and return for heating and cooling. The total length in a single direction of the DHC is 4.6km. A noteworthy feature of this district network is that some of the branches provide simultaneous heating and cooling to certain users. Nevertheless, most of the users are seasonal users that have heating demand in winter and cooling demand in summer. Moreover, according to the customers' energy profile, they can be split into three categories: office buildings, educational, and specific usage (residential, swimming pool, and IT room). These profiles are also differentiable between workdays and weekends.

The power plant that generates the thermal energy to cover the demand is placed at the beginning of the branches and is run by SAMPOL. This power

Table 4.1: Generators installed in Parc Bit

Generator	**Technology**	**Installed figure**
CHP Engine (2)	Diesel	2x1.36MW_e
Solar Collectors	Flat plate	864m^2
Biomass	Wood chip	1MW_h
Burner (2)	Diesel	$1.2 + 0.8MW_h$
Absorption (2)	Single. Li-Br	$1.32 + 0.43MW_c$
Electric Chiller	Compressor	1.2MW_c
Electric Chiller	Screw	1.3MW_c
Cooling Tower	Open	80kg/s
Dry cooler	-	118kg/s
Heating storage	Water	200m^3
Cooling storage	Water	200m^3

plant is composed of 2 CHP engines of 1.36MW, 700kW of solar collectors, 1MW of biomass, two diesel burners of 2MW total on the heating side, and two absorption chillers of 2MW total and two electric chillers of 2.5MW total on the cooling side.

The main figures of the installed machines are depicted in Table 4.1. Figure 4.1 depicts the schema of the power plant and the connection between the generators.

The heated or cooled water to be pumped to the branches is taken from water storage tanks that are used as energy buffers. There are four tanks of 100m^3; two for cooling and two for heating. The thermal energy generation from the power plant is delivered to an equilibrium collector and then straight to the tanks. The return flow is directed to the generation plant to be heated again. The power plant provides heated water at a maximum temperature of 95°C, and the return temperature is fixed at 65°C. For the chilled water, the minimum supply temperature is 6°C, and the return is fixed at 12°C. Both the returns have fixed temperatures due a load side design, which is achieved through a variable flow pump in the pumping station. The flow that moves through the network is pumped with pumps which usually are equipped with a variable frequency drives (VFD). The energy consumed by the pump is then considered linear with the movement of the flow.

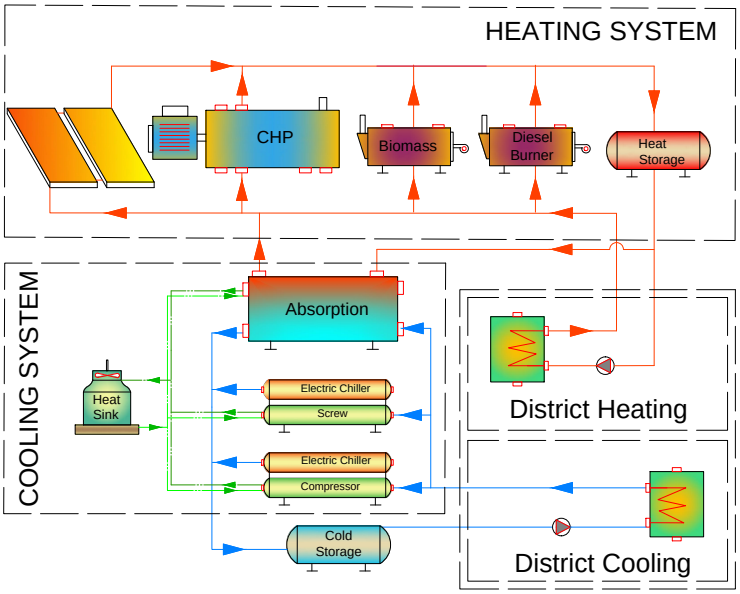

Figure 4.1: Parc Bit power plant configuration

4.1.1 Heating Generators

In this section, the technical characteristics and features of the machines are briefly described to enhance understanding of the power plant and its generation's configuration. The Parc Bit's heating system provides heating power to a local district heating network in the form of hot water. Usually, the supply temperature to the customer is 90°C, and the return temperature is 60°C. The heating generators also provide heating power to the absorption chillers installed on the power plant as forms of input power.

4.1.1.1 Combined Heat and Power

The CHP engines are supplied with diesel and provide electricity and heating power in the form of high-enthalpy water, low-enthalpy water, and exhaust gases. In this case, the electric production is subsidised by the Spanish government, and the generators receive an extra benefit per MWh generated,

Table 4.2: CHP parametrization

Load	Consumption	HT	LT	WHB	Ele
104%	$3,461$kW	568kW$_{\mathrm{t}}$	235kW$_{\mathrm{t}}$	674kW$_{\mathrm{t}}$	$1,460$kW$_{\mathrm{e}}$
78%	$2,622$kW	459kW$_{\mathrm{t}}$	127kW$_{\mathrm{t}}$	509kW$_{\mathrm{t}}$	$1,095$kW$_{\mathrm{e}}$
42%	$1,525$kW	298kW$_{\mathrm{t}}$	27kW$_{\mathrm{t}}$	296kW$_{\mathrm{t}}$	590kW$_{\mathrm{e}}$

which will always be fed into the grid. The electricity has dispatch priority over other technologies not considered to be renewable. This extra operation revenue is provided by the generated MWh$_{\mathrm{e}}$ and is added on top of the benefits of the wholesale price. As a condition to receive the governmental subsidy for generation, the CHP engine must achieve a thermal-electric performance of 55% as measured yearly [111]. The CHP generation is constrained by its performance. However, its performance is not constrained by the consumption of primary fuel.

The thermal energy generation comes from three different sources and is represented in Figure 4.2:

- CHP high temperature (HT) circuit that has an output temperature of approximately 90°C, coming from the engine jacket water.
- CHP low temperature (LT) circuit that has an output temperature of approximately 50°C, coming from the lubricant oil and charge air cooling.
- Co-generated energy coming from exhaust gases. The temperature of the exhaust gases at the CHP is 464°C. After passing through the waste heat boiler (WHB), the temperature that is released to the atmosphere is 196°C. The temperature should not be lower to avoid corrosion problems at the boiler.

In this case, the low temperature circuit cannot be harvested for any need, and the energy is wasted because it is cooled down by dry coolers. According to the operational data retrieved from the power plant, the amount of energy converted from primary energy in each circuit is depicted in Table 4.2.

The generation of energy using the CHP entitles a cost per O&M. This cost is related to the amount of energy generated and is usually expressed in terms of MWh$_{\mathrm{e}}$. The consumption of primary energy in the CHP engine is depicted in Table 4.2 in kW. The primary energy comes from diesel, and its

economic cost can be calculated with the low heating value of energy, density, and price per unit of volume.

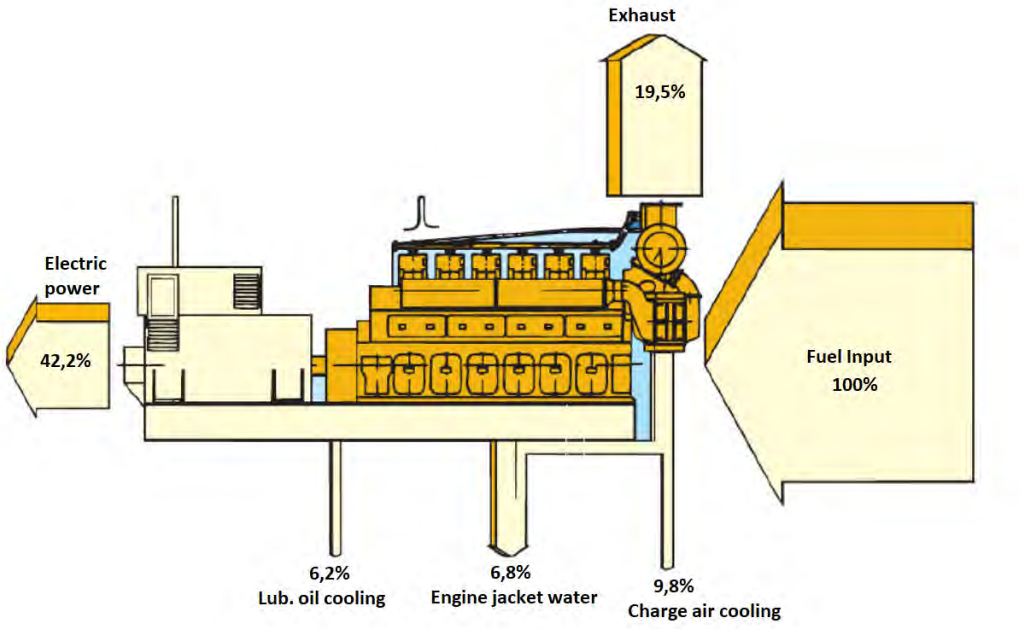

Figure 4.2: Engine Sankey diagram

4.1.1.2 Solar Collector Field

The solar collector field in the power plant is composed of 864m^2 of Arcon Solvarme HT Solar collector that is distributed in nine rows and directly installed on the ground in concrete slabs. The tilt angle of the collector field is a south-oriented 30° and therefore provides for greater generation during the summer period. The total area used by the collector field is $1,900$m^2, and the distance between the rows is 4m. The fluid running inside the collectors is a mixture of water-glycol in $60\% - 40\%$ proportions. The cost of O&M per MW_t generated in the collector field is 1€.

Table 4.3 depicts the efficiency figures used in Equation 4.19, which are according to the European Standard EN12975 and have been rated for the collector at the Technical University of Denmark's testing facilities in 1993.

$$P_{sh} = A(\eta_0 G - a_1(T_c - T_a) - a_2(T_c - T_a)^2) \tag{4.1}$$

Table 4.3: Solar Collector Field

Parameter	**Value**	**Unit**
Exterior Area	864	m^2
Interior Area	800	m^2
η_0	0.78	-
a_1	3.5	W/m^2K
a_2	0.02	W/m^2K^2

However, collector efficiency nowadays is expected to be much lower due to aging, technical problems, and damages that arise from stagnation and operation at high temperatures.

The collector field has two connection options, depending on whether demand for heating or cooling is greater:

- Summer configuration, which directly feeds the absorption chillers and is depicted in purple in Figure 4.1, or
- Winter configuration, to the equilibrium collector, which is connected to the heating energy buffer and is depicted in orange in Figure 4.1.

Currently, the information on generation is not retrieved from the field. The solar collector field was never connected during the duration of this PhD research because it was decommissioned due to leakage problems. Data from previous years was used in the studies. During this research, studies were carried out to study the viability of fixing the field and to acquire a new solar collector field; neither option was economically viable.

4.1.1.3 Diesel Burner

The diesel burner was installed in the original generation plant. The nominal power of generation is $2,000\text{kW}_\text{t}$ that is divided in two steps of $1,200\text{kW}_\text{t}$ and 800kW_t. The burner generates thermal energy by using diesel as fuel and provides an efficiency of 92% at nominal load. The cost of O&M in the boiler is 1€per MW_t generated. During nominal generation, the burner can increase by ΔT that is not greater than 20°C, where 65°C is the minimum return temperature to avoid corrosion problems. The burner's minimum technical fumes exit temperature is 140°C.

4.1.1.4 Biomass burner

The biomass burner was installed in Parc Bit in 2013 as a renewable support or heating generation. This installation was made as an enlargement of the heating generation side to fulfil customer demand. The burner's nominal power of generation is $1,000\text{kW}_\text{t}$ and burns wood-chips as fuel. The efficiency of this boiler reaches 90% on nominal generation. The cost of O&M in the boiler is 3€per MW_t generated. In nominal generation, the burner can increase ΔT up to 15°C, where 60°C is the minimum return temperature.

4.1.2 Cooling generators

The Parc Bit power plant is providing cooling power to a local network. Usually, the supply temperature is 7°C, and the return temperature is 12°C. Cooling power is provided by two types of technologies: electric chillers and absorption chillers. The electric chiller's input energy is supplied either by the electric grid or by the local CHP, while the absorption input energy come from the heat produced in the power plant by the CHP, boilers, or solar collector field.

The coefficient of performance (COP) of the cooling generators varies with the load they work at, the temperature of the cooling output, the temperature of return from the cooling tower [112, 113], and in absorption chillers the temperature of the heating source. The effect of partial loads on the nominal COP of the generator is depicted in Figure 4.3. Nominal COP is achieved at 100% load, nevertheless, the COP can be higher than the nominal at partial loads.

The usual temperature of the cooling energy output provided by the chillers is 7°C, and the input temperature into the absorption is usually 12°C. The influences of the cooling output temperatures and its ΔT are depicted in Figure 4.4.

4.1.2.1 Absorption chillers

The power plant generates cooling energy through absorption chillers. Both chillers are single stage and uses as refrigerant lithium bromide (Li-Br). The rated COP at design temperatures is 0.62 for the 1.32MW_c chiller and 0.64 for the 0.43MW_c chiller. The thermal energy input is provided by the thermal generators at the power plant. The rated temperature arriving from the hot

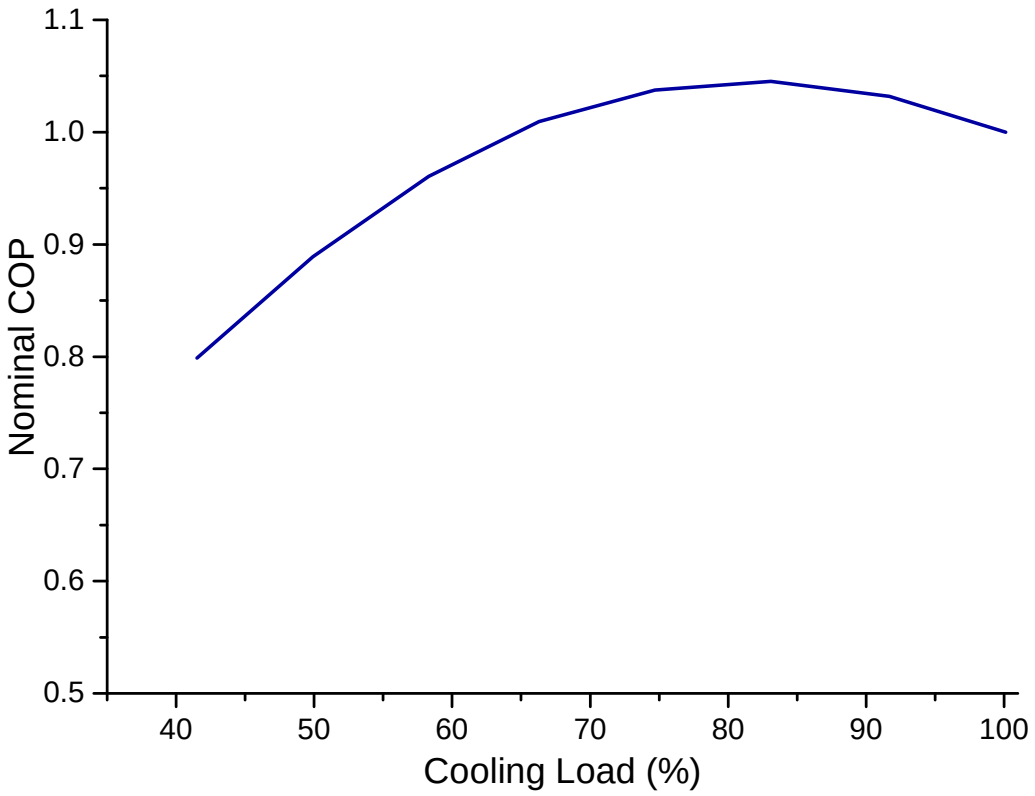

Figure 4.3: Influence on cooling capacity of partial loads

source is 90°C, and the return temperature is 85°C. The influences of the thermal energy input temperatures and its ΔT are depicted in Figure 4.5.

Both the absorption chillers are connected to the same cooling tower for condensation; the temperature entering to the tower is around 35°C from both absorptions, and the return should be 29°C or lower.

4.1.2.2 Electric Chillers

Part of the cooling generation is provided by the two auxiliary electric chillers. Therefore, cooling generation does not depend solely on the absorption chillers. One of the electric chillers uses screw technology and is connected to the cooling tower to meet condensing requirements. The cooling tower is shared with the absorption chillers. The other electric chiller uses compressor technology and condenses in a dry cooler. The screw electric chiller nominal power is

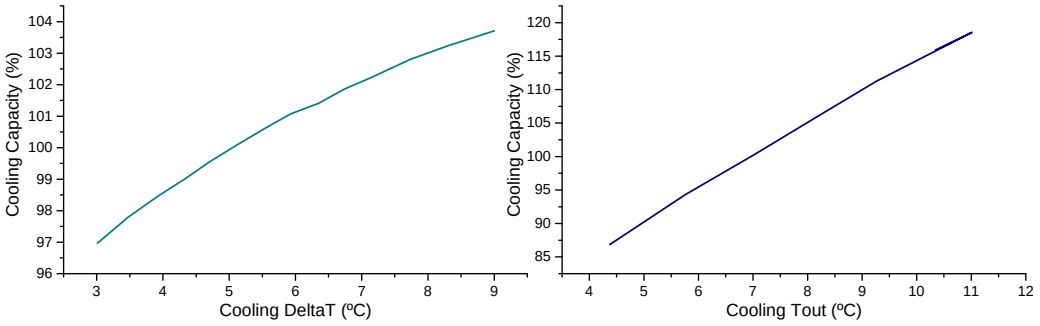

Figure 4.4: Influence on cooling capacity of cooling temperature

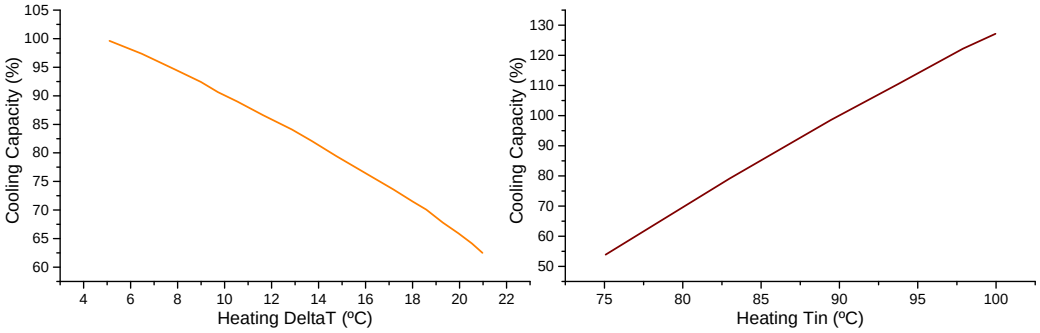

Figure 4.5: Influence on cooling capacity of heating circuit temperatures

$1,297\text{kW}_\text{c}$, the usual temperature of the cooling energy output is 6°C, and the input temperature is usually 12°C. The COP of the machines also varies with the load. The rated COP at design temperatures is 4.17. The condensing temperature that enters the tower from the chiller is 35°C, and the return should be 29°C for the best performance.

The compressor electric chiller's nominal power is $1,170\text{kW}_\text{c}$, the usual temperature of the cooling energy output is 6°C, and the input temperature is usually 12°C. The COP of the machines also varies with the load. The rated COP at design temperatures is 3.08.

The compressor electric chiller is connected to the dry cooler, where the temperature entering the cooler is 32°C and. For the best performance, the return should be at 22°C.

4.1.3 Condensing Dissipators

Cooling demand in buildings is directly related to ambient conditions, particularly to ambient temperature and relative humidity. These two variables directly influence the calculation of the condensing capacity in cooling towers since they influence the air's enthalpy that enters the refrigeration system. In the case of dry coolers, only the ambient temperature influences their condensing capacity. Ergo, cooling demand and condensing capacity are inversely related. This might lead to a problem when generating cooling energy at the power plant.

In the hybrid polygeneration power plant configuration that has been proposed as a problem to solve in this thesis, both cooling generators are connected to the same condensing node and thus the same heat sink. It is assumed that the water temperature from the cooling generators entering and exiting the condensing dissipators are equal and fixed. The water temperature that is exiting the cooling tower regulates the fans that provide the air stream through the tower.

For some environmental conditions, the cooling demand leads to condensing power that is larger than the maximum defined for the condenser in the Equation 4.2.

When this happens, the cooling demand is not satisfied, and the user's needs are not meet.

$$P_{cn} = \dot{G}_s \left(H_2 - H_1\right) \tag{4.2}$$

where G_s is the maximum air flow that can be forced through the tower or dry cooler and is defined by the rated power of the fans and design parameters such as height, and air filters. H_1 and H_2 are the entering and exiting enthalpies of the air in the cooler. To ensure heat transfer along the cooling tower, the exiting bulk liquid temperature must have a temperature difference that is greater than 2.8°C with an entering air wet bulb temperature according to [114]. Otherwise, the exiting bulk liquid temperature will be of higher temperature than desired. In a cooling tower, there is an efficiency drop because the exiting bulk liquid temperature is seldom more than 0.3K above the exiting air stream temperature, which can be assumed to be saturated for calculation purposes [115].

The temperature that enters the tower is 33°C and the return should be 29°C. If the return temperature is higher than the 29°C that is fixed as the set point, the efficiency of the chiller will drop. On the other hand, the return

temperature cannot be lower than 20°C to avoid crystallisation problems on the absorption solution. The influence in cooling capacity of cooling tower's return temperature to chiller is depicted in Figure 4.6.

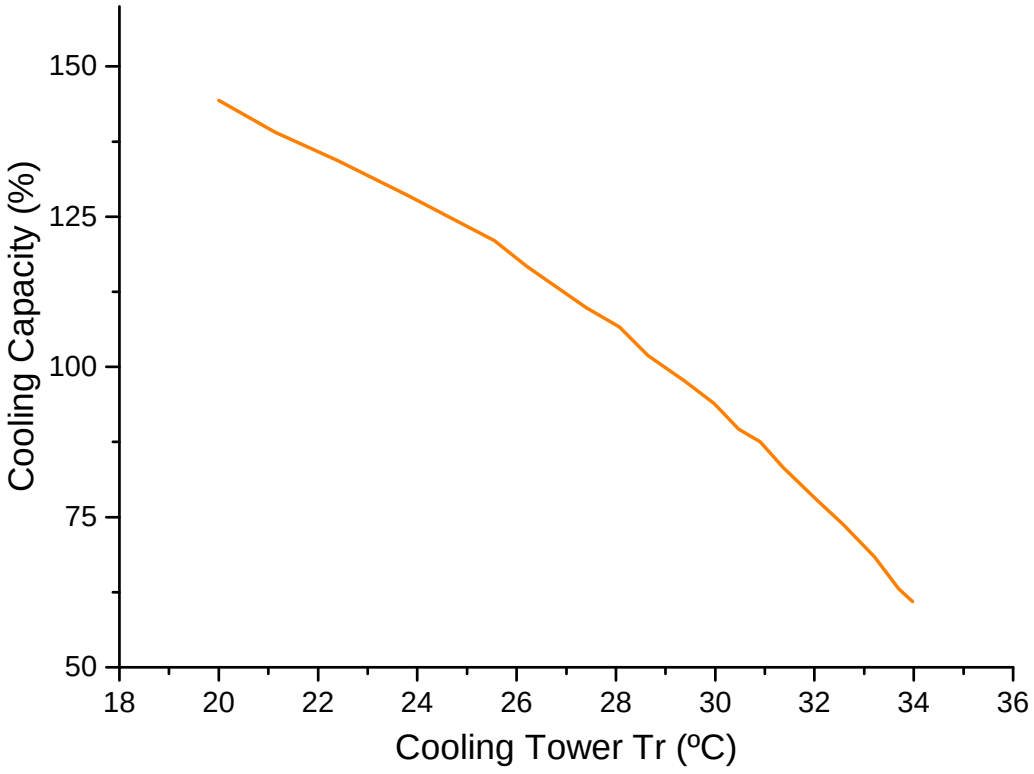

Figure 4.6: Influence on cooling capacity of condensing return temperature

4.1.3.1 Cooling tower

The cooling tower is designed to dissipate the condensing energy requirements from the absorption chillers and the electric chiller. The cooling tower is open, which means that the condenser water is sprayed counter-flow with the forced air from the ventilators at the tower; the water is recovered in a tray at the bottom of the tower. The cooling tower comprises three modules of fans that each have an electrical power of 16.5kW$_e$ and a total electrical power of 49.5kW$_e$. The mass flow of air (G_s) that can move through the tower is 315kg/s. The refrigeration occurs due to an exchange of enthalpy

between the condenser water and the surrounding air, which is carried out through an increase of the temperature and humidity in the incoming air. It is generally accepted that the relative humidity of the air exiting from the cooling tower is equal to 100%.

4.1.3.2 Dry cooler

The dry cooler is designed to dissipate the condensing energy requirements from the electric chiller. The refrigeration occurs due to an exchange of enthalpy between the condenser water and the surrounding air. This exchange is carried out only through an increase of temperature in the incoming air since the relative humidity along the dry cooler does not vary. The dry cooler comprises six fans that each have an electrical power of 7.5kW$_e$, or 45kW$_e$ in total. The mass flow of air that can be moved through the dry cooler is 118kg/s.

4.1.4 Storage

The power plant at Parc Bit also includes energy storage. This energy is stored as hot water for heating and cold water for cooling. All the energy generators inject their energy productions into the tanks and from there the load is flown to the customer. Therefore, the tanks are also energy buffers.

Table 4.1 states that there is 200m^3 of water for heating and cooling. This volume of water is separated into two water tanks. Consequently, there are four identical tanks of 100m^3 each that are installed at the generation site. The tanks are cylindrical; horizontally oriented; and have a total length of 14m, a diameter of 3m, and a thickness of 12mm. The insulation material that covers the surface is rock wool and has a thickness of 40mm. The tanks may not be effectively stratified because there is no system to help the phenomena and the tanks are installed horizontally. This is the reason why the tanks are considered to be more of energy buffers than energy storage. The maximum amount of energy stored in the tanks can be calculated using Equation 4.3 and the minimum supply temperature and normal generation values expressed in Table 4.4. The heat loss can be estimated with the help of the work presented in [116].

$$E_{stored} = \rho_w V_{stored} c_{pw} (T_g - T_f) \tag{4.3}$$

Table 4.4: Storage installed in Parc Bit

Type	Volume	Generation T.	Supply T.	Return T.	Energy
Heating	200m^3	89°C	75°C	60°C	$3,248\text{kWh}_\text{t}$
Cooling	200m^3	6°C	8.5°C	12°C	580kWh_c

4.1.5 District Heating and Cooling Network

The DHC under analysis in this study has branched topology and provides heating and cooling to the UIB and Parc Bit. The whole network comprises of four branches of pre-insulated steel pipes. Each branch has two pairs of pipes: supply and return for heating and cooling. The total length of a single direction of the DHC is 4.6km. A noteworthy feature of this district network is that some of the branches provide simultaneous heating and cooling to certain users [21, 117]. The effective peak power of the network is 4.4MW_h for heating and 2.5MW_c for cooling. The annual energy consumption of the network is $4,800\text{MWh}_\text{h}$ for heating and $2,500\text{MWh}_\text{c}$ for cooling. Heat loss represents 29% of the annual supplied energy. A map of the DHC can be seen in Figure 4.7.

Figure 4.7: DHC network's birds-eye outline

4.1.5.1 Pumping

Pumping optimisation at the power plant is achieved using VFD. The VFD linearly adjusts the electric pump consumption with the flow. Figure 4.8 depicts the power-flow relation of the pumps installed in the DHC. As mentioned, the DHC is comprised of four branches. Therefore, four pump sets for heating and four pump sets for cooling are used. For the sake of simplification, this thesis considers the regime where the pump works as having a linear relation with flow-power, and the sets of pumps are summed up in an equivalent pump. The equivalent pump constant is described in Equation 4.4 for heating and Equation 4.5 for cooling. The flow and electric power depicted in the equations are the aggregation of the working pumps at the branches.

$$k_{eleH} = \frac{P_{ele,p}}{\dot{m}} = \frac{64.5kW_e}{660m^3/h} \tag{4.4}$$

$$k_{eleC} = \frac{P_{ele,p}}{\dot{m}} = \frac{243kW_e}{1805m^3/h} \tag{4.5}$$

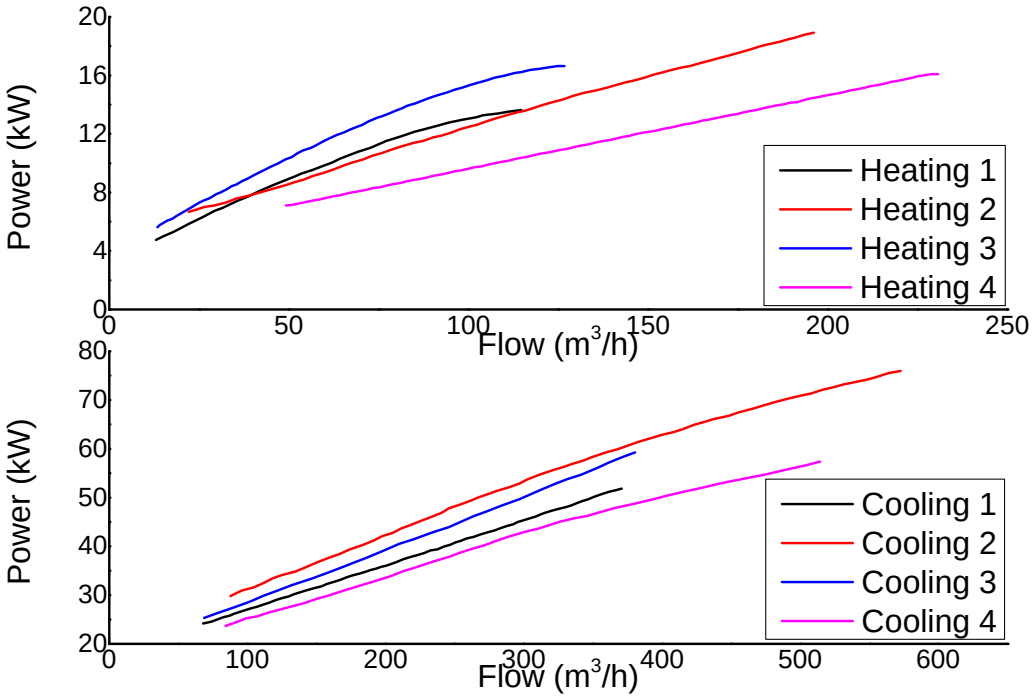

Figure 4.8: DHC pumping power and flow

4.1.5.2 Network Description

This section describes the values used in calculations regarding the network. The pipes' diameters in the DHC range from 33 to 193mm in heating and from 90 to 280mm in cooling. The pipes are pre-insulated with a carbon steel core of 8mm thickness. The insulation used is expanded polystyrene with an assumed thermal conductivity of 0.033W/mK, since the heat conductivity coefficient of the insulation increases with aging [35]. The insulation thickness varies between 13 and 106mm in heating and between 17 and 112mm in cooling. The depth to which the pipes are buried is assumed to be 1.5m for the whole network, and the considered distance between centre of pipes is 0.5m. The total volume of water in the pipes is 127m^3 for heating and 296m^3 for cooling.

Table 4.5: DHC design temperatures

Temperatures	**Heating**	**Cooling**
Tf_{max}	89°C	8.5°C
Tf_{min}	75°C	6°C
Tf_{common}	86°C	6°C
Tr	65°C	12°C

In the DHC supply, temperatures are subject to modifications, but return is fixed by design. Table 4.5 depicts the maximum, minimum, and commonly used supply and return temperatures. These values are determined by the design of the DHC and its customers. For the sake of simplification, the average pipe temperature is considered for the whole length of the network pipe.

4.1.5.3 Heat Losses

Thermal energy losses in the distribution network are identified as heat transference from the pipes to the soil. In the DHC networks, thermal transference is dependent on the temperature difference between the soil and the pipes. Therefore, a lower temperature difference leads to lower heat loss. Similarly, the thermal conductivity of the materials enveloping the heat source and heat sink plays an important role in heat loss calculation. Generally, the main factors that affect heat losses are as follows:

- Pipe insulation
- Pipe cross-section
- Length of pipes
- Distance between pipes
- Depth at which pipe is buried
- Thermal conductivity of the soil
- Soil temperature

The ground surrounding the network is not in a thermally stable state, although steady-state conditions have usually been assumed in the literature. It is important to notice that the heat loss in a DC network produces increases of temperature of the fluid in the pipe. Thermal losses can be easily calculated using the approximate steady-state method that is explained in [118, 119] and summarised in Equation 4.6. This method is used to calculate heat loss for a pair of pipes (supply and return) considering the topology of the network, its construction, and soil properties. From the district network's description, an overall heat transfer coefficient or U value is calculated. This value depends on variables that are fixed by design in a district network. An extensive explanation of the formulas used to calculate the heat loss in a pipe pair are explained in Annex A.

$$\phi_s + \phi_r = 2U \left(\frac{T_f + T_r}{2} - T_{soil} \right) \tag{4.6}$$

If the simplified method is used that considers a calculated soil temperature T_{soil} and a return temperature T_r that is fixed by design, then the only variable that influences the heat loss is the supply temperature Ts because all the other values can be considered fixed. In the case of DH, the greater the T_f, the greater the heat loss in distribution. On the other hand, in DC, the lower the T_f, the greater the heat losses. Therefore, for a given case of pipes or network with a known U value, the heat loss can be formulated as per Equation 4.7:

$$\phi = \phi_f + \phi_r = k_\phi T_f + \phi_r \tag{4.7}$$

Soil Temperature Soil temperature is an important factor for calculating heat loss as it is necessary to calculate the thermal difference to DHC pipes. This temperature is dependent on the depth and the ambient temperature. Simplified models are generally used to calculate soil temperature [36, 120]. The proposed model in [36] describes the annual variation of the daily average soil temperature at different depths as a sinusoidal function. The model assumes that at an infinite depth, the soil temperature is constant and equal to the annual average ambient temperature. The expression that calculates the mean daily temperature at a given depth is presented in Equation 4.8.

$$T_{soil}(z,t) = T_a + A_0 e^{-z/d} sin \left[\frac{2\pi(t - t_0)}{365} - \frac{z}{d} - \frac{\pi}{2} \right] \tag{4.8}$$

where $T_{soil}(z,t)$ is the soil temperature at time t in days and depth z in metres, Ta is the average ambient temperature difference in °C, A_0 is the annual amplitude of the surface soil temperature in °C, t_0 is the time lag in days from an arbitrary starting date to the occurrence of the minimum temperature in a year, and d is the damping depth defined in [36]. According to [121], the model must be corrected when using air temperatures. The model proposed by [36] consistently underestimates by about 2°C when using air temperatures instead of measured soil surface temperatures.

The presented model calculates the soil temperature at a given depth, day, and set of soil characteristics. The model does not consider hourly temperature variations which may be considered negligible at the depth considered [37]. The model only estimates the soil temperature based on ambient parameters and does not consider the possible influence of the DHC pipes on operation. The soil heat conductivity coefficient λ_s of the surrounding soil is difficult to estimate due to inhomogeneous and partly unknown soil composition and moisture content. This coefficient ranges between 0.5W/mK in the case of dry sand to 2.5W/mK. In this case the value is 1.3W/mK [31].

Soil temperature is calculated using the soil temperature model expressed in Equation 4.8, the parameters expressed in this section, and the climatic conditions from the DHC site. Figure 4.9 depicts the temperatures at different depths.

Table 4.6: Heat loss parameters for DHC

Case	k_ϕ	**Winter** ϕ_r	**Spring** ϕ_r	**Summer** ϕ_r	**Autumn** ϕ_r
Heating	1.379	54.608	40.019	19.940	33.096
Cooling	-1.459	19.557	34.998	56.247	42.324
Soil temperature	-	12.7°C	18.0°C	25.3°C	20.5°C
Number of day	-	24	115	205	293

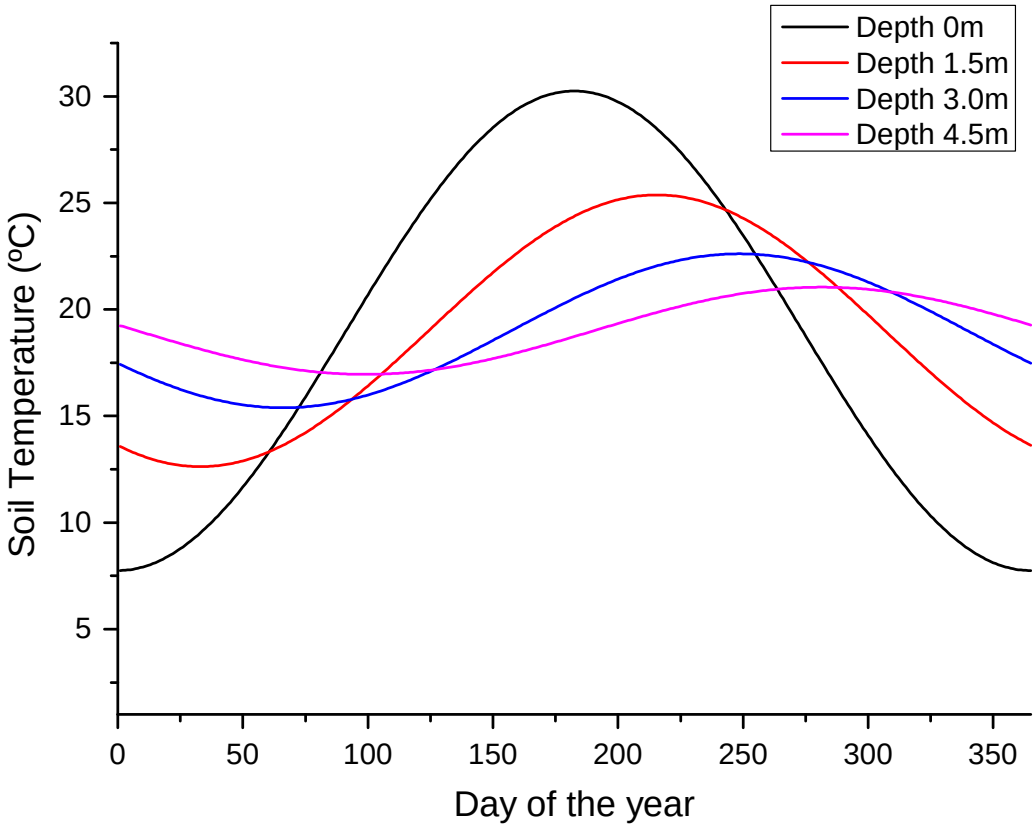

Figure 4.9: Soil temperatures at different depths

Heat loss from the DHC is calculated using the assumptions and information presented. The results expressed according to Equation 4.7 are presented in Table 4.6.

4.1.5.4 DHC Thermal Mass

The usage of a district network to carry the energy from the generation point to the consumption point implies a large amount of water inside the distribution pipes. This in turn implies that there is a significant amount of energy stored within the network that works as passive storage and inertia.

Usually, due to the covered extension and the total pipe length, the network has a significant thermal mass and thus response time to changes. The thermal mass in a DHC comes from fluid that carries the energy, pipe, and soil. This section quantifies the thermal mass of a DHC is quantified and studies the DHC's usage as active storage. The energy stored in a branched DHC thermal mass is considered invariable for fixed temperatures of supply and return. Therefore, it is unprofitable as active storage. On the other hand, when these temperatures are variable, the energy stored in the thermal mass can be profitable as active storage. Nevertheless, when return temperature T_r is considered fixed by the user's substation and by all the users in a district network, the only variable in the equation is the supply temperature T_f. The supply temperature can be managed from the generation site by either providing energy at a variable temperature or by using a three-way valve and mixing the return water with the water from the generation.

In cases where T_r is invariant, the energy stored in the thermal mass of the DHC is referred to the supply only. As T_f is considered variable within some boundaries, this means that the energy stored in the thermal mass on the distribution network varies and should be considered in energy simulations. The supply temperature has higher and lower boundaries; the higher boundary is delimited by the maximum temperature the power plant is able to generate, and the lower boundary is determined by the district network's most restraining user requirement. Therefore, the energy stored in the thermal mass is calculated in accordance with the range of temperatures considered. In this case, such temperatures only refer to T_f. When thermal mass is considered, the variable is included in Equation 4.9 at the n_{th}hour.

$$\begin{aligned} EG_{(n)} =& U_{h(n)} + \phi_{(n)} + (E_{TM(n)} - E_{TM(n-1)}) \\ =& U_{h(n)} + \phi_{(n)} + TM(T_{f,(n)} - T_{f,(n-1)}) \end{aligned} \tag{4.9}$$

The thermal mass of a DHC can be calculated considering the individual thermal mass of fluid and pipe.

Soil thermal mass is not considered when calculating the total thermal mass of the DHC. The energy accumulated in the soil is not suitable to be

used as active storage due its lower temperature than the supply and the low heat transference back to the pipe through pipe's insulation [116].

Fluid Thermal Mass The thermal mass of fluid refers to the capacity of passively stored energy in the fluid (usually water) inside the DHC. As the return is not considered, the amount of thermal fluid to consider as active storage depends on the half volume of fluid inside the DHC network. The thermal mass of supply can be calculated as per Equation 4.10.

$$TM_f = c_p \rho V = c_{pw} \rho_w \frac{V_{DHC}}{2} \tag{4.10}$$

where V_{DHC} is the volume of fluid on the distribution network, ρ_w is the density of the water, and c_{pw} is the specific heat capacity of water.

Pipe Thermal Mass The thermal mass of a pipe refers to the pipe's capacity to passively store energy in the material of the pipe that is in contact with the fluid. The temperature of the fluid is the same as the temperature of the material. The work by [47] has studied the delay for a metallic pipe to reach a steady state when modifying a temperature resulting 200s, which is negligible in hourly terms. The thermal mass of the pipe is calculated considering the material in the DHC pipes as depicted in Equation 4.11.

$$TM_p = c_p \rho V = c_{pm} \rho_m \frac{\pi L \left(D_{out}^2 - D_{in}^2\right)}{4} \tag{4.11}$$

where ρ_m is the density of the material, c_{pm} is the thermal capacity of the material, V is the total volume of material in the pipes, L is the length of the pipes, and D_{out} and D_{in} are the external and internal diameters of the pipe.

Using the same approach the thermal mass of pipe's insulation can be calculated. However, as the distance from the pipe within the insulation increases, the temperature decreases [116]. Therefore, the insulation cannot be considered as active storage because the supply temperature is always greater than the temperature in the insulation, and no heat is transferred to the fluid under any circumstances.

Table 4.7 presents the description of the network in terms of length and volume through the pipes. The inertia in the network can be stored in the flow and the return pipes by increasing the temperature for heating or decreasing for cooling. To achieve this, it is necessary to regulate the pumping

Table 4.7: DHC network pipe information

Branch	**Length**	**Volume**
Heating 1	1,103m	16.78m^3
Cooling 1	1,103m	44.67m^3
Heating 2	752m	22.79m^3
Cooling 2	752m	51.46m^3
Heating 3	1,002m	32.29m^3
Cooling 3	1,002m	69.18m^3
Heating 4	1,772m	55.54m^3
Cooling 4	1,772m	130.65m^3
Total Heating	4,629m	127.4m^3
Total Cooling	4,629m	295.9m^3

Table 4.8: Thermal mass calculation parameters

Energy	**Mass** [kg]	TM [kJ/K]	TM [%]
Water Heating	63,700	267,620	81.41%
Water Cooling	147,980	621,709	86.82%
Steel Heating	121,659	61,124	18.59%
Steel Cooling	187,848	94,378	13.18%

station in accordance with the temperatures instead of the differential pressure between flow and return.

The thermal mass of the DHC is calculated by considering the fluid in the pipes and the carbon steel core that is in contact with the fluid. The calculation of this mass considers the specific heat capacity of carbon steel c_{pm} to be 502.416J/kgK with a density ρ_m of $8,050$kg/m^3. The calculation considers the specific heat capacity of water c_{pw} to be $4,184$J/kgK with a density ρ_w of $1,000$kg/m^3. Table 4.8 depicts the main parameters and the thermal mass of carbon, steel, and water that are considered in this DHC.

4.1.6 Primary Energy Considerations

This section explains the boundaries and considerations that are involved in simulating the power plant. Four weeks are studied, one for each season. In the case of stored raw material, the prices and values are fixed for the whole optimisation period and will be kept invariable across the seasons. On the

other hand, energy demand and electricity prices vary on an hourly basis. The reported costs in this section are obtained from Sampol and the current market situation.

- CHP Diesel: Lower heating value 10.4kWh/l; Cost = 0.45 €/l.
- Boiler Diesel: Lower heating value 10.4kWh/l; Cost = 0.50 €/l.
- Biomass: Lower heating value 3.2kWh/kg; Cost = 0.22 €/kg.
- Energy generation subsidy: 100 €/MWh_e.
- Water cost: 3 €/m^3.
- Solar power: Free O&M cost.
- Electricity: Purchasing and selling values are depicted in Figure 4.10.
- Thermal demand: Heating and cooling demand are depicted in Figure 4.10.

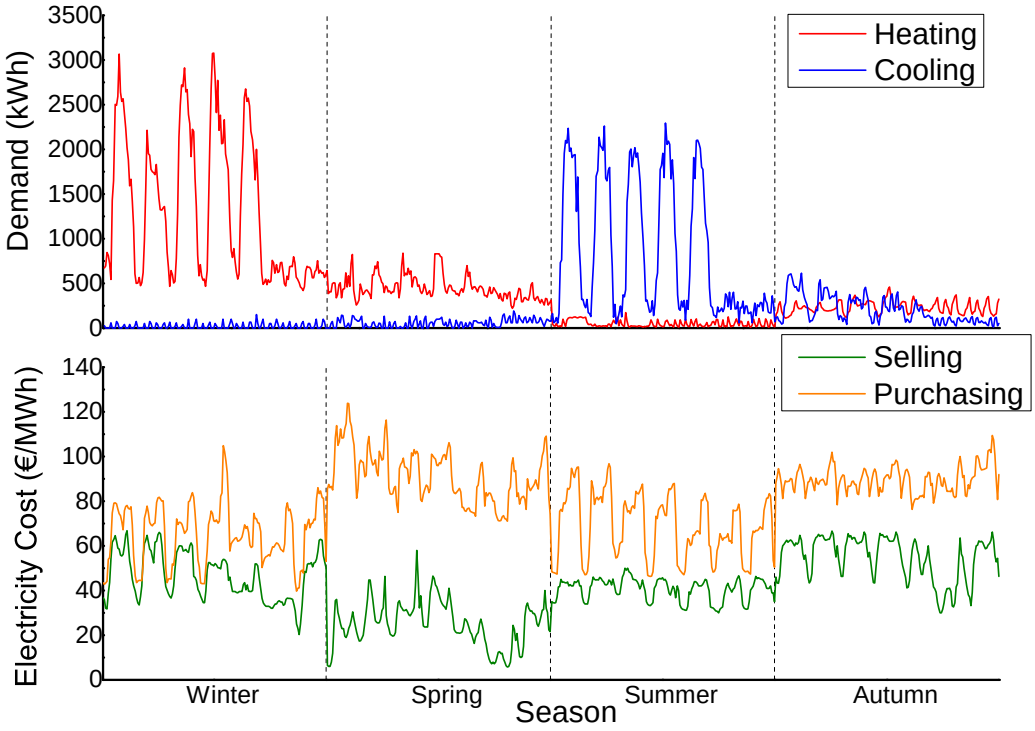

Figure 4.10: Electricity price and thermal demand variation

4.2 MILP Formulation

4.2.1 Power Plant

The aim of an EMS is to create generation strategies for complex problems and to provide possible alternatives to unfeasible solutions for the energy manager, thereby broadening the view of energy operation management. When optimising the power plant, climatic information should be taken into consideration, especially if the heat sink or energy generators depend on the climate. This chapter contributes to the field of energy optimisation by presenting a case study of the developed EMS, which solves real operational problems. Figure 4.11 presents a node distribution of the pilot power plan.

In this section, the technical characteristics of the generators that form the power plant are translated into linear equations. These features and boundaries are introduced in the optimiser as constitutive equations.

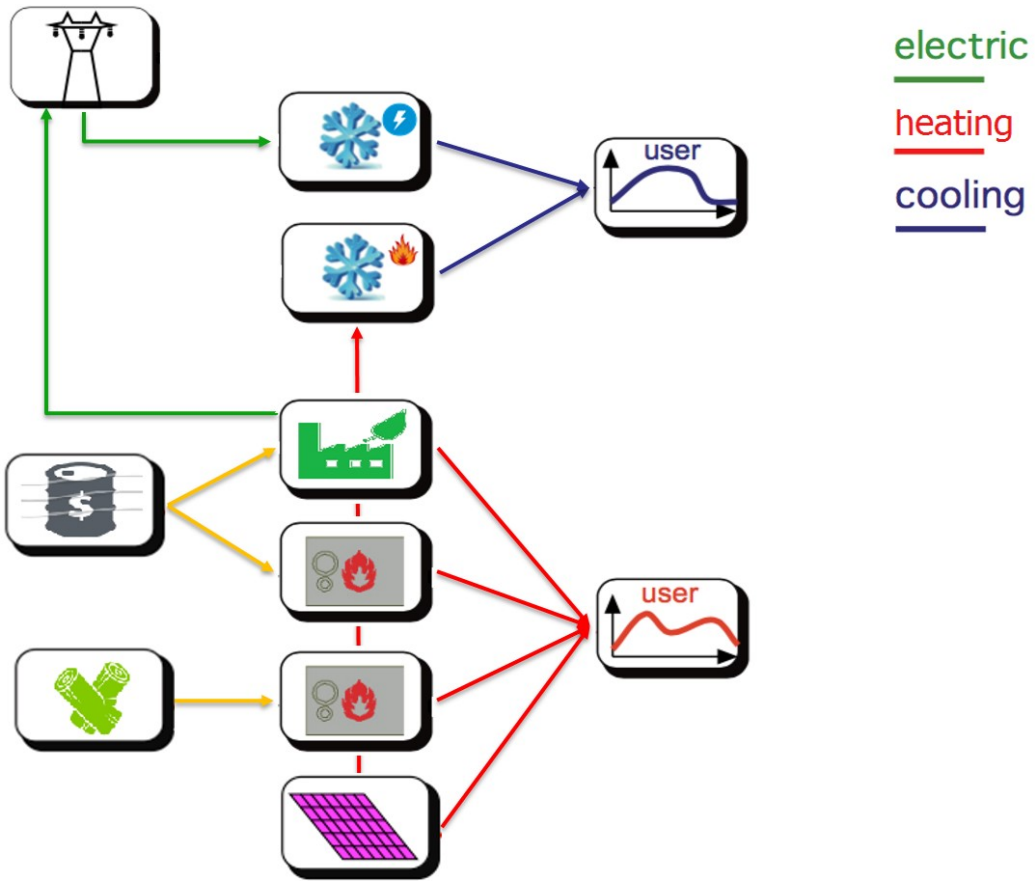

Figure 4.11: Parc Bit Power plant's node distribution

4.2.2 Heating Node

In the heating node, the generation side balances out the loads from the consumers and the energy used by the absorption chillers. It is assumed that the hot water output is generated under acceptable premises of temperature and flow to be harvested in either load or absorption. In this EMS, the following heat generators are modelled:

4.2.2.1 Combined Heat and Power

The main aspect to be modelled in a CHP generator is the relationship between electricity E_e, and thermal E_h energy generated, and its input power

E_{IN}. This characteristic is expressed by the following equations:

$$E_h(t_i) = k_0\delta(t_i) + k_1 E_e(t_i) \tag{4.12}$$

$$E_{IN}(t_i) = C_0\delta(t_i) + C_1 E_e(t_i) \tag{4.13}$$

where the coefficients k_1 and C_1 are constant or linearised using a piecewise linear approach. To do so, the working range is subdivided into intervals where those coefficients are constant. Using the therm C_0 the fuel unit cost decreases with the increase of electric power generation. To define the generator as on or off in a time interval, a binary variable $\delta(t_i)$ which is involved in the limits of operation is defined as follows:

$$\delta(t_i)E_{e_{min}} \leq E_e(t_i) \leq \delta(t_i)E_{e_{max}} \tag{4.14}$$

Therefore, the cost and benefits from a CHP engine are defined on basis of the energy generation, fuel consumption, and governmental benefits:

$$\sigma_{CHP} = \sum_{i=1}^{i} E_{IN}(t_i)\sigma_{diesel} + \delta_{CHP}E_e(t_i) \tag{4.15}$$

$$B_{CHP} = \sum_{i=1}^{i} E_h(t_i)\beta_t + (\beta_e(t_i) + \sigma_{OMIE}(t_i))E_e(t_i) \tag{4.16}$$

4.2.2.2 Boilers

The auxiliary boilers are supplied with a primary fuel, which can be either biomass or fossil fuel, and it provides heating in the form of hot water. The purpose is to generate heating to match the heating demand on the node. The relation between the fuel consumed and energy generated is explained in Equation 4.17, where E_h is the output from the boiler, η_B is the efficiency, and B_{IN} is the energy used by the boiler. In Equation 4.18, the cost of the boiler σ_B is introduced as the cost of the fuel per unit of fuel mass (σ_{bio}) times the fuel consumed added to the cost for O&M per unit (δ_B) times the boiler output.

$$E_h(t_i) = E_{IN}(t_i)\eta_B \tag{4.17}$$

$$\sigma_B(t_i) = E_{IN}(t_i)\sigma_{bio} + E_h(t_i)\delta_B \tag{4.18}$$

4.2.2.3 Solar Thermal

Solar resource is intermittent and uncontrollable. For practical reasons, the approach used in the EMS considers resource forecast to be ideal and without deviations from the real generation. This energy is added into the node in the form of heating generation. The energy is calculated using irradiation forecasts, and the energy produced by the collector field is calculated using the methodology explained in [70], which uses a model based on the steady state test of the European Standard EN12975.

$$P_{sh} = \left[\eta_0 G - a_1(T_f - T_a) - a_2(T_f - T_a)^2\right] S \tag{4.19}$$

4.2.3 Cooling Node

In the cooling node, cooling generators match the cooling demand. The cooling generators proposed in the EMS are absorption and electric chillers. Both options work analogously by means of simulation. The input energy E_{IN} is converted by the generator into cooling power through the efficiency or COP.

The different working points where the chiller can effectively generate cooling have different COPs. These efficiencies are represented using piecewise approximation. A practical constraint is fixed for chillers that are unable to generate if the load is lower than a percentage of its nominal power; such information can be retrieved from the data-sheet. Different loads correspond to different energy consumptions, and this relation is defined by Equation 4.20, where E_c is the cooling output, E_e is the input energy into the chiller, and COP_t is the efficiency at a given time.

$$E_c(t_i) = k_0\delta(t_i) + COP_t E_e(t_i) \tag{4.20}$$

In the case of the absorption chiller, the energy input is provided by the thermal generators at the power plant and is therefore considered to be part of the thermal demand at the heating node. For the electric chillers, the energy input is obtained from the power generators at the site or from the electric grid.

When a chiller is in operation, it generates excess heat that must be rejected. This excess heat is addressed as condensing power. The condensing power balances the thermodynamic state of the chiller and can be calculated as a sum of the generation E_c and the energy used E_{IN} (see Equation

4.21). The chiller absorbs energy from both E_c and E_{IN} because the cooling generation is a subtraction of energy from the energy carrier.

$$E_{cn}(t_i) = E_{IN}(t_i) + E_c(t_i) \tag{4.21}$$

The condensing requirements for the chiller to generate cooling energy are calculated with reference to the generated cooling power and the energy consumption of the generator. Therefore, taking Equation 4.21 and Equation 4.20 into account, the condensing requirements can be expressed in Equation 4.22:

$$E_{cn} = E_{c_t}\left(1 + \frac{1}{COP_t}\right) \tag{4.22}$$

The required condensing power is calculated as depicted in Equation 4.23. This power depends on the cooling power generated at the chillers and their COP.

$$E_{cn} = \sum_{i=1}^{i} E_{INi} + E_{ci} \tag{4.23}$$

Another source of cooling, the slack generator, is activated in case the demand is not matched and to keep the node balanced. This generator keeps the balance of the cooling node satisfied, but at a high cost of c_{ext}. This high cost is fixed to penalise the use of this peak module and thus should be avoided by the optimiser. The energy generated by this slack generator is defined as a shortage in cooling demand.

To solve such a problem, it is necessary to precisely calculate the power plant generators and their capacities when working under different environmental boundaries. To do so, technical specifications must considered and simulated together to find a techno-economical solution that allows the generator to fulfil the user's demands. To succeed in fulfilling the demand and finding the most optimal solution, it is necessary to retrieve information about the load, ambient temperature, and relative humidity for every time step. This information is fed into the optimiser to provide a solution that fulfills the user's request of energy, if possible.

4.2.4 Condensing Node

In the condensing node, a balance of energies is pursued between the heat sink and the cooling generator's condensing requirements. The concept of a heat sink refers to the element designed to dissipate excess heat. In this case, the element must fulfil the rejection requirements of the cooling generators, otherwise their generation capability is reduced. Equation 4.24 depicts the calculation of condensing power, where $\dot{m}$ is the mass flow of the fluid, H_{in} is the entering enthalpy, and H_{out} is the exiting enthalpy of the fluid.

$$E_{cn} = \dot{m}(H_{in} - H_{out}) \tag{4.24}$$

There are two kinds of heat sinks that are defined in the optimisation tool: geothermal systems and cooling towers or dry cooler.

4.2.4.1 Cooling Tower/Dry Cooler

The condensing capacity that is delivered from a condenser is constrained technical and environmentally. Technically, this capacity depends on the air stream moved by the fans through the machine; such air flow is limited by the fan system's power. Environmentally, the capacity depends on the entrance conditions of the air stream as the exiting enthalpy from the tower is fixed. Figure 4.12 depicts a schema of a cooling tower. The condensing power available on a tower is calculated as the air flow multiplied by the difference between entering and exiting enthalpies, as depicted in Equation 4.25.

$$E_{cn} = \dot{m}_G(H_{G,out} - H_{G,in}) \tag{4.25}$$

In the pre-processing phase, enthalpy calculation is made through a calculation routine based on the psychometric diagram of the air. The air conditions are also calculated with the routine. To calculate the enthalpies of the air exiting from the condenser, the following assumptions are made from the required values:

- Dry Cooler: Relative humidity (RH) = Entering RH
- Cooling tower: RH = 100%
- Exiting temperature = Condensing water temperature to chiller -0.3K

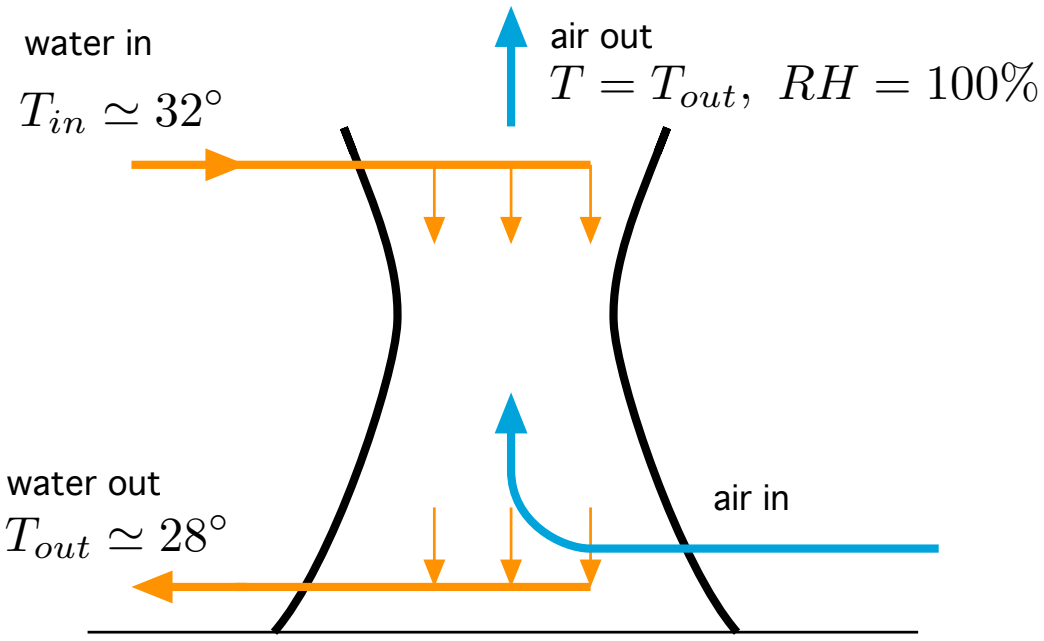

Figure 4.12: Schematic view of a cooling tower

The psychometric routine calculates the enthalpies using the following inputs:

- T_{db}: Dry bulb temperature
- RH: Relative Humidity
- Pa: Air pressure

From the component list, information is retrieved regarding the $T_{w_{in}}$ that the chiller is rated at and the desired $T_{w_{out}}$ for which the chiller provides the best performance. In principle, if more than one chiller uses the same condenser, the desired $T_{w_{out}}$ values should be the same.

The condenser type is modelled to understand how much electrical power and water is consumed to condense a certain amount of condensing power.

The electric consumption from the cooling tower comes from the fan, P_{efan}. The electrical power is proportional to the air flow, as expressed in Equation 4.26.

$$P_{efan} = k_{CT} G_s \tag{4.26}$$

The k_{CT} parameter can be calculated using the equipment information from the data-sheet, as expressed in Equation 4.27.

$$k_{CT} = \frac{\hat{P}_{efan}}{\hat{G}_s} \tag{4.27}$$

In one plant, the same cooling tower can be shared by several cooling modules so that the condensing power required by each machine must be summed up with the power required by the other machines . This interaction requires the definition of a condensing power vector and of a condensing power node where all machine requests are summed up.

4.2.4.2 Geothermal system

This work models a closed-loop geothermal system. It is assumed that the underground water has a constant temperature in the same way that the water returning from underground has a fixed temperature. The maximum temperature difference is set by the local government. Using these assumptions, the condensing power that can be delivered by the system is dependent on the mass flow of water pumped from underground and is expressed in Equation 4.28, which relates to the mass flow of water m and the difference of temperatures with the condensing capacity.

$$C_{cn} = \dot{m}_w c_p (T_{in} - T_{out}) \tag{4.28}$$

The electric consumption of the system comes directly from the pumping efforts and is estimated to be directly proportional. The relation is understood as an electric coefficient $kgeo$ and is depicted in Equation 4.29.

$$E_e = \dot{m}_w kgeo \tag{4.29}$$

4.2.5 Electric Node

In the electric node, the grid acts as an energy buffer that all the consumptions are taken from and all the generations are fed into. The proposed generators in this case are the CHP engines and as consumers there are electric chillers, pumps and generators self-consumption. In the electric node, it is possible to fix different prices for buying, selling, and by the hour.

4.2.6 Thermal Storage

Thermal storage retains excess energy generation when there is no demand for it to be released when convenient. The convention for the storage term $E_t(t_i)$ is described as positive during the discharging phase and negative during the charging phase. There is a maximum amount of energy to store and an energy loss per unit of time. The status of the storage at time t can be represented as per Equation 4.30.

$$P_{St}(t_i)\Delta t = (\eta_{HL} E_{St}(t_{i-1}) - E_{St}(t_i)) \tag{4.30}$$

The maximum amount of energy that can be kept on the thermal storage depends on the range of flow temperatures T_f to the customer, the volume of water stored V, the specific heat capacity of water c_{pw}, and it is calculated as shown in Equation 4.31.

$$E_{St,max} = c_{pw}\rho V(T_{fmax} - T_{fmin}) \tag{4.31}$$

Heat losses are considered in the storage and are estimated using [73]. Similarly, an electric consumption of the pumps whenever there is a charge or discharge from the storage is considered in Equation 4.32.

$$E_e(t_i) = \beta_{E,St} \left|P_{St}\right| (t_i)\Delta t \tag{4.32}$$

The $\beta_{E,St}$ introduced in Equation 4.32 represents the electricity consumption per each unit of heat stored or discharged through the thermal storage unit. This parameter is supposed to be constant and independent from the energy accumulated or released, as a first approximation. In addition, the thermal power during the charge or discharge phase is further constrained by a ramp limit which avoids unrealistic solutions with extremely rapid charging or discharging times.

4.2.7 District Heating and Cooling Network

This section introduces formulations for the DHC pumping consumption, thermal mass and heat loss to linearly approximate the thermodynamic behavior of the network. The approach was presented in [117].

4.2.7.1 Heat Loss Calculation

To simplify the calculation of heat loss in a network, it is expressed using only one variable: supply temperature T_f, as already described in Equation 4.7. Equations 4.33 and 4.34 depict the linear formulation implemented in the optimiser for calculating the heat loss at each time interval for the DH and DC network respectively.

$$\phi_{DH}(t_i) = k_B^{DH}\ T_f^{DH}(t_i) + \phi_B^{DH} \tag{4.33}$$

$$\phi_{DC}(t_i) = k_B^{DC}\ T_f^{DC}(t_i) + \phi_B^{DC} \tag{4.34}$$

For the sake of simplicity, but without losing generality, the coefficients k_B and ϕ_B, which are the base or minimum heat loss at the distribution network due to technical reasons, are assumed to be constant. This assumption is derived by imposing the soil temperature T_s and the return temperature T_r at a fixed value within the time horizon of the simulation. In fact, the weekly variation of soil temperature is negligible, and the return temperature is fixed by design condition. Finally, the variation of supply temperature T_f is bounded within an operational range from $T_{f,min}$ to $T_{f,max}$ which is based on the design, network topology, and technical restrictions.

4.2.7.2 Network Thermal Mass

The thermal mass effects on the DH and DC are evaluated in the MILP formulation in Equation 4.9. In practice, the thermal mass is added both in the energy balance equation for the heat energy vector and in the energy balance equation for the cold energy vector. The hot and cold balance equations are modified in each time interval as follows:

$$\left[\sum_{h=1}^{N_{chp}} E_{h,CHP}(t_i) + \sum_{k=1}^{N_b} E_{h,B}(t_i)\ + E_{h,St}(t_i) - \sum_{k=1}^{N_{abs}} E_{h,INabs}(t_i) - D_h(t_i) - U_h(t_i) - \right.$$
$$\left. - \phi_{DH}(t_i)\right] \Delta t = TM_{DH}\left[T_f^{DH}(t_i) - T_f^{DH}(t_{i-1})\right] \tag{4.35}$$

$$\left[\sum_{h=1}^{N_{ele}} E_{c,ele}(t_i) + \sum_{k=1}^{N_{abs}} E_{c,abs}(t_i) + E_{c,St}(t_i) - U_c(t_i) - \phi_{DC}(t_i)\right]\Delta t = \\ = TM_{DC}\left[T_f^{DC}(t_{i-1}) - T_f^{DC}(t_i)\right] \tag{4.36}$$

The balance equations are modified to include supply temperatures for the DH and DC networks as additional control and decision variables of the optimisation problem, according to Equation 4.9. The sum of the energy generated by the plant after subtraction of the demand and heat loss is substantially equal to the energy stored in the network, considering thermal mass at a given time interval. This stored energy corresponds to the variation of the energy content of the thermal mass for the DH and DC. Hence, the variation is calculated as the difference of temperature between two consecutive time intervals on the right side of Equations 4.35 and 4.36.

4.2.7.3 Network Flow Distribution

The mass flow of water $\dot{m}$ is measured in m^3/h and is used as an energy carrier on the DH or DC network. The corresponding heat generated (EG_{DH}) equates the user's heating demand for a given ΔT, which refers to the heat loss and the thermal mass. Hence, can be also thermodynamically expressed as follows:

$$EG_{DH}(t_i) = \dot{m}_{DH}(t_i) c_{pw} \rho_w \left(T_f^{DH}(t_i) - T_r^{DH}\right) \Delta t \tag{4.37}$$

where the heat generated EG_{DH} in the DH is also assumed to be equal to:

$$EG_{DH}(t_i) = \left[\sum_{h=1}^{N_{chp}} E_{h,CHP}(t_i) + \sum_{k=1}^{N_b} E_{h,B}(t_i) + E_{h,St}(t_i) - E_{h,INabs(t_i)}\right] \Delta t \tag{4.38}$$

Equation 4.37 correlates water flow, energy generated, and supply temperature. It is possible to conclude that the greater the value of ΔT the less $\dot{m}$ is required to deliver the same amount of energy; therefore, the electric consumption of the pumps will be lower. As the T_r is fixed by the customer, it is concluded that the greater T_f is, the lower the electricity consumption.

4.3 Results of Optimisation

4.3.1 Generation Optimisation

4.3.1.1 Case Description

The case proposed for this optimisation is an approach to a generation problem under strict climatic conditions. The goal pursued is the optimal generation of cooling power when it is constrained due to critical environmental conditions. In this study, five scenarios are presented that combine condensing constraints and storage. The condensing constraint options used are non-constrained, cooling tower, or geothermal system as heat sink. This case uses the descriptions of the power plant's configurations, its components, and constraints as well the time profiles of loads that were already presented in previous chapters. The optimisation period is the summer week. The described information is input to the optimising tool XEMS13 to find a feasible generation solution.

Ambient Considerations Ambient conditions are studied due their crucial importance to energy generation when using a dependent heat sink. Relative humidity and dry bulb temperature are used to calculate the wet bulb temperature, which directly affects cooling tower performance. Figure 4.13 depicts dry and wet bulb temperatures at the power plant site for 2015 in terms of the number of occurrence hours for a specific temperature.

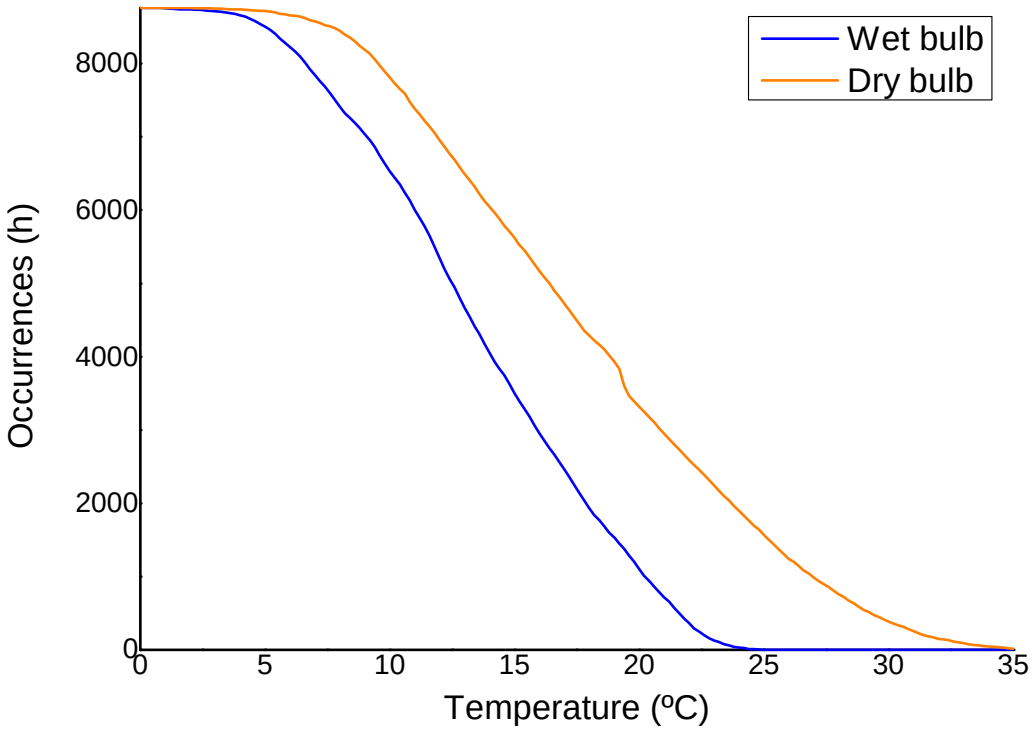

Figure 4.13: Occurrence hours for dry and wet bulb temperatures in 2015

Figure 4.13 indicates that the highest wet bulb temperature for 2015 is 25°C. If this value is considered for the incoming air stream, the desired water outlet temperature is 28°C, the maximum air stream exiting flow is 150kg/s , and the condensing power is equal to 2.0MW_{cn}.

The geothermal system is designed to simulate the worst-case scenario for the cooling tower without considering its efficiency gap. As the condensing capacity of the geothermal system is not dependent on external climatic conditions its fixed capacity is equal to 2MWh_{cn}.

The cooling tower's condensing power depends on external climatic conditions. The available condensing power of the cooling tower that considers the efficiency gap of 0.3K is calculated for a exiting air temperature that is equal to 27.7°C. In that case, the condensing power along the study week varies from a minimum of 1.75MW_{cn} to a maximum of 5.5MW_{cn}.

Proposed Configurations To determine the best solution for the described problem, two possible variables are considered in this work and their

combination generates the following different cases:

- Condensing mode: non-constrained, cooling tower, or geothermal system;
- With or without cooling storage.

The configuration used for each scenario is depicted in Table 4.9.

Table 4.9: Different scenarios configuration

Case	**C. Tower**	**Geo. Sys.**	**C. Storage**
Case 0	-	-	-
Case A	✓	-	-
Case B	✓	-	✓
Case C	-	✓	-
Case D	-	✓	✓

Case 0 is a scenario where there is no condensation constraint. Therefore, the chillers can generate freely without restriction from the condensing node. This case does not include any thermal storage.

Case A is a scenario constrained by the condensing node. In this case, the chosen heat sink is the existing cooling tower. This case does not include any thermal storage.

Case B is constrained with the same condensing constraints as in case A. In this case, cooling storage is included for $3MWh_c$.

Case C is a scenario that is also constrained by the condensing node, in this case, the chosen heat sink is a $2MWh_{cn}$ geothermal system. This case does not include any thermal storage.

Case D is constrained with the same condensing constraints as case C. However, in this case, $3MWh_c$ of cooling storage is included.

The five scenarios are run on the optimiser for the summer week, which is between 27^{th} July 2015 and 2^{nd} August 2015. Climatic values such as temperature and humidity in hourly steps are provided, as are wholesale electric market prices as well as heating and cooling demand for the DHC network.

Table 4.10: Summary of results

Case	0	A	B	C	D
Absorption Chiller	84.09%	21.16%	33.94%	14.23%	14.59%
Electric Chiller	15.91%	68.64%	61.57%	74.01%	82.68%
Slack Generator	0%	10.20%	4.50%	11.76%	2.74%
Waste Cooling	19.98%	10.25%	0%	11.53%	0%
Waste Heating	23.95%	84.70%	77.16%	91.08%	94.08%
Cooling Heat Losses	0%	0%	0.24%	0%	0.21%
Energy Price (€/MWh)	0.22	21.49	14.67	28.23	22.86

4.3.1.2 Results

Two kinds of heat sinks are proposed in this study: a cooling tower and a geothermal system for condensing purposes. The principles behind the working of these heat sinks are different. The geothermal system provides a constant and invariant condensing power of 2MWh_{cn} across the day and the year. Meanwhile, the cooling tower provides a condensing power that is dependent on ambient conditions varying from $1.75\text{MWh}_{\text{cn}}$ to $5.5\text{MWh}_{\text{cn}}$. The lower condensing power availability coincides with the higher cooling demand and the midday: this is a major drawback for cooling towers. Once the optimisations are carried out, the generation schedules are shown for heating and cooling. The results from these cases are economically motivated, and neither the impact of emissions nor energy efficiency considerations are accounted for. A summary of the results is depicted in Table 4.10.

Case 0 The first case proposed is a base case where no condensing restrictions are applied in the optimisation. Therefore, the results from this case fail to fulfil the technical constraints of condensing for a cooling power plant. However, the results are used to demonstrate how the cooling generation would be if no condensing constraint was used. In Figure 4.14, it is possible to see how the 84.09% of cooling demand is covered by the absorption chillers which harvest free thermal energy from the CHP engines. The electric chillers are only switched on when the demand for power is higher than the nominal power of the absorptions. No energy is purchased from the slack generator. Of the total cooling generation, 19.98% is wasted due to the minimum working point of the chillers.

This is the only case where the annual thermal-electric efficiency for the

CHP value is met. In the rest of the cases, more heating waste comes from the non-harvesting of the thermal energy generated by the CHP. Figure 4.14 depicts the heating optimisation. The CHP engines work a combined 234.10 equivalent hours, and 23.95% of the heating generation is unused.

The cost per unit of energy in this scenario is 0.22€/MWh.

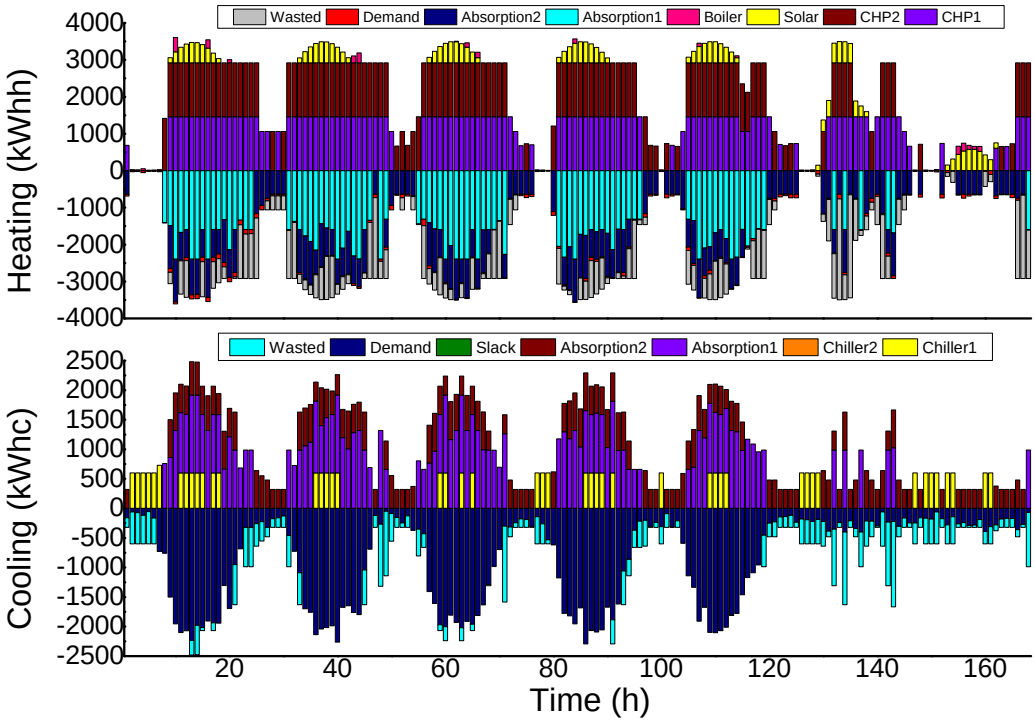

Figure 4.14: Heating and cooling optimisation for case scenario 0

Case A Figure 4.15 depicts how 68.64% of cooling power is generated by electric chillers which have lower condensing requirements than the absorption chillers. It is possible to observe from the figure that whenever there is enough condensing power available, the absorption chillers take over. However, if there is significant demand and the enthalpy of the incoming air is high, only the electric chillers are used. The results also indicate that at certain points it was necessary to buy energy from a fictitious generator: 16.19MWh$_c$ was purchased, which means that the power plant was unable to generate 10.20% of the total cooling demand. Additionally, the figure indicates that 16.27MWh$_c$ of cooling is produced and wasted. This is generated

when the demand is lower than the minimum production power and is triggered by the absence of cooling storage. This represents 10.25% of the total cooling generation.

Figure 4.15 depicts the heating optimisation. The CHP engines work a total of 207.16 equivalent hours, and 84.70% of the heating generation is unused. The cost per unit of energy in this scenario is 21.49€/MWh_c, which does not consider the energy or its cost when there is a shortage of cooling generation.

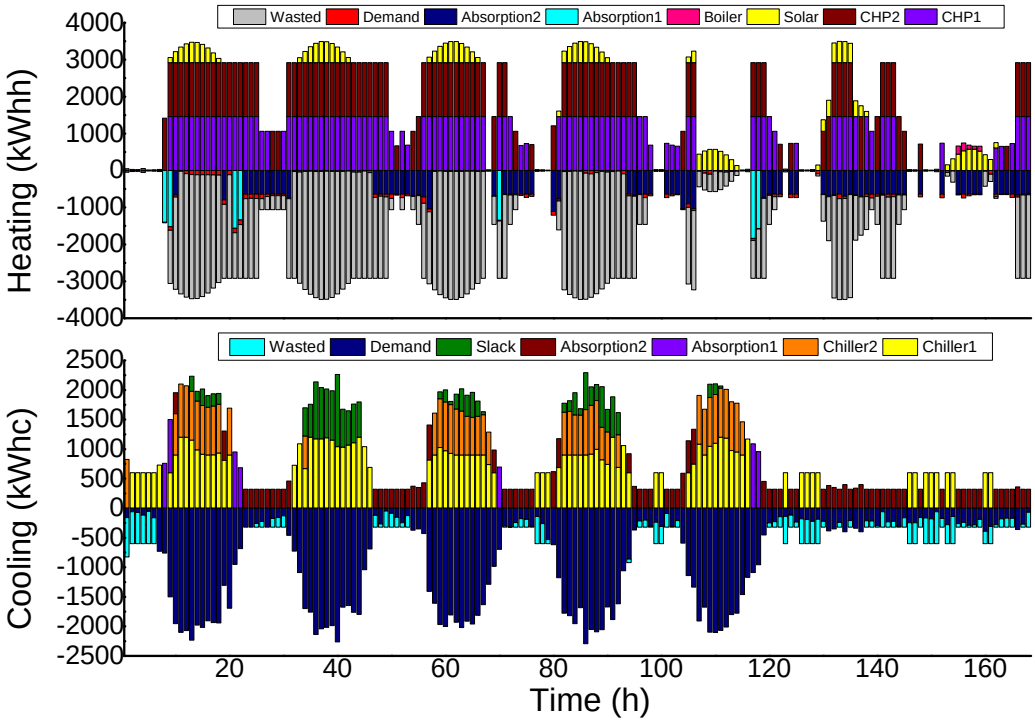

Figure 4.15: Heating and cooling optimisation for case scenario A

Case B Analogously to case A, in case B, 61.57% of the cooling energy is generated by electric chillers during midday when the demand and enthalpy are high. Figure 4.16 depicts the optimisation result. It illustrates how the storage loads in the early parts of the day and unloads in mid-day to avoid purchasing energy from the slack generator. In the same way, the storage completely avoids cooling waste by unloading the energy when the demand is not enough to turn on any chiller with a load higher than 50%. On the other

hand, the cooling storage provides 18.68% of the total demand and its heat losses represent 0.24% of the total generation. The percentage of energy that cannot be generated is 4.50% of the total cooling demand. Compared with case A, this reduction is achieved through the storage. Figure 4.16 depicts the heating optimisation. The CHP engines work 198.42 equivalent hours in total, and 77.16% of the heating generation is unused. The cost per unit of energy in this scenario is 14.67€/MWh_c, which does not consider the energy or its cost when there is a shortage of cooling generation.

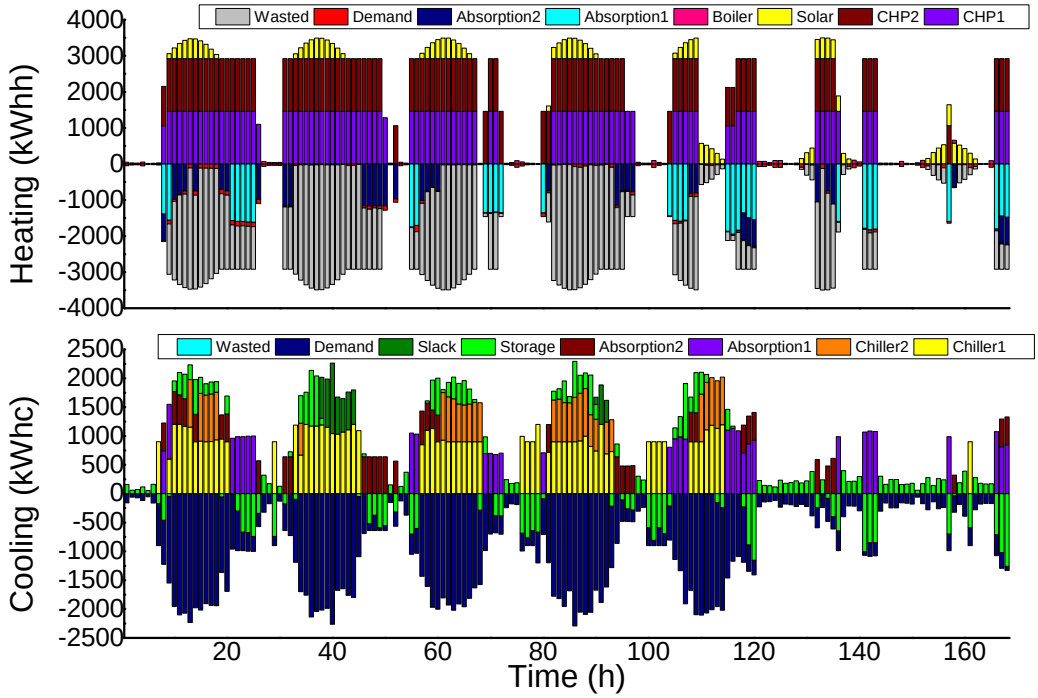

Figure 4.16: Heating and cooling optimisation for case scenario B

Case C Figure 4.17 depicts how 74.01% of the cooling power is generated with electric chillers for the same reason as in case A. It is possible to see how the maximum condensing power of the geothermal system is reached during the central hours of the day. Once this happens, the cooling power must be purchased from the slack generator. A total amount of 18.94MWh_c was purchased, representing 11.76% of the total cooling demand. Cooling waste also appears due the absence of storage and the minimum load of the chillers; this waste represents 11.53% of the total generation. Figure 4.17

depicts the heating optimisation. The CHP engines work a total of 190.13 equivalent hours, and 91.08% of the heating generation is unused. The cost per unit of energy in this scenario is 28.23€/MWh$_c$, which does not consider the energy or its cost when there is a shortage of cooling generation.

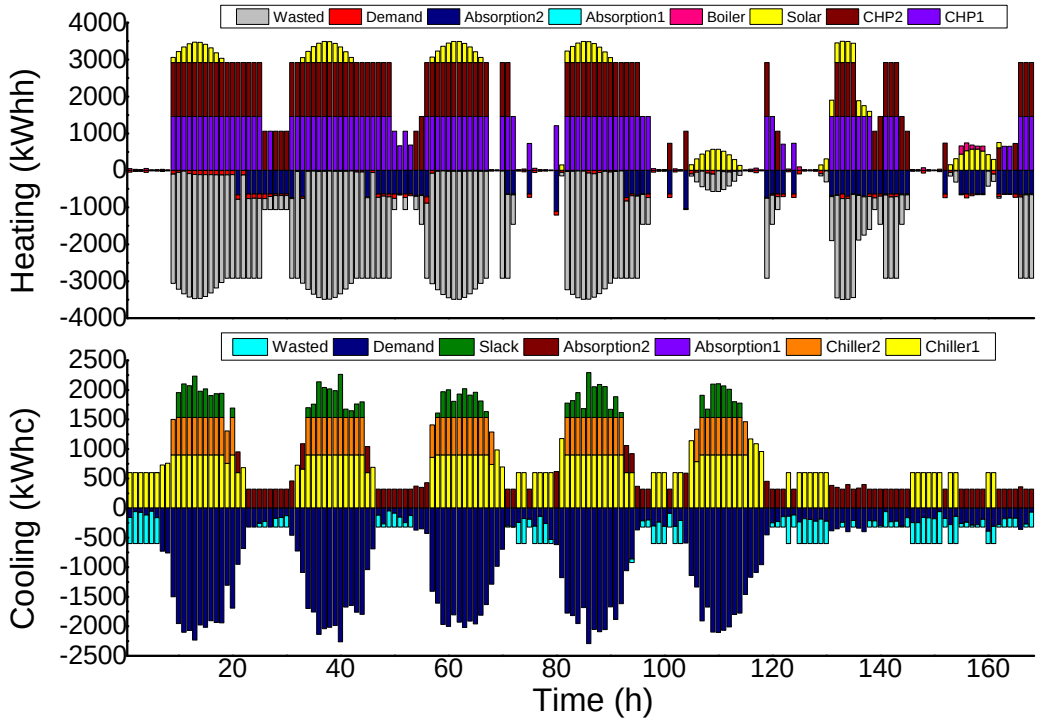

Figure 4.17: Heating and cooling optimisation for case scenario C

Case D Figure 4.18 depicts the optimisation result. Again, most cooling generation is produced by electric chillers with a share of 82.68%. The figure depicts how the storage works identically to case B: loading in the early day and unloading in midday to avoid cooling waste and purchasing energy from the slack generator. The amount of energy that cannot be generated is 3.93MWh$_c$, which represents 2.74% of the total cooling demand. This reduction, unlike case C , is achieved through the storage. On the other hand, the cooling storage provides 17.56% of the total demand, and its heat losses represent 0.21% of the total generation. The cost per unit of energy in this scenario is 22.68€/MWh$_c$, which does not consider the energy or its cost when there is a shortage of cooling generation. Figure 4.18 depicts the

heating optimisation. The CHP engines work a total of 173.06 equivalent hours, and 94.08% of the heating generation is unused.

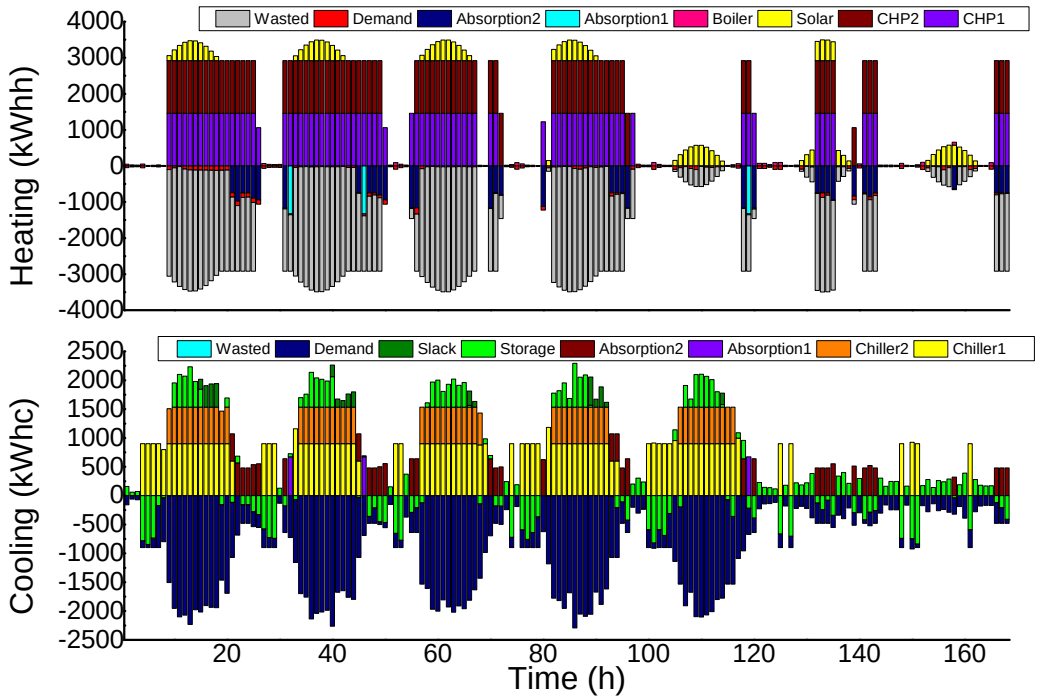

Figure 4.18: Heating and cooling optimisation for case scenario D

4.3.1.3 Conclusions

An application for the optimisation tool was proposed in this section and has been published in [61]. The problem that was studied is a current generation problem under strict climatic conditions. The goal pursued is the optimal generation of cooling power when it is constrained due to critical environmental conditions. In this case, the optimisation tool has been applied to five cases in the hybrid power plant of Parc Bit, which provides heating and cooling to the DHC. In this chapter, a cooling generation problem has been assessed, and the limitations that arise from the condensing requirements of the generators have been discussed. Such limitations directly affect the cooling generation and the strategies that the power plant manager should follow. As can be seen from the above cases, cooling generation is preferably carried out by generators with lower condensing requirements. Therefore, electric

chillers usually take over the generation when the condensing availability is low. This is motivated by a higher COP than absorption chillers and a lower condensing power requirement for the generation of cooling power. This means that even when the heating power is a free resource, the cooling demand of the power plant should be fulfilled by electric chillers where electric consumption is purchased from the grid. Otherwise, the cooling demand is not covered, and the power plant fails to fulfil client demand. The geothermal system provides condensing power that is almost as low as the cooling tower's worst case scenario. This motivates higher energy generation prices in the geothermal system's scenarios. Nevertheless, the cooling power shortages are very similar to the scenario without storage for both condensing constraints. Furthermore, the geothermal system outperforms the cooling tower in the scenarios with cooling storage in terms of cooling power shortage. Another set of scenarios is also proposed that depends on the cooling storage. One scenario does not include cooling storage, and the other includes storage of $3MWh_c$. The cooling storage allows the power plant to generate more efficiently. It completely avoids cooling waste due to minimum chiller operation, partially reduces the system difficulty of generating cooling demand, and improves the final economic result compared to the non-storage scenarios. On the other hand, heat loss from cooling is attributed to the water tanks used as cooling storage. Nevertheless, these heat losses are not as influential to the final optimisation result as the shortages in power that the storage avoids. To conclude, the optimisation tool can indicate generation strategies that otherwise would have been difficult to prove and apply because they are not straightforward. As the tool can manage several variables, including climatic ones, and the results are more precise than any other method.

4.3.2 Energy Supply Optimisation

4.3.2.1 Case description

The case proposed in this optimisation evaluates the impact of optimising the supply temperature in a DHC network. Thermal efficiency in distribution and generation is sought. The main issues covered in this section are pumping optimisation, heat loss impact on the network, and thermal mass. Two scenarios are proposed to evaluate the suggested method: a fixed supply temperature defined by design and a variable supply temperature which is optimised. Once the optimisations are carried out for 4 typical weeks; each

Table 4.11: Energy KPIs

KPI	Winter		Spring		Summer		Autumn	
	NoTM	**TM**	**NoTM**	**TM**	**NoTM**	**TM**	**NoTM**	**TM**
Heating Energy [MWh]	248.55	247.11	102.05	99.82	31.19	30.07	64.48	62.78
HL Heating [%]	11.6%	11.1%	25.9%	24.2%	73.9%	72.9%	39.2%	37.5%
Heat stored TM [MWh]	0	17.42	0	4.61	0	10.71	0	15.28
Cooling Energy [MWh]	5.32	5.01	13.80	13.48	150.51	150.24	39.41	39.10
HL Cooling [%]	34.1%	30.1%	32.0%	30.4%	5.3%	5.1%	14.3%	13.6%
Cold stored TM [MWh]	0	4.34	0	10.49	0	17.60	0	18.92
Total Energy [MWh]	253.86	252.11	115.85	113.30	181.70	180.32	103.88	101.88

Table 4.12: Economic KPIs

KPI	Winter		Spring		Summer		Autumn	
	NoTM	**TM**	**NoTM**	**TM**	**NoTM**	**TM**	**NoTM**	**TM**
Pumping Cost [€]	79	112	64	97	233	244	92	106
HL Cost [€]	1,731	1,393	1,842	1,114	878	647	1,556	942
Supply Cost [€]	1,810	1,504	1,906	1,211	1,110	891	1,648	1,049
Generation Cost [€]	12,591	10,745	5,081	3,350	4,262	3,288	3,675	2,381
Total Cost [€]	14,401	12,250	6,986	4,561	5,373	4,180	5,323	3,429
LCOE [€/MWh]	56.41	48.15	59.75	39.40	28.29	21.82	50.36	32.62

week represents the four seasons of the year, the generation schedules are obtained for heating, cooling, and electricity. The optimisation results in these cases are economically motivated and no environmental or energy efficiency considerations are considered. In this section, energy economics, energy balance, and flow temperature optimisation are presented as the results. For the sake of simplicity, no energy generation mix is depicted when comparing the two scenarios.

4.3.2.2 Energy KPIs

In this section, the main key performance indicators (KPI) from the two scenarios are depicted. The results are extracted from the simulations carried out by XEMS13. Table 4.11 compares the main KPIs from scenarios that either consider thermal mass (TM) or do not (NoTM). Heating and cooling energy refers to the user demand plus the heat loss to supply the load. The levelized cost of energy (LCOE) is calculated by dividing the generation cost by the user's total energy demand.

Table 4.11 indicates that even if the flow temperature optimisation is focused on harvesting the thermal mass, it decreases the heat loss in the network and the total energy consumption in the network. The heat and

Table 4.13: Comparison and summary of most important KPIs

KPI	Winter	Spring	Summer	Autumn	Average
Total Energy Savings [%]	0.69%	2.20%	0.76%	1.93%	1.39%
Total Cost Savings [%]	14.94%	34.72%	22.20%	35.58%	26.86%
Savings on LCOE [€/MWh]	8.27	20.35	6.46	17.74	13.21

cold-stored thermal mass refers to energy recovered from the network thermal mass that has been previously stored. Table 4.11 indicates that the amount of stored energy for both heating and cooling have similar ranges from 4MWh to 18MWh. The amount of energy stored is not always related to the total energy consumed in the season.

The economic KPI in Table 4.12 indicates the costs of generation, supply, and total costs. This information indicates how the generation costs are reduced when using thermal mass, which is the main goal of the optimisation. It is also noteworthy that the total supply costs are also lower when using thermal mass. The cost for pumping is higher when thermal mass is used, but this expense is lower when compared to the savings in heat loss costs. Similarly, Table 4.12 indicates lower total costs when thermal mass is used, compared to the fixed supply temperature scenario.

Table 4.13 presents the economic savings of using thermal mass. The values are expressed in percentages of savings compared with the scenario where thermal mass is not used. Generally, the use of thermal mass results in energy and economic savings, but they are not correlated because low-energy savings correspond to high-cost savings. In fact, the economic savings indicate the gains that can be achieved when the thermal mass is used as active energy storage. Hence, generation units can overproduce with respect to the demand and losses to store energy in the network when economic conditions are favourable. The network is discharged later to cover energy demand in disadvantageous economic conditions. Energy savings are instead mainly related to the reduction of power losses, whereas weekly energy generated is substantially unchanged. Table 4.13 presents annual average energy savings of 1.39% coming from heat loss. The annual average total cost savings are 26.86%, which represent a reduction in the LCOE by 13.21€/MWh.

4.3.2.3 Energy Balance

The energy balance indicates how the network demand is met with the help of the thermal mass. For a better understanding of energy balancing and

the influence of thermal mass, Figure 4.19 indicates the generation from the power plant which is supplied to the DHC in comparison with the network demand (which includes heat losses).

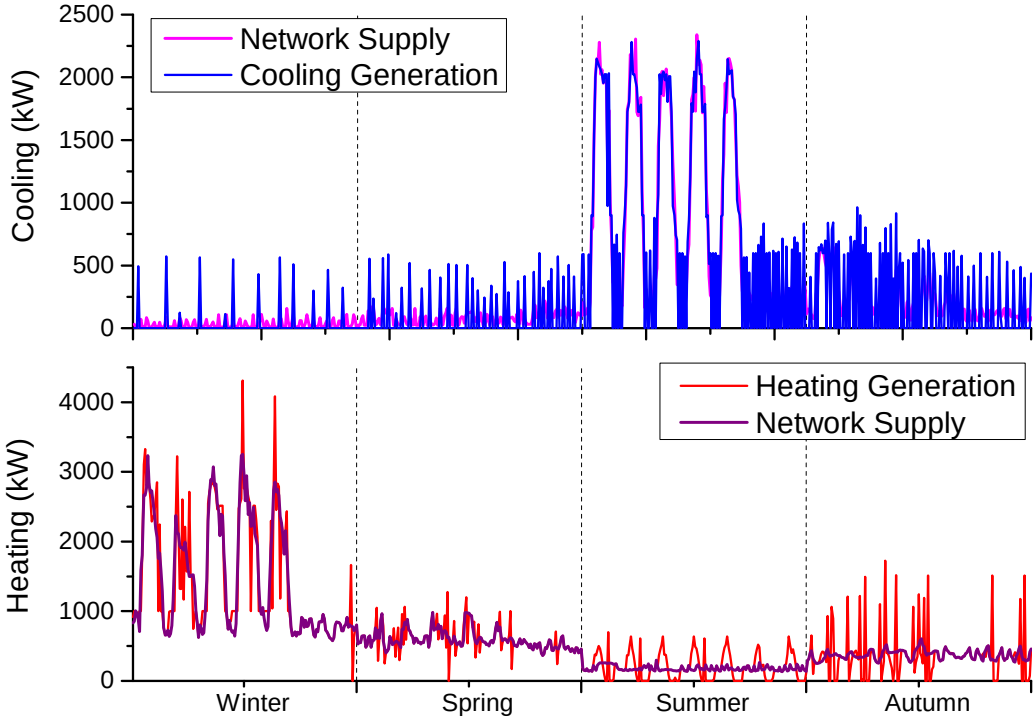

Figure 4.19: Heating and Cooling Energy balance

Figure 4.19 illustrates how the generation has a changing pattern, unlike the network demand. This is observable in both figures for heating and cooling but is especially apparent when the cooling demand is low. When the energy supplied is greater than network demand, the network is being charged with energy, and the opposite is occurring when the demand is greater than the supplied energy. The thermal mass is used as an energy storage in the supply side and can be compared to thermal energy shifting or a forced thermal demand response.

4.3.2.4 Mass Flow and Supply Temperature Optimisation

This section compares optimal temperature harnessing thermal mass TM and fixed supply temperature without harnessing of thermal mass $NoTM$. Consequently, mass flow M_f rates in both scenarios are compared. Figure 4.20 depicts the mass flow, temperature of supply T_f, and temperature of return T_r in both scenarios for the four weeks that consider heating power. Likewise, Figure 4.21 considers cooling power for the four weeks.

Figures 4.20 and 4.21 illustrate that the mass flow rate is generally higher in the scenarios using thermal mass than the scenarios with fixed supply temperature. Nevertheless, Figure 4.21 indicates that during the summer week, the mass flows are very similar as the supply temperature is mostly the same in both scenarios. Both graphs illustrate how supply temperature reaches the upper boundary when the demand is high or is loading the thermal mass. On the other hand, the temperature drops to the lower temperature boundary during low-demand hours. This is observable from Figure 4.20, where supply temperature is steady in the lower boundary during spring week.

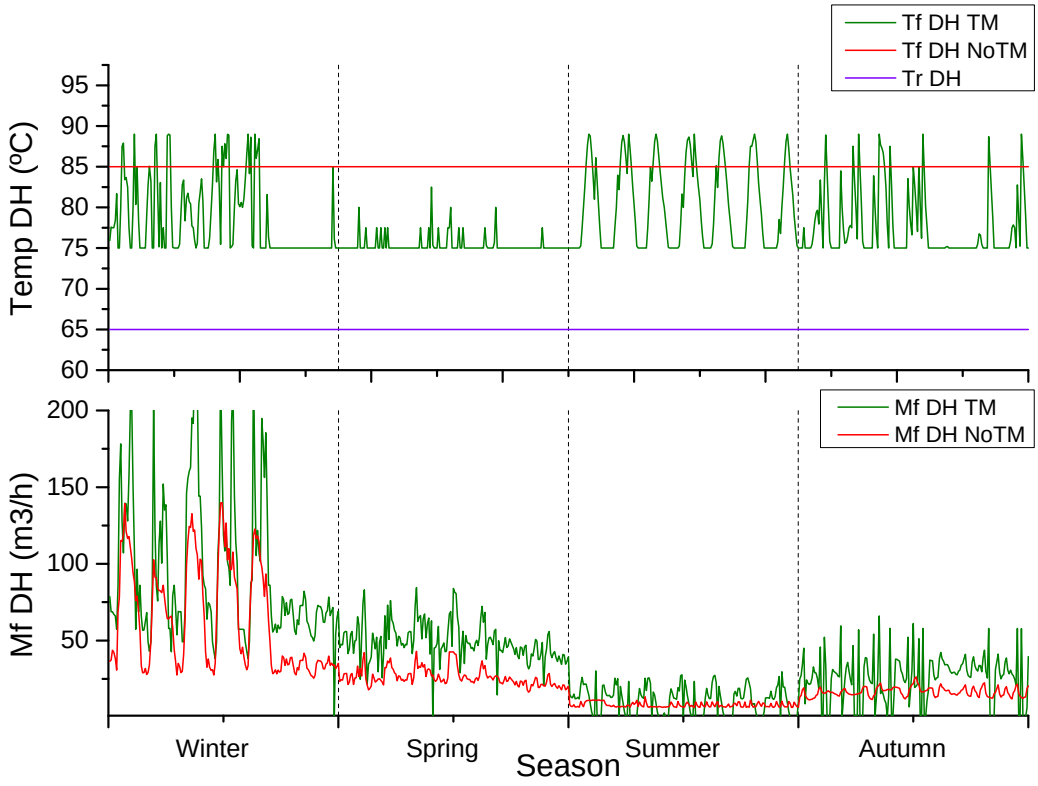

Figure 4.20: Optimal and fixed flow temperature and mass flow for heating

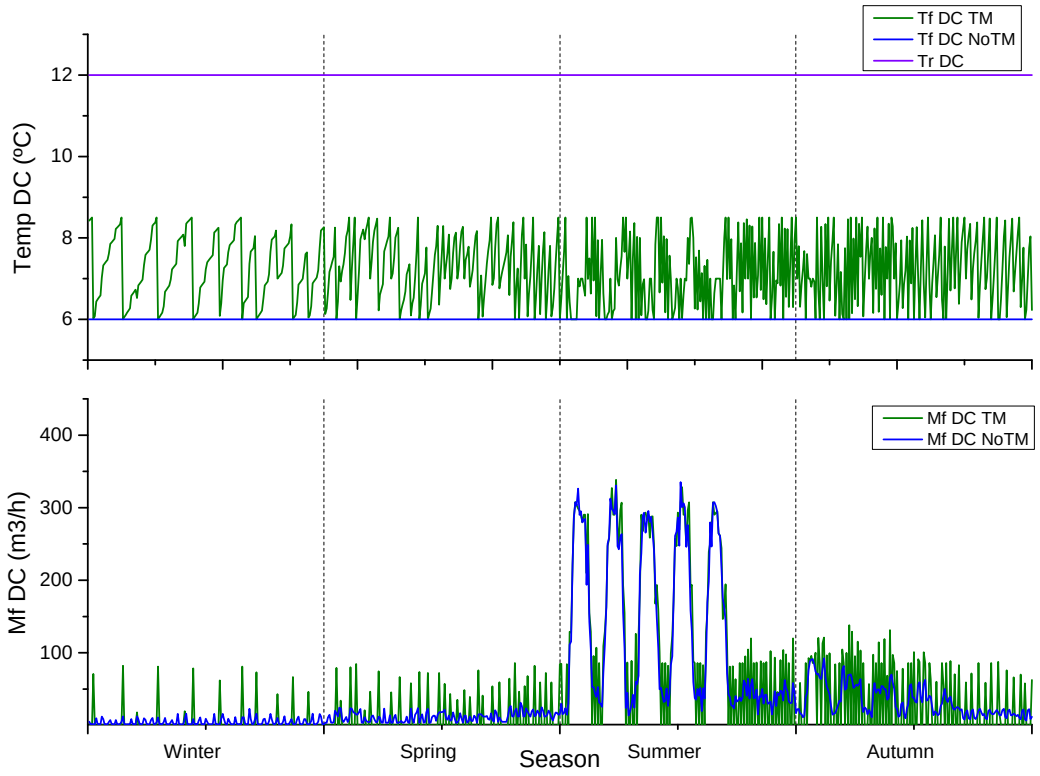

Figure 4.21: Optimal and fixed flow temperature and mass flow for cooling

4.3.2.5 Conclusions

In this case, the optimisation tool is applied to improve the supply energy through the DHC network. More specifically, this case addressed a problem regarding thermal mass harnessing and supply temperature optimisation. Energetic and economic benefits for a hybrid power plant supplying thermal energy to a DHC are presented. To compare the benefits of applying this idea, two scenarios are compared: one in which thermal mass is neglected and the other in which thermal mass is considered. The results presented in [117] for both scenarios are compared in 4 typical weeks; each week represents the four seasons of the year and their peculiarities. The main conclusions are as follows.

The simulation results indicate that the thermal mass is used similarly to energy storage that decouples the energy generation and demand, which allows for more cost-effective energy generation. Generally, thermal mass

is used to store energy, but the amount of energy stored is dependent on the scenario. This suggest that the use of thermal mass might provide less savings for power plants with standard energy storage. The thermal shifting ability of thermal mass is such that during low demand weeks, most of the energy demand is supplied to the network before its actual use. Figure 4.19 depicts a change in the heating and cooling generation pattern compared to the network demand. Those figures graphically represent how the energy is shifted to cheaper generation hours and the decoupling of demand and generation. A higher mass flow rate is used to achieve this energy shifting through thermal mass; the rate supplies more energy than requested by the network. Simulation results indicate how the supply temperature is changing along the defined boundaries to achieve energy matching and energy optimisation. Therefore, supply temperature boundaries are a constraint with a significant impact on the exploitation of thermal mass. This suggests that greater savings can be achieved with broader supply temperature boundaries, but this range is usually fixed by design.

Supply temperature optimisation enhances energy efficiency because it lowers the heat losses in the DHC. That behavior is pronounced during low demand seasons where the energy supply reduces heat loss. In all cases, the total energy consumption of the DHC is greater than the cases where thermal mass is used. The simulations indicate that regardless of the demand, thermal mass and supply temperature optimisation provide substantial energy and economic savings. These savings are presented and quantified through the LCOE, which decreases an average of 13.21€/MWh using thermal mass. The biggest reduction on LCOE occurs during spring and autumn, when it is not high demand season. The most significant results are the annual average energy and cost savings of 1.39% and 26.86% respectively. These savings are obtained from a change of supply strategy and energy management. These energy savings could be even greater if the return temperature was not fixed. In such cases, the return side could be considered for thermal mass, and energy supply strategies could be applied to both supply and return temperatures. In the studies presented in [49, 51], where only the thermal inertia of the DHC was comparable with this work, the cost savings are 7.0% and 10.38% respectively. In this work, the cost savings are 26.86%.

4.3.3 Smart Energy Distribution

4.3.3.1 Case Description

In this case, real life operations are used to compare the previous power plant operation and the new strategy for supplying temperature. The new strategy is motivated by the results obtained in Section 4.3.2. The strategy is based on two pillars:

- Control supply temperature to lower heat loss as much as possible and
- Store excess heat from CHP in the DHC network's thermal mass to be used when needed.

To achieve a controllable supply temperature, a three-way valve actuator is used and controlled from the SCADA. This valve mixes generated hot water with DHC return water to obtain the desired supply temperature. Figure 4.22 depicts the actuator and valve.

Figure 4.22: Valve actuator to control supply temperature

Table 4.14: Energy savings due optimal supply temperature

Energy	**Before**	**After**
Demand [MWh]	98.95	98.12
CHP generation [MWh]	89.26	95.29
Aux Boiler generation [MWh]	38.24	14.04

4.3.3.2 Results

In this case, the supply temperature is controlled based on a set point at the power plant. Figure 4.23 depicts a day before the supply temperature control is applied and a similar day when the supply temperature control is applied. The figure depicts the supply, return, and set-point temperature for the UIB and Parc Bit branch. The day when the control is applied has lower supply and return temperatures than the non-controlled day. The figure also depicts how the set-point can be fixed for a temperature so high that the power plant cannot reach it. In those cases, the return water is not mixed with the generated hot water. Evidence of greater power plant efficiency and auxiliary boiler generation decreases is depicted in Figure 4.24. This figure compares two batches of 3 mid-week days in February 2018, before and after using controlled temperature energy distribution. These two batches are similar in terms of CHP schedule and energy demand. Table 4.14 depicts the figures for demand, CHP, and auxiliary boiler generation. As presented, the energy input of the auxiliary boiler is massively reduced due to a higher cogeneration fraction, energy storage, and better energy supply strategy.

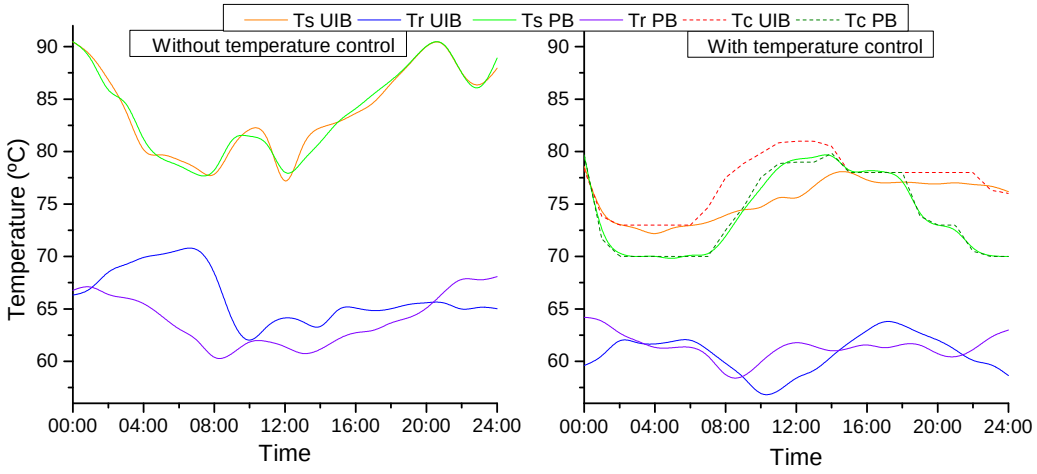

Figure 4.23: Optimal supply temperature using three way valve

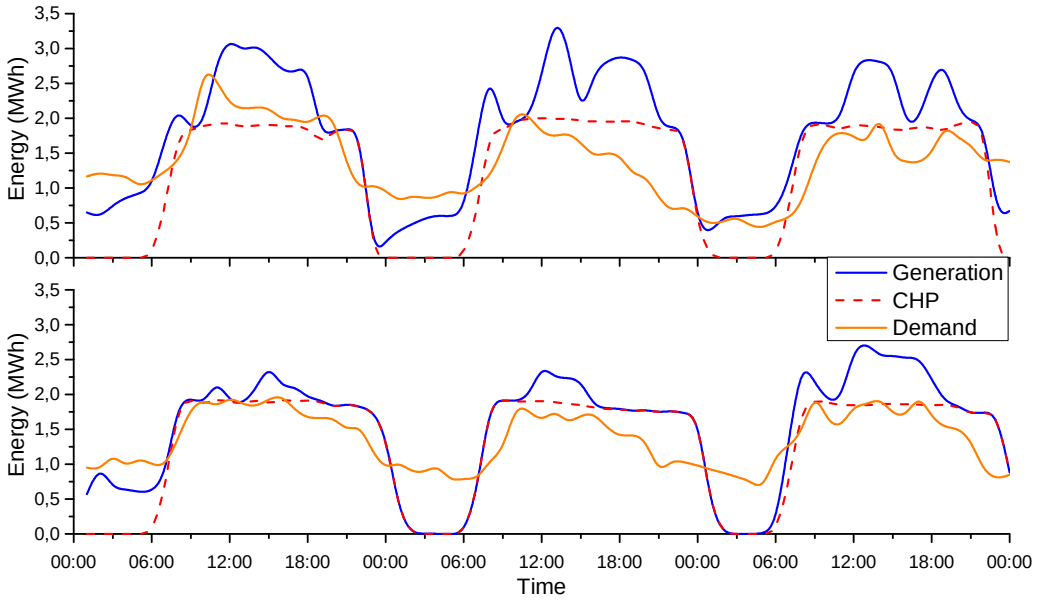

Figure 4.24: DH thermal inertia harnessing

4.3.3.3 Conclusion

One of the goals of controlling supply temperature is to decrease heat loss in energy distribution without failing to fulfil the customer's demand. Decreas-

ing heat loss in DHC is based on decreasing supply temperature in heating and increasing supply temperature in cooling. The decrease of heat loss implies lower energy requirements in power plant generation. This translates to more energy stored in case of a day when the scheduled CHP generation is enough to cover the demand. On the other hand, if the scheduled CHP generation is not enough to cover the demand, these lower energy requirements are translated into a decrease in auxiliary boiler generation and savings for primary energy consumption. Figure 4.24 provides evidence for a decrease in auxiliary boiler generation and thermal inertia harnessing. The figure compares similar days in terms of CHP schedule and energy demand. The figure compares total power plant energy generation with CHP generation and DHC demand. Another benefit to controlling supply temperature is to store excess heat from the power plant in the DHC. Excess heat in the power plant occurs when the energy generated by the CHP is greater than the users' energy demand. Either this excess heat is not harnessed in co-generation, and the exhaust gases is dumped into the atmosphere, or the exhaust gases is harnessed and the energy is stored in the DHC network. To do so, the supply temperature is increased only during the time when this fact takes place. In the power plant, the control of the supply temperature is performed with help of an hourly scheduled table that is programmed in the SCADA where the set point is inserted. Figure 4.25 depicts the schedule table.

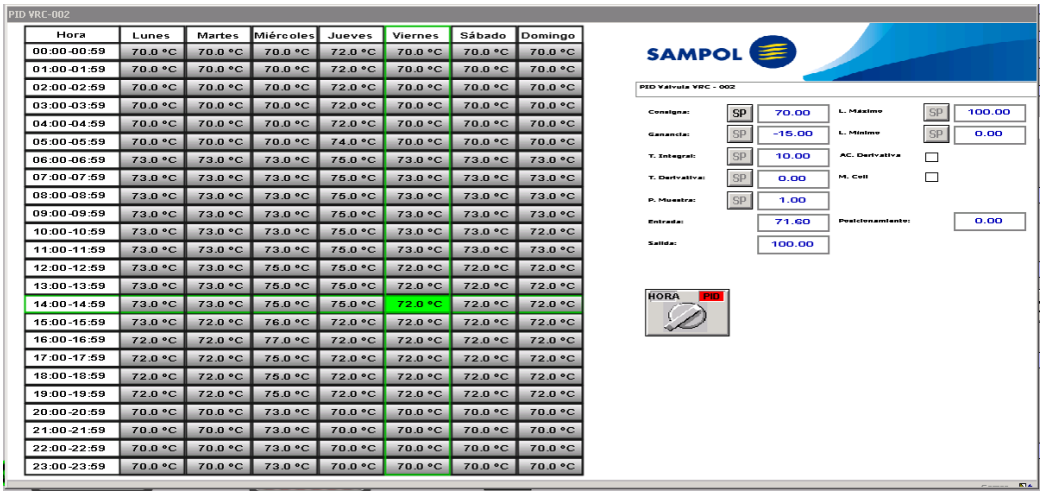

Figure 4.25: Supply temperature scheduling table

4.3.4 Forecasting Optimisation Scenarios

4.3.4.1 Case Description

In this case, the simulator determines generation strategies by optimising the production mix that minimises the energy cost and maximises revenues using energy forecasts. The strategies obtained from the forecasted information are compared with the strategies obtained using real information or the ideal strategy. The deviation from the ideal strategy is the error that is due to the forecasts. The resulting strategies that use forecasted and real values are compared to evaluate the forecasting error propagation in the final economic result. This comparison will demonstrate the influences of each forecasting error on the power plant revenue and the differences between the ideal operation and the forecasted strategies.

4.3.4.2 Comparison Strategy

A strategy is proposed to compare the propagation of the forecasting error into the final optimisation result. This strategy compares the results obtained using forecasted or real information. In this case, there are four possible combinations:

- **Real Price – Real Demand.** Ideal optimisation results. These are the results that would be obtained if the forecast were not in any error.
- **Real Price – Forecasted Demand.** Optimisation results that are influenced by a demand error. These are the results obtained using forecasted demand. Therefore, the impact of the error can be observed upon comparison with the ideal results.
- **Forecasted Price – Real Demand.** Optimisation results that are influenced by a price error. These are the results that were obtained using a forecasted price. Therefore, the impact of this error can be seen upon comparison with the ideal results.
- **Forecasted Price – Forecasted Demand.** Forecasted optimisation results.

Once the generation schedule of the different options is proposed, the CHP schedule is forced in the optimiser using the real values of energy price and

Table 4.15: MAE and MAPE forecasting errors for demand and price

Season	Heating		Cooling		Price	
	MAE	**MAPE**	**MAE**	**MAPE**	**MAE**	**MAPE**
Winter	153.20	4.98%	26.56	1.16%	6.10	3.39%
Spring	81.17	2.64%	6.58	0.29%	6.25	3.47%
Summer	72.78	2.36%	132.95	5.80%	3.43	1.91%
Autumn	51.41	1.67%	74.92	3.27%	4.03	2.24%
AVERAGE	89.64	2.91%	60.25	2.63%	4.95	2.75%

demand. Consequently, the rest of the power plant behaves to match the demand. The calculated economic result for the different scenarios is compared with the ideal result.

4.3.4.3 Forecasted Input

The demand forecast algorithm is explained in Section 3.2, and further results are explained in Section 5.2.3. In combination, these enable the estimation of hourly energy values for each customer. These values would be aggregated to a total demand for either cooling or heating, including supply heat loss, and compared afterward with the real demand at the power plant. Figure 4.26 enables the comparison of the real heating or cooling demand with the aggregated forecast. Similarly, the energy price forecast algorithm is explained in Section 3.2, and the forecasted results as further results are explained in section 5.2.1. In this case, the selected results are from the ARIMAX method and a 1-day ahead forecast that uses the open market as an explanatory variable. Figure 4.27 enables the comparison of the historical OMIE's energy prices with forecasted values. As may well be appreciated, the forecast values are very similar to the real values. The results of these forecasts are only used as one step in the optimisation process; the error is not relevant, and only the difference between the final results should be taken into consideration.

Table 4.15 depicts the errors in terms of MAPE and MAE for price and demand. The MAE units used for demand and price are kWh and €/MWh respectively.

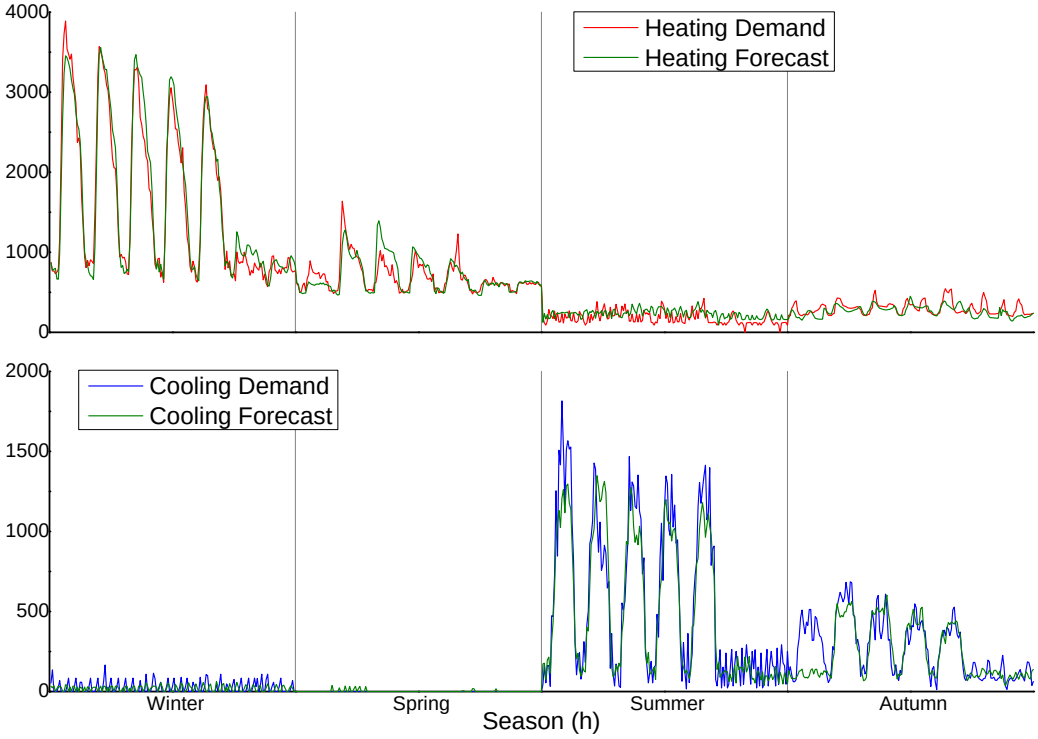

Figure 4.26: Thermal demand and forecast comparison

4.3.4.4 Economic Optimisation Forecasting Results

This section presents the optimisation results, which are the final results. Energy price and demand information are used to achieve these results. Depending on the scenario, this information is either forecasted or real. To compare the different forecast-based scenarios, the economic results obtained from real values are assumed to be the ideal results. The error induced by the forecasts is evaluated in comparison with the ideal scenario. This error is a deviation from the ideal economic benefits and therefore a decrease of benefits due to misleading forecasts. The difference between the ideal scenario and the forecast-based scenarios is the different use of the CHP or its generation schedule. The rest of the generators actuate accordingly to the decision taken by the CHP because they are auxiliary or dependent. Table 4.16 depicts the results from the optimisation and compares them to the ideal scenario. Figure 4.28 enables the comparison of the different hourly values of the four studied cases.

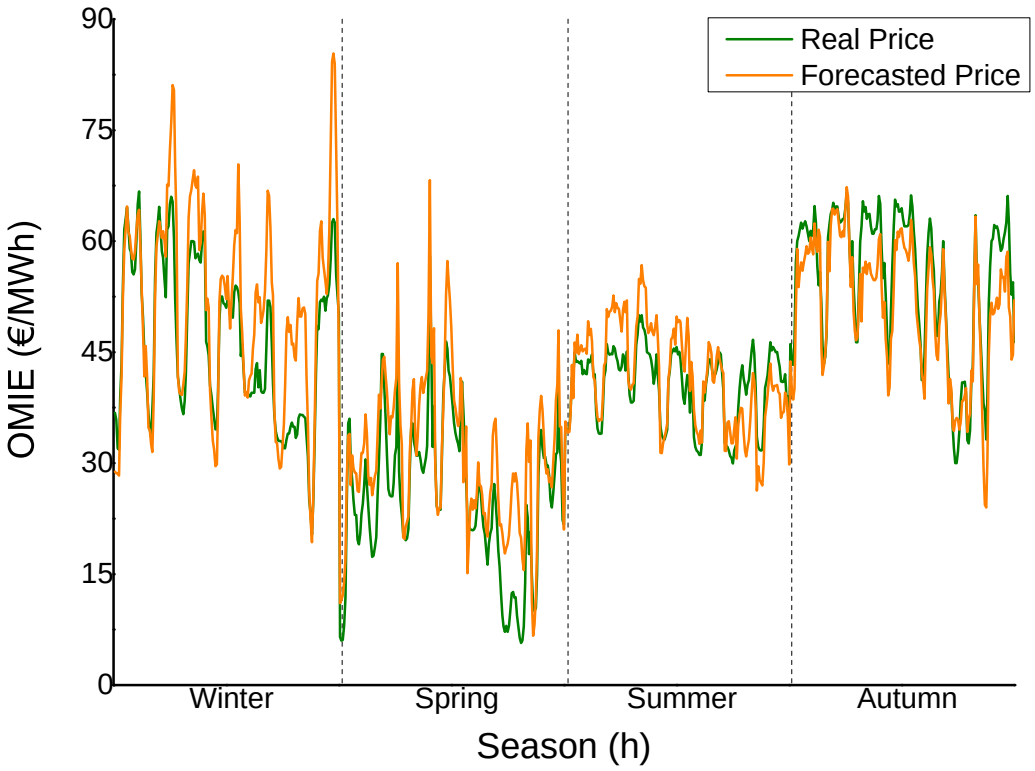

Figure 4.27: ARIMAX one-day ahead energy price and forecast comparison

4.3.4.5 Conclusions

In this section, generation strategies have been proposed and compared, and economic benefit was used to evaluate the influence of forecasting errors. This evaluation was achieved by using the EMS to generate energy generation strategies with different information. The strategies were generated for 4 typical weeks that corresponded to the different seasons.

An ideal generation strategy was calculated to evaluate the accuracy of the strategies. This strategy used real information from energy prices and thermal demand.

Therefore, the optimisation result proved to be the best possible option. The strategies generated using forecasted information were compared using the real values of price and demand [122]. The results are presented in Table 4.15, which depicts the errors induced by the forecast when the economic results are compared with the ideal scenario. The results indicate how the

Table 4.16: Errors in optimisation due to forecasting error propagation

Scenario	Winter	Spring	Summer	Autumn	MAPE
Real Price – Forecasted Demand	14€	55€	70€	0€	0.48%
Forecasted Price – Real Demand	366€	884€	104€	7€	4.74%
Forecasted Price and Demand	366€	825€	90€	6€	4.49%

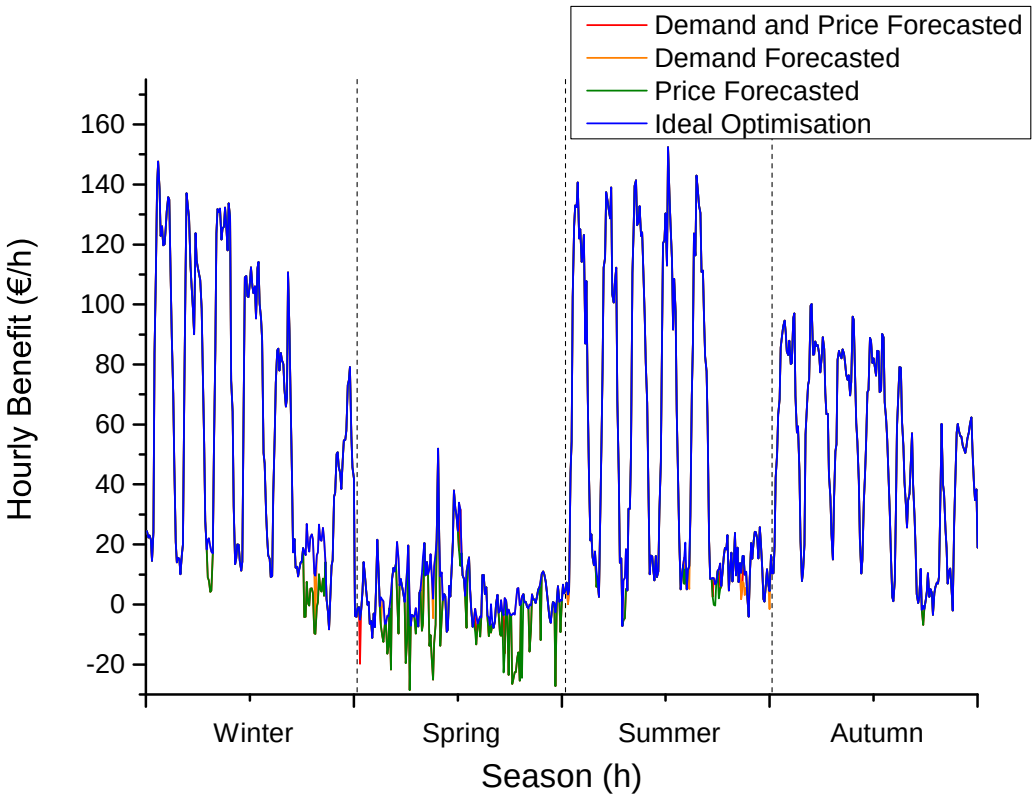

Figure 4.28: Comparison of hourly benefits depending on forecasts

forecasting error propagates the economic error in the optimisation. In the case of the energy price, the average error of 2.75% had an average impact of 4.74% on the optimisation. In the case of thermal demand, an average error of 2.91% for heating and 2.63% for cooling error had an impact of 0.48% on the optimisation. Moreover, when combining both forecasting errors, the average reduction of benefits was equal to 4.49%, which was even lower than the average error from only using energy-forecasted information.

These results indicate how the most influential factor in the optimisation

is the energy price forecasting error. This error directly propagates and strongly affects the power plant's hourly benefits. This fact is particularly pronounced during the spring week, when the market prices are close to the break-even point for running the CHP. On the other hand, the autumn week is less affected. Demand forecasting errors were less influential in terms of power plant optimisation, most likely due their lower influence on CHP benefits. In fact, demand error of 2.91% for heating and 2.63% for cooling decreased to 0.48% benefit impact.

The results depicted in Table 4.15 also indicate that error propagation is strongly dependent on the case. Therefore, it is possible for there to be weeks where the combined error is higher or lower than the greater individual error. One conclusion which could be drawn here is that the error *per se* is not important; what is important is the error that is close to the breakeven point. The impact of the forecasting error in the final generation schedule depends on may factors such as the quantity of errors in forecasts; the errors' sign; and whether the error modifies the generation strategy, which does not necessarily happen. Similarly, as more than one forecast is used, the different errors may cancel each other. These considerations indicate that a tremendous amount of possibilities could be studied. Nevertheless, as is evident from the final results of Figure 4.28, the deviation of the forecasted scenarios did not differ much from the ideal scenario. Therefore, forecasts can be used to create generating strategies. The errors influenced by the forecasts were as low as 4.49% on average.

Chapter 5

Energy and Price Forecasting

5.1 Forecasting Methodology

5.1.1 Explanatory Variables

Section 2.5 explains how an explanatory variable can improve the accuracy of an energy forecast. Both the ARIMAX and NARX forecasting models, are supported with an explanatory variable based on suitable information. As mentioned in Section 2.5.1, for the explanatory variable to be helpful, it must be related to the time series for forecasting and should include future observations.

5.1.1.1 OMIE Explanatory Variable

In principle, the relation between total electric demand and electric energy price suggests that electricity demand can be an explanatory variable for electricity price forecasting. On the other hand, and as seen in Section 2.3.1, the demand is not the only factor related to energy price. The energy price is built when matching the energy bids and the demand. Therefore, the price requested in the generation bids is as important as the demand and the price offered for it. In the energy market, it is possible to discern between two kinds of generators: manageable and not-manageable. The first kind can generate depending on the price and therefore match in the energy auction whenever certain economic boundaries are met. By contrast, the unmanageable power plants can generate independently of the selling conditions. These technologies are solar, wind, and nuclear power. The behaviour of the un-

manageable power plants affects the final auction price because their energy bids are close to 0€/MWh, so the energy is purchased. Relatedly, another explanatory variable can be considered: the energy that will be produced regardless of economic boundaries that are subtracted from the total energy demand. This amount of energy is what is left for manageable generators to match and can be defined as 'Competitive Market' or 'Open Market', and is defined in equation 5.1.

$$CompetitiveMarket_h = Demand_h - Solar_h - Wind_h - Nuclear_h \quad (5.1)$$

In this thesis, three possibilities are studied to understand the impact of an explanatory variable on forecasts:

1. No explanatory variable
2. Demand as an explanatory variable
3. Competitive market as an explanatory variable

A Pearson correlation study is carried out for the two explanatory variables on the historical values for 2016 to determine which one is more suitable to be used in energy price forecasting. The results of the relation between energy price and demand are depicted in Figure 5.1 with a Pearson correlation factor of 0.412.

The results of the relation between energy price and competitive market are depicted in Figure 5.1 with a Pearson correlation factor of 0.719. The relation depicted for Competitive Market and energy price is much higher than the relation with the demand. Even the relation is not perfect and is in fact far from being close to 1 (which means a perfect and direct relation), it is a better support for forecasting for both methods and should improve the forecasting accuracy.

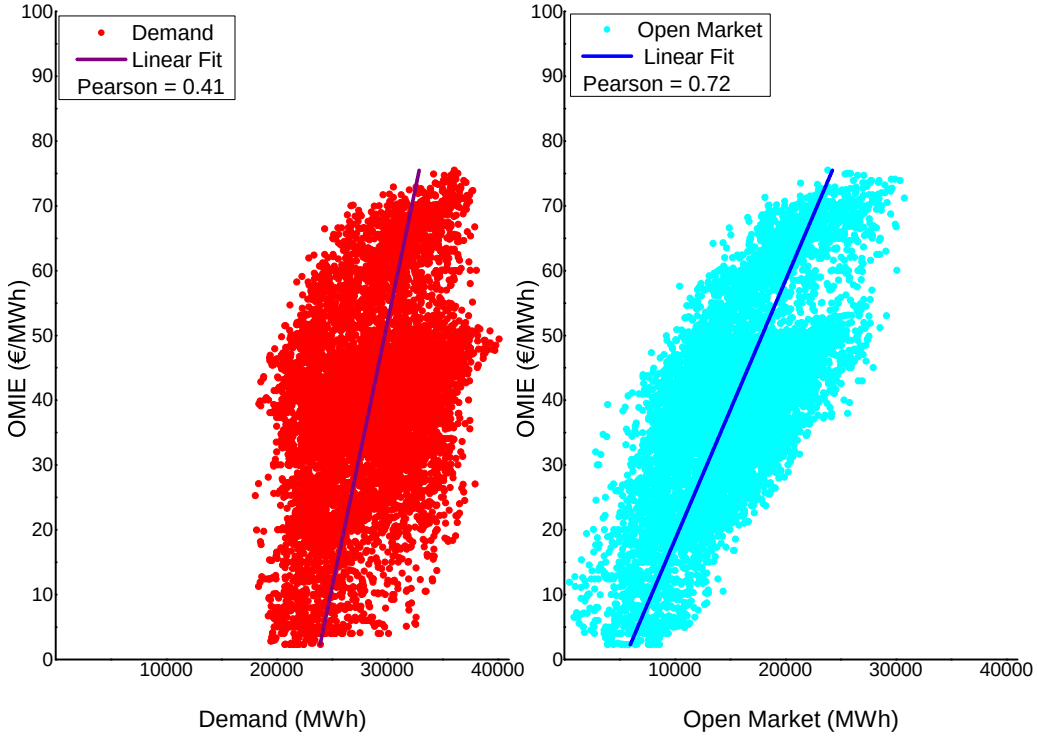

Figure 5.1: Explanatory variables relation to energy price

5.1.1.2 Solar Energy Explanatory Variable

The energy forecasters may use solar radiation, ambient temperature, and cloudiness as its inputs, whereas power is given as an output [123]. As mentioned before, the relation between irradiation and solar generation is direct for a certain power plant. Therefore, a precise irradiation value is presumed to have an outstanding explanatory variable. In the same way, the cloudiness index has a negative relation with solar energy generation and is hence presumed to be a useful explanatory variable. A generation forecast that is based on cloudiness is deemed to be the most successful method for long-term solar forecasting [96].

The importance for forecasting energy generation lies in the markedly different generation between stations that change from a 540MW peak in winter to a $5,600$MW peak in summer and achieve a maximum of 12% of the total renewable power injected into the grid. It is also important to understand that solar electricity generation in Spain includes two technologies that can

produce electricity:

- Photovoltaic technology generates energy that is influenced only by the solar irradiation on the panel surface at a certain time and is not supported with storage. The installed power of this technology is 4.16GW [124].
- The thermo-solar power plants are able to generate electricity through a process that is dependent on solar irradiance and temperature; additionally, these power plants sometimes have storage systems. The installed power of this technology is 2.3GW [124].

To provide reliable explanatory data for Spain, it is necessary to acquire data from an NWP, which provides the cloudiness index for a certain location. This information would help to model solar radiation by considering of geographical information. The model is based on a clear-sky radiation calculation and the satellite cloudiness indices in different locations in the country. The calculation of the irradiation for a given location is performed by subtracting the fraction blocked by the clouds from the clear-sky radiation [125, 126]. The calculation of the average irradiation in Spain would be the weighted irradiation with the installed power in the area under study [127].

Figure 5.2 [128] illustrates the fundamental relationship between the satellite observation of the planetary albedo and ground-level irradiance. The difference between the net incoming irradiance at the top of the atmosphere ($I_{in}TOA$) and the net irradiance at the ground level (Ig_{in}) must be equal to the flux lost (either reflected, scattered, or absorbed).

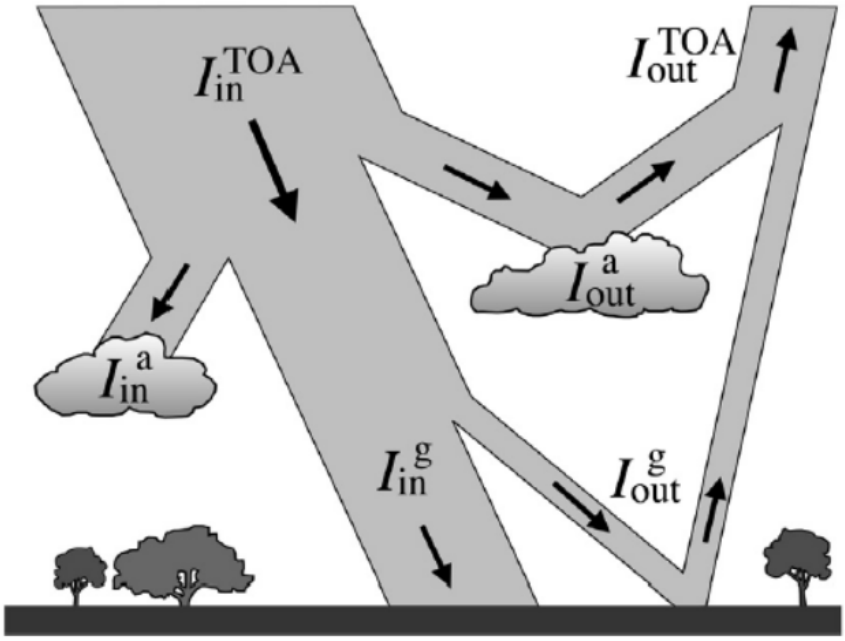

Figure 5.2: Solar irradiation reaching ground after cloud block

To obtain the irradiation with the developed method, it is necessary to calculate the extraterrestrial hourly irradiation on a tilted surface (G_{0T}) for a given point and the tilt angle of a south-oriented surface [129]. This calculation depends upon the location of the plant, the time of the year, and the slope of the solar collectors. The irradiation on a tilted surface (G_{0T}) is calculated according to Equation 5.2:

$$G_{0T} = G_{SC}\left(1 + 0.033\cos\frac{360n}{365}\right)\cos\Theta_z \tag{5.2}$$

Where G_{SC} is a solar constant ($1,367\mathrm{W/m^2}$), n is the day number of the year, and Θ_z is the incidence angle calculated in 5.3:

$$\cos\Theta_z = \cos(\phi - \alpha)\cos\delta\cos\omega + \sin(\phi - \alpha)\sin\delta \tag{5.3}$$

ϕ is the latitude of the location, α is the slope of the collecting surface, δ is the declination or angular position of the sun calculated in Equation 5.4, and ω is the hour angle or the angle of displacement of the sun calculated in Equation 5.5.

$$\delta = 23.45 \sin\left(360 \frac{284 + n}{365}\right) \tag{5.4}$$

$$\omega = (h_s - 12)15 \tag{5.5}$$

The solar time is denoted by h_s. The difference between the solar time and the standard time is calculated through Equation 5.6, and the result is given in minutes.

$$SolarTime - StandardTime = 4(L_{st} - L_{loc}) + E + DLS \tag{5.6}$$

where L_{st} and L_{loc} are the longitudes for the standard meridian, and the location, day light savings, and E are a values that are calculated through Equation 5.7:

$$\begin{aligned} E = 229.2(0.000075 + 0.001868 \cos(B) - 0.032077 \sin(B) \\ - 0.014615 \cos(2B) - 0.04089 \sin(2B)) \end{aligned} \tag{5.7}$$

Finally, B is calculated according to Equation 5.8.

$$B = (n - 1)\frac{360}{365} \tag{5.8}$$

The intensity of the solar radiation that reaches the surface of the earth decreases with increasing values of the cloudiness index or sky cover [130, 128]. Taking this hypothesis as valid, the method forecasts the irradiance (I_f) for a given location to be dependent on the extraterrestrial hourly irradiance (G_{0T}). The method also holds the irradiance to be the complement to the forecasted cloudiness measured in $[0 - 1]$ range (N_f). The values are calculated hourly according to Equation 5.9.

$$I_f = G_0(1 - N_f) \tag{5.9}$$

A similar model was presented by [131], where global irradiance is obtained by adding the cloud's transmissivity to the model. The value of the weighted explanatory variable used for Spain is calculated by considering the forecasted time series, irradiance in the measured places, and the installed powers in those places. Spain's weighted averaged irradiance values (I_E) are calculated according to Equation 5.10.

$$I_E = \frac{1}{P_s} \sum_{n=1}^{50} I_{fn} P_{sn} \tag{5.10}$$

Where I_{fn} the forecasted irradiance on the n location, P_{sn} is the installed solar power for a given location, and P_s is the total solar power accumulated in Spain that is calculated using Equation 5.11.

$$P_s = \sum_{n=1}^{50} P_{sn} \tag{5.11}$$

As a result, three variables are obtained for the forecast, cloudiness, extraterrestrial irradiation, and irradiation. The calculated national extraterrestrial irradiance is on a plane that is parallel to the collector aperture, and the solar national generation in hourly steps indicate a strong relation in Figure 5.3(a). It is important to bear in mind that the units and factors do not match for the variables, as the irradiation is measured in [W/m^2] and its maximum value is $1,367$W/m^2. Solar power is measured in [MW] and its maximum value is $6,460$MW. This relation reaches 0.86 and an R^2 of 0.741 when measured with the Pearson factor.

In the case of the cloudiness index, the relation with the aggregated energy generation is less obvious in terms of indexes or graphs in Figure 5.3(b). The Pearson factor provides a result of 0.09 and an R^2 of 0.008. Nevertheless, the relation between cloudiness and solar generation is easily understandable from the perspective of physics: the existence of clouds blocks the solar energy generation, as depicted in Figure 5.2. For the irradiance, which is calculated using the radiation and the cloudiness factor, the relation with the aggregated energy generation in Figure 5.3(c) reaches the highest value. The Pearson factor provides a result of 0.90 and $\mathrm{R}^2 = 0.816$. Therefore, this time series will be used as an explanatory variable for solar energy forecasts in further calculations.

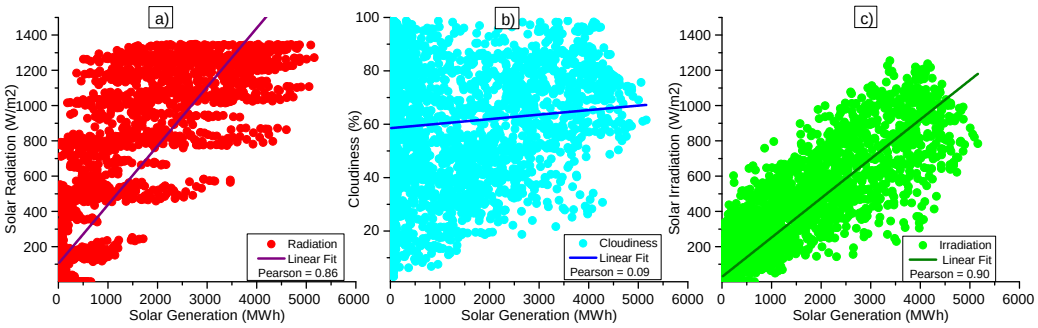

Figure 5.3: Explanatory variables relation to solar generation

5.1.1.3 Wind Power Explanatory Variable

The capability of a wind turbine to generate power is directly related with wind speed and direction. In the case of wind direction, it would be useful to understand how the wind turbines shadow each other on a wind farm [132, 133] to improve the calculation of the explanatory variable. To do so, the wind farms' turbine distribution is required. Unfortunately, this information is not easily accessible. Therefore, the only contribution to the explanatory variable is the wind speed in the location. Equation 5.12 illustrates the power delivered by a wind turbine:

$$P = \frac{1}{2}\rho A v^3 \tag{5.12}$$

Where ρ is the air density, A is the area swept by the rotor, and v is the wind speed through the blades.

The value of the weighted explanatory variable used for Spain is calculated by considering the forecasted time series and the wind speed in the measured places and the installed powers in those places. Spain's weighted average wind speed (v_E) values are calculated according to Equation 5.13.

$$v_E = \frac{1}{P_w}\sum_{n=1}^{50} v_{fn} P_{wn} \tag{5.13}$$

Where v_{fn} n is the forecasted wind speed in the n location, P_{wn} is the installed wind power for a given location, and P_w is the total wind power accumulated in Spain that is calculated using Equation 5.14.

$$P_w = \sum_{n=1}^{50} P_{wn} \tag{5.14}$$

The resulting data provides a time series for wind speed. To study the correctness of the above-mentioned suppositions, two correlation studies were carried out on the time series: a Pearson correlation study and an R^2 correlation study. After wind speed and national wind generation were taken into consideration, the results were a correlation of 5.4, a Pearson factor of 0.79, and an R^2 of 0.63. In the case of wind speed, the same study is made to the power of three (cubic wind speed, v^3) because it is related to wind power, as seen in Equation 5.12. This study provides a Pearson factor of 0.73 and an R^2 of 0.54, which is lower than the initial results. Thus, simple wind speed should be used to forecast.

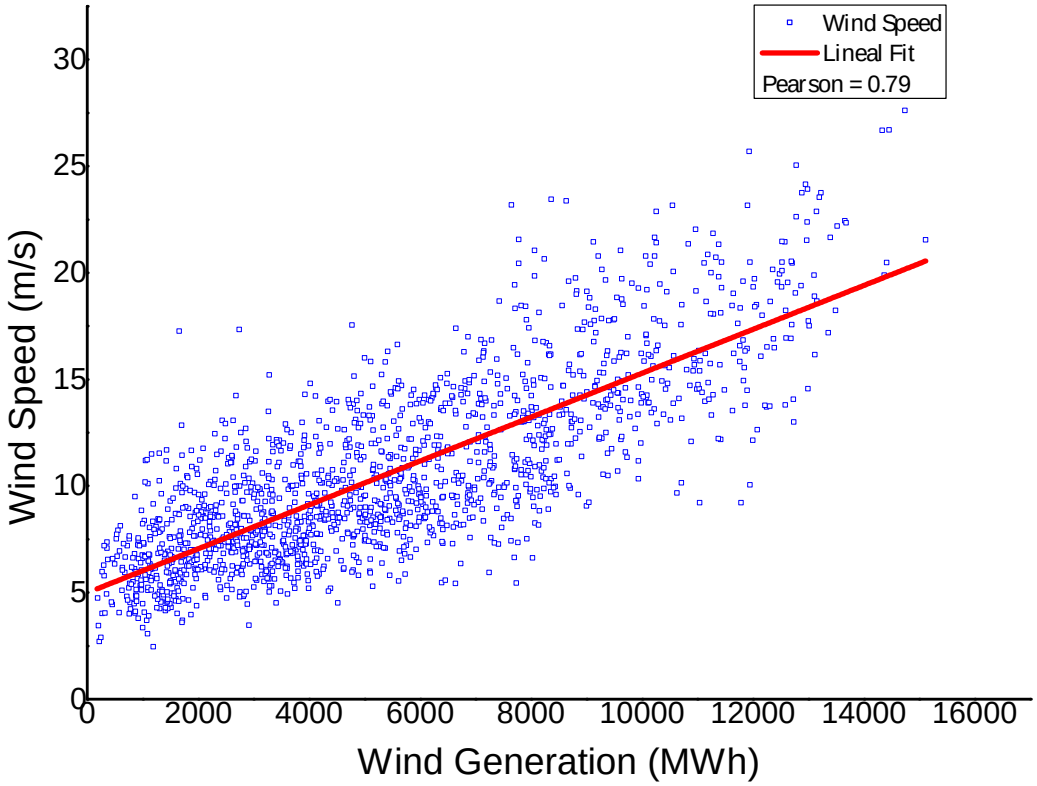

Figure 5.4: Wind power and speed correlation

5.1.1.4 Thermal Demand Explanatory Variable

Accurate energy demand forecasts can be obtained using simple models that combine weather forecasts with the historical load and weather curves [134, 78]. The demand forecast model could be improved by using a sufficient data series as an explanatory variable that would support the historical demand values [135]. A straight approach to the problem would be to use the ambient temperature as explanatory variable [136]. The relations between the demand and the ambient temperature are inverse with a Pearson value of -0.51 for heating demand and direct with a Pearson value of 0.52 for cooling demand; both relations are depicted in Figure 5.5.

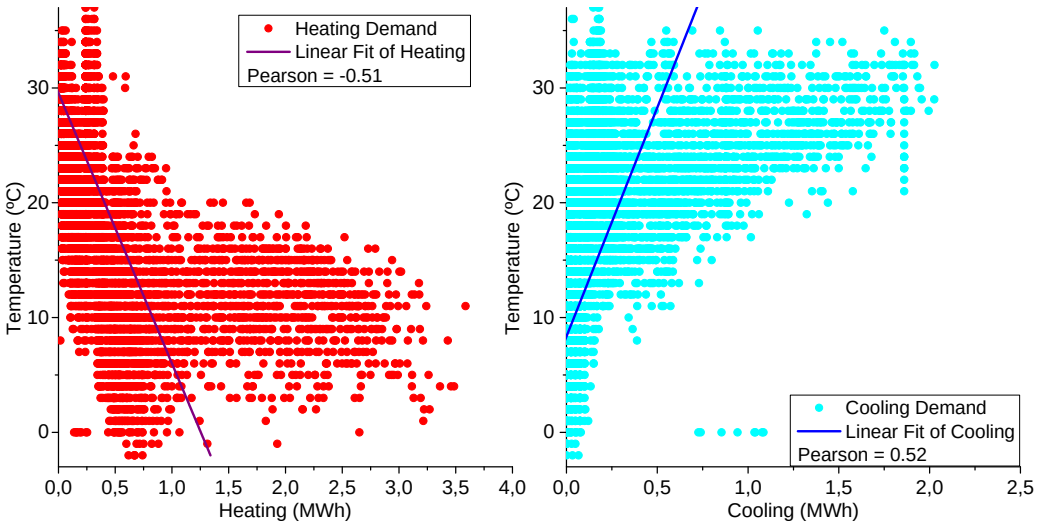

Figure 5.5: Thermal demand and temperature correlation

5.1.2 Data Acquisition

This section describes the process of data acquisition from different sources. Three sources are used in this work:

- Spanish energy market
- Climatic data
- DHC Network

Figure 5.6 depicts a graphical interpretation of the data acquisition system.

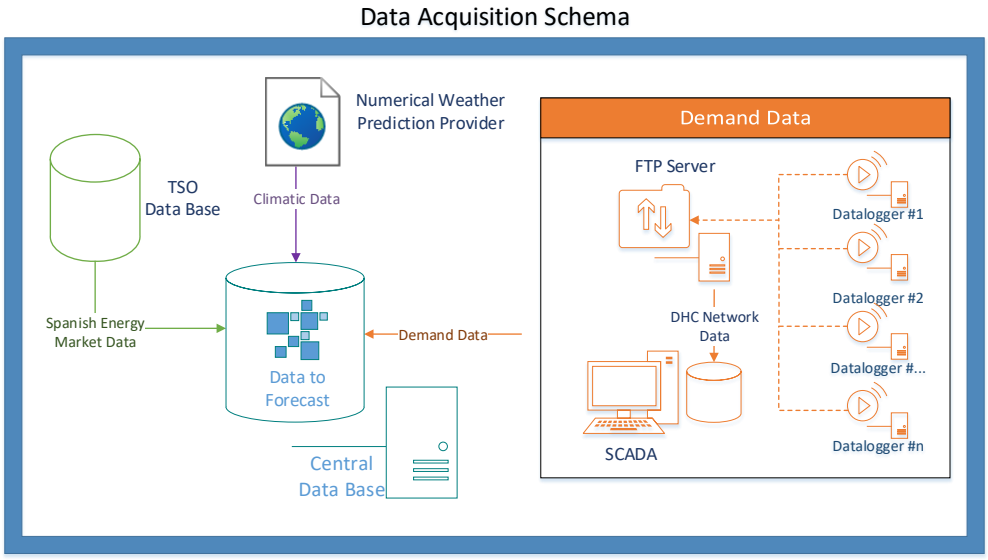

Figure 5.6: Data acquisition schema

5.1.2.1 Spanish Energy Market Data acquisition

Energy market information is acquired from the Spanish transport system operator, Red Electrica Española. This information is necessary to understand the market and evaluate the energy mix at every hour and the OMIE energy market's price. This information is available on the Red Electrica Española website and provides the demand and generation data of the Spanish energy mix in 10-minute steps [137]. Energy price information can also be found at the same source in hourly values and from all the different markets. This information is acquired through recurrent queries to their DB and is stored in SAMPOL's SQL DB, which has been created as part of this thesis. The information is stored with the same periodicity as acquired but it is always used as hourly values.

The generation of solar and wind energy and market energy price is based on the historical data acquired with this method. Moreover, the transport system operator has been providing a demand forecast of up till 1 week ahead

and a solar and wind power forecast of up till 3 days ahead since the summer of 2015. These forecasted values are used in the thesis. The installed power for solar and wind technologies that is used to calculate the explanatory variable is provided by the Ministry of Industry [124]. Detailed information of the installations is provided, such as location, technology, power, and whether the installation is connected to the grid. This information is processed and clustered according to the provincial division in Spain. In this way, 50 aggregated installed powers are obtained.

5.1.2.2 Climatic Data Acquisition

Climatic data is required to forecast demand, solar, and wind power. This information is acquired from an NWP and acquired from the web service in hourly steps [138]. The NWP is based on an algorithm that analyses satellite images and predicts the climatic data [139]. The NWP data covers 3 days ahead. To have a homogeneous database for Spain, one station per province is used; those stations are usually located in each province's main city, which results in 50 stations being selected for Spain. Stations are marked with black dots in Figure 5.7.

The variable grid that takes the provinces as units may lead to errors because the NWP value is given for a point and is used in the whole area regardless of the station and the power plant's location. The asymmetry in the location of weather stations and the different shapes and sizes of the provinces avoid the possibility of spatially averaging the NWP data used in [127]. Furthermore, only the aggregation of the weighted data in the whole country is carried out in this study. That there is only one station per province and that station's data is used for the whole province may lead to errors because the station's value is used for the whole province without considering its exact location. The shadowing effect within wind farms that arises due to the location of the wind turbines in the land and the wind direction may decrease the local wind power generation, thus affecting the aggregated generation. From this service, the following information is retrieved:

- Cloudiness
- Wind speed
- Ambient temperature

For the extraterrestrial hourly radiation calculation, a value of slope (α) is estimated. This value is fixed for all the solar power plants and during the year. The most common slope value for Spain is fixed at the average latitude value of 40°. The optimum yearly slope value for an installation is the same as the latitude where it is located [140]. The acquisition and processing of the information and calculations are conducted by an automatic tool designed in Matlab®.

Figure 5.7: Weather Stations Localizations

5.1.2.3 DHC Network Data Acquisition

Due the inherent variability of the load, it is necessary to acquire information on energy demand. Each customer in the network is equipped with an energy meter (Kamstrup Multical 601) that is supported by a data logger that retrieves historical information every 2 minutes and communicates with the SCADA in the generation plant. The data acquired with this method are flow and return temperature, mass flow, instant power, and aggregated energy consumed. On one hand, the energy meters were installed from the

beginning on the client's side and record the aggregated energy consumed. On the other hand, the data-logger solution has been installed as part of this PhD thesis. The equipment is depicted in Figure 5.8. The communication of the data-logger with the SCADA is performed through GSM, which allows communication even in remote points. Once the information is received, it is stored in the DB for further use and analysis. Figure 5.9 depicts the principles of thermal data acquisition and processing.

Figure 5.8: Datalogger + Kamstrup Multicall 601

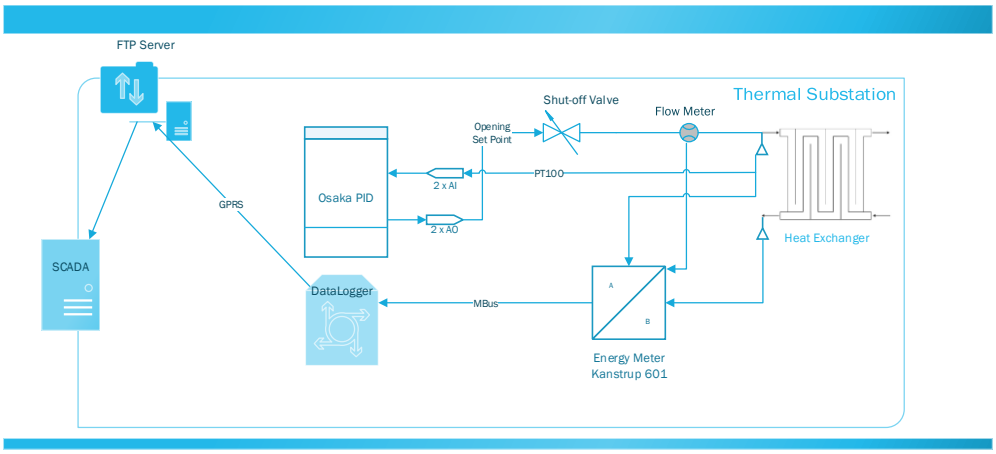

Figure 5.9: Substation data acquisition principle

5.1.3 Configuration of Forecasting Methods

This section contains a brief description of the configurations used in forecasting. Many configurations have been tried for the different forecast models. The best performing set of configurations are depicted in the following sections. The main options for configuration pertain to the amount of inputs and the values of those inputs. The amount of inputs relate to the amount of steps needed to forecast, which is generally 24. The values of those inputs are selected from the ACF and PACF studies, which indicate which lags have greater impact on the time series.

5.1.3.1 ARIMAX

For ARIMAX forecasting, the data is split: 95% for the training set and 5% for the result comparison set. The derivative part, D, is fixed as 0. The data-set is divided between weekdays, Saturdays, and Sundays only for price forecasting. The best performing configurations for the different variables have been used in the studies carried out in this thesis.

5.1.3.2 NARX

For NARX forecasting, the data is split randomly in three different sets: training 70%, validation to avoid overfitting 15%, and result comparison and testing 15%. The training method used is the Lavenberg-Marquardt algorithm. The attempted methods and ANN configurations that performed the best are depicted in Table 5.1. The values of neurons per layer correspond to input, hidden, and output layers. L stands for linear, ST stands for sigmoid tangent, and I stands for the input layer. The proposed input and feedback delays are different for the type of day (weekday, Saturday, or Sunday) and for the forecasting variable.

Table 5.1: NARX Configuration

Variable	**Configuration**
Neurons per layer	48-24-1
Activation Function	I-ST-L
Gradient	5×10^{-9}
Epochs	2,000

5.2 Forecasting Results

5.2.1 Energy Price Forecast Results

5.2.1.1 Case Description

This section compares the forecasts of energy prices using forecasting methods and the three explanatory variable options. The study covers January 1st 2016 - December 31st 2016. The length of historic data used on the forecasts starts on January 1st 2015 and ends the previous day to the first forecast day. Different forecasting time horizons that cover 1 to 6 days ahead are studied. To compare both forecasting methods, several combinations of inputs, lags, and configurations of ARIMAX and NARX models have been attempted to obtain the most accurate results. However, only the best-performing combinations are presented. For both methods, a study has been conducted to understand the influence of the explanatory variable on the quality of the prediction. The options used were no explanatory, demand, or competitive market as explanatory variable, as explained in Section 5.1.1.1. The methodology applied considers the forecasted days to be part of the historical values when forecasting a later day. Therefore, to perform the last forecast of 6 days ahead, the target vector should use the historical values plus the last 5 days obtained from forecasts. This methodology demonstrates the impact of forecasted days on future forecasts and enables the evaluation of the impact on the accuracy over time [141].

5.2.1.2 Results

Table 5.2 depicts the results of MAPE for $D1$, which corresponds to 1-day ahead, until $D6$, which corresponds to 6 days ahead. Figure 5.10 plots the results for the MAE to visually compare how both methods perform and compete along the forecasted time horizon. It can be observed that the ARIMAX method outperforms NARX method. Figure 5.10 illustrates how the error increases with the size of the time horizon. The following explanatory variables presented in Section 5.1.1.1 are also compared:

1. No explanatory variable
2. Demand as an explanatory variable
3. Competitive market as an explanatory variable.

Table 5.2: MAPE figure for ARIMAX and NARX in price forecasting

Method	**ARIMAX #1**	**ARIMAX #2**	**ARIMAX #3**	**NARX #1**	**NARX #2**	**NARX #3**
D1	2.88%	3.60%	2.65%	3.69%	3.95%	3.51%
D2	3.22%	3.73%	2.61%	3.71%	4.06%	3.51%
D3	3.36%	3.89%	2.80%	3.80%	4.07%	3.66%
D4	3.57%	3.83%	2.67%	3.79%	4.12%	3.67%
D5	3.60%	3.91%	2.75%	3.80%	4.39%	3.63%
D6	3.62%	4.26%	3.19%	3.85%	4.55%	3.70%

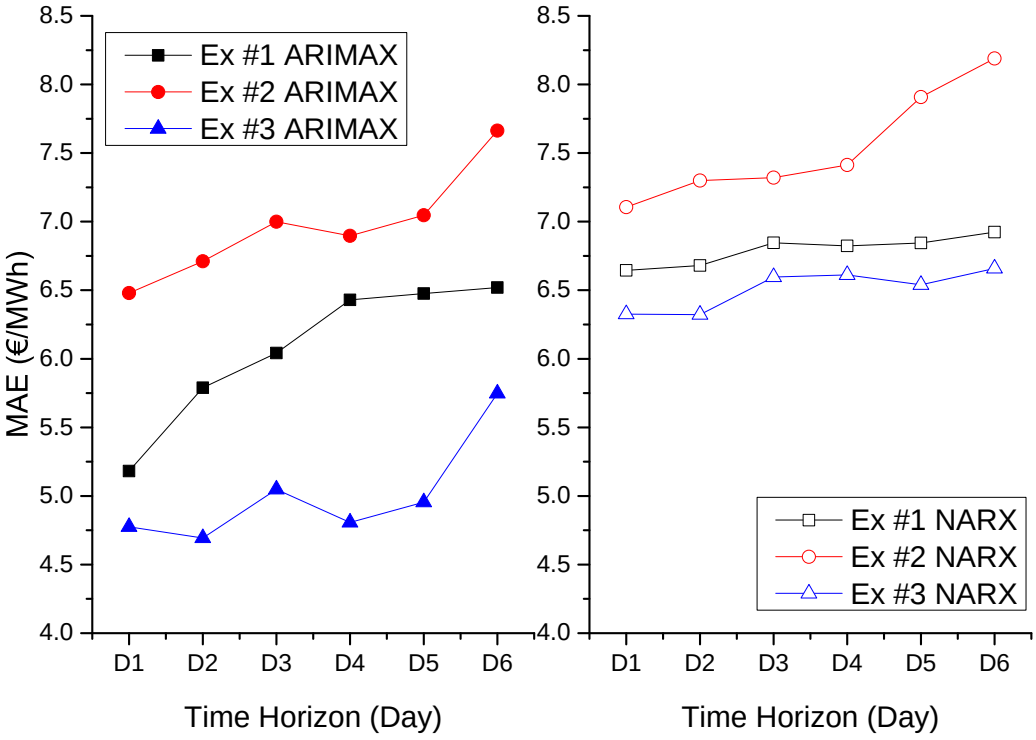

Figure 5.10: Forecasting MAE for both methods

5.2.1.3 Conclusion

This section presents the conclusions obtained from the energy market's forecasting results. Comparing the forecasts with the error figures presented in Section 5.2.1 indicate that the proposed ARIMAX method outperforms NARX in most cases. The lower average MAE is 4.78€/MWh, which was achieved by the ARIMAX model in the 1-day ahead forecast and using (#3) the competitive market as an explanatory variable. The highest average

MAE achieved is 8.19€/MWh, which was achieved by NARX model in the 6 days ahead forecast and using demand as the explanatory variable.

The best resulting explanatory variable option is the competitive market (#3), which is followed closely by the no explanatory variable option (#1). Using demand as the explanatory variable (#2) would be counterproductive because it is the worst option due to the low correlation between the variable and the target vector (0.41). Although the competitive market is the best option, its results are obtained with historical values, and no forecast error is included or evaluated. In reality, the competitive market variable is a forecasted variable that is composed of the forecasts of demand, solar, wind, and nuclear power; these forecasts are themselves subject to errors.

Similarly, the results indicate the influence of the time horizon on forecasting accuracy. The larger the time gap to the forecasted value, the higher the error. The influence of time is different for the different forecasting methods. When comparing the two best performing explanatory variable options, ARIMAX increases the MAE by an average daily base of 0.23€/MWh. However, NARX increases the error by an average daily base of 0.06€/MWh. Therefore, the NARX method is much less sensitive to errors for forecasted days. Figure 5.10 depicts both error trends. For the ARIMAX method, changing the forecast from 1 to 2 days ahead decreases the error from 4.76€/MWh to 4.69€/MWh.

5.2.1.4 Discussion

For a practical use of the 1-day ahead forecast, the no explanatory variable option would probably be the most accurate method. This is because of the small error difference between the no explanatory and competitive explanatory options (5.18€/MWh - 4.76€/MWh). The final error of the competitive explanatory option may increase in real life operation considering the error impact of forecasting the explanatory variable.

On the other hand, the ARIMAX method with no explanatory variable is the method that is the most sensitive to the time horizon, with a daily error increase of 0.27€/MWh. The results indicate that the ARIMAX method performed better than the NARX method for all explanatory variable options. The ARIMAX method had less errors, which results in a lower annual error average. However, both methods are accurate enough to be used as reliable forecasting tools. They indicate dependence on the time horizon, but this did not have much of an effect on accuracy. In any case, even long-term

forecasts can be useful for power generators and consumers.

5.2.2 Renewable Energy Forecast Results

5.2.2.1 Case Description

This section presents the results for solar and wind energy forecasting in Spain. The aim of this work is to propose a comparison between the two forecasting models for solar and wind power. Both methods are improved with a valid explanatory variable obtained from an NWP method. This comparison is carried out within the specific boundaries of the Spanish energy market. The forecasts focus on the daily market, forecast for 24 hours, and have a forecast horizon from +12 hours to +36 hours. The simulations are carried out for a significant week during winter: 10^{th} January 2015 to 17^{th} January 2015. The week is selected for having a typical variability in RES energy production. The results obtained for this week are similar to the results from other weeks.

A common approach to the forecast problem over a wide region is to calculate individual forecasts and sum the results up [142]; it can be expected that individual errors will partially cancel out when summing up the forecasts and thus result in a more accurate prediction [57]. An aggregated forecast approach for a country like Spain is an extremely complicated process due to the numerous installations, the variety of technologies, and the lack of historical generation information from each generator. Therefore, the approach taken in this section is to forecast the aggregated power for the Spanish peninsular market for each technology. The forecast methods are therefore supported with a valid explanatory variable that comprises a time series of hourly values.

Several combinations and configurations of ARIMAX and NARX models have been attempted to obtain the most accurate results. The configuration of each model is different for each energy source. The parameters that achieve the best set of results are presented in this section.

Two explanatory variables that improve the forecast are used here: one for solar forecasting, and the other for wind forecasting. To study the correlation between variables, Pearson and R^2 correlation studies have been carried out for the time series. The results for solar, where irradiation and national solar generation are taken into consideration, indicate a strong correlation: a Pearson factor of 0.90 and $\mathrm{R}^2 = 0.816$ as depicted in Figure 5.3. The data

series is depicted in Figure 5.11. The results for wind, where wind speed and national wind generation are taken into consideration, indicate a Pearson factor of 0.79 and an R^2 of 0.63 as depicted in Figure 5.4, the data series is depicted in Figure 5.11.

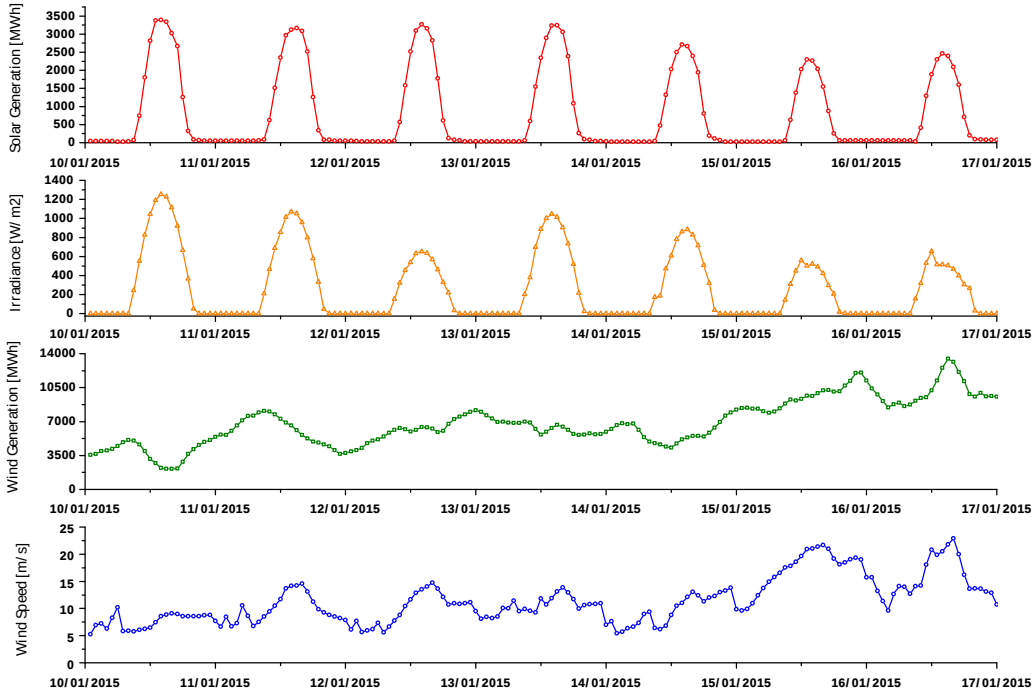

Figure 5.11: Renewable energies data series for forecasting

The errors between the forecasted values and the real data are analysed in this section to measure the accuracy of the predictions. To validate the forecast methods in this work, the following parameters are calculated:

- MAE, depicts the absolute deviation of the forecast. This provides the perception of the accuracy of the method in terms of energy. This parameter is particularly useful for market deviations.
- MAPE, depicts the same error divided by hourly generation. This parameter is useful for understanding the accuracy of the forecast method. The percentage of error escalates when the value of generation is close to zero.

- MADPE, depicts dividing the sum of the daily MAE by the sum of the daily generation: this parameter represents a relative daily error. This parameter is useful to understand the accuracy of the method on a daily basis and can address the MAPE drawback when generation is close to zero.

5.2.2.2 Results

ARIMAX and NARX models for solar and wind energy generation for 1 day ahead forecasts have been developed. Both the proposed models accept either the hourly irradiation or the wind speed as inputs. The outputs are the hourly values of either the solar generation or the wind generation in Spain. After several simulations for the four proposed methods, the best configuration provides the results for the evaluated representative weeks (10/01/2015 – 17/01/2015); these results are depicted in Table 5.3 and in Figure 5.12. The best configurations are found by following the methodology presented in Section 3.2.2. This methodology is based on selecting the most important lags for the ACF and PACF studies. The selected lags give information about correlation on the time series and only those which high impact are used.

Table 5.3: Renewable energy forecast error

	Error	**D1**	**D2**	**D3**	**D4**	**D5**	**D6**	**D7**	**Mean**
ARIMAX Solar	**MAE**	118	66	121	79	182	190	77	119.24
	MAPE	33.0%	32.9%	44.7%	20.5%	34.3%	51.6%	40.8%	36.83%
	MADPE	12.1%	7.3%	14.5%	8.9%	24.9%	32.7%	11.4%	15.98%
ARIMAX Wind	**MAE**	1054	1371	2377	1479	891	1597	1587	1479.30
	MAPE	25.3%	21.9%	36.2%	23.4%	15.2%	15.4%	14.3%	21.67%
	MADPE	27.4%	22.5%	39.1%	22.9%	15.0%	16.7%	15.7%	22.77%
NARX Solar	**MAE**	179	133	116	134	61	61	95	111.04
	MAPE	22.2%	32.5%	32.3%	36.9%	44.3%	43.7%	41.7%	36.26%
	MADPE	18.3%	14.6%	13.8%	15.1%	8.3%	10.5%	14.0%	13.51%
NARX Wind	**MAE**	1121	1423	900	388	581	410	1156	854.31
	MAPE	26.1%	24.2%	14.8%	5.9%	8.9%	4.2%	11.2%	13.62%
	MADPE	29.1%	23.4%	14.8%	6.0%	9.8%	4.3%	11.4%	14.12%

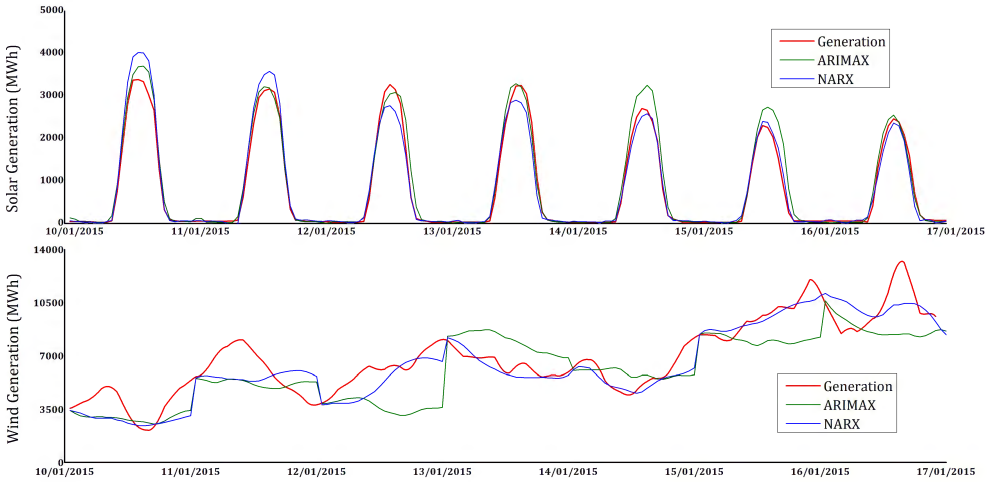

Figure 5.12: Renewable energy forecast results

5.2.2.3 Conclusion

This section presents the conclusions for the renewable forecast. The model is developed to obtain 24 hourly values as results for the 1 day ahead forecast or the main market that cover +12h to +36h. Both proposed models accept the time series to forecast and explanatory time series as inputs to improve the accuracy of the results. Solar power uses irradiation as the explanatory variable, as explained in Section 5.1.1.2. Wind power uses wind speed as the explanatory variable, as explained in Section 5.1.1.3. Once the forecasts are compared with the error figures, the results indicate that the proposed NARX method outperforms ARIMAX for both generation forecasts. The results also indicate that solar forecasts are more accurate than wind forecasts.

Nevertheless, the solar generation results for the ARIMAX and NARX methods are very close. The MAE and MAPE values are practically the same, and there is only a slight difference for MADPE when the NARX method (13.51%) outperforms the ARIMAX method (15.98%). This indicator is the most reliable for generations that have low values that are close to 0MWh: solar generation during dusk is one such example. The results are much clearer for wind generation. The NARX method outperforms the ARIMAX method for every error figure. In terms of MAPE, the average value for NARX and ARIMAX are 13.62% and 21.67% respectively. The MADPE

values are similar to MAPE in this case.

The results of the performance achieved with the NARX method for solar and wind forecasts in terms of MADPE are very similar: 13.51% for solar and 14.12% for wind. On the other hand, the results obtained with the ARIMAX method in terms of MADPE differ for solar and wind forecasts. The solar forecast is 15.98%, which is similar to the result for NARX, but the result for wind generation is much worse: 22.77%. This is the worst result from any of the proposed forecasting methods. These error figures are for 1-day ahead market forecasts; if the time horizon were longer, the error would escalate.

5.2.3 Thermal Energy Demand Forecast Results

5.2.3.1 Case Description

The optimal management of a DHC addresses problems such as the optimisation of the pumping supply energy and the minimisation of heat loss. The variability of the load creates situations where predicted information becomes very useful for managing different possibilities to supply that energy. This chapter evaluates the effect of forecasting error when optimising supply temperature. This evaluation is carried out on the 4 typical weeks selected for each season that were presented in Section 4.1.6.

Demand forecasts are based on historical data, and temperature is used as the explanatory variable. This forecast uses ARIMAX because it is more stable and has accurate forecasting values. The results of the demand forecast are depicted in Table 5.4. Once the forecasted energy demand and supply requirements are known, it is necessary to develop a model to calculate the future associated heat loss in the district network. This model should accord with the expected demand and be based on the topology of the district network, as explained in Section 4.1.5. Energy supply heat losses are related to distribution temperature. In this calculation, return temperature is fixed, and the supply temperature varies with the optimisation. A network operator that possesses information about future behavior in the DHC would be able to manage and optimise the energy generation of the power plant as well as minimise the cost of the pumping station and the heat loss without reducing service quality.

Once the total supply demand is calculated, it is possible to optimise the pumping station's consumption, which will vary with the different flow temperature. When energy costs are assigned to the heat loss and pumping

requirements, it becomes possible to pursue an optimum supply temperature to deliver energy to the customers .

The demand forecast algorithm estimates hourly energy values for each customer. These values are aggregated to a total demand of either cooling or heating and are compared with the real demand afterward. The demand forecast results that were calculated in Section 4.3.4 are used in this section. Figure 4.26 compares the real heating or cooling demand with the aggregated forecast. Table 5.4 presents the MAE demand (in kWh) and MAPE errors for comparison. The real demand is similar to the predicted values. Nevertheless, the results of forecasting are only used as one step in the optimisation process. Ergo, the error is propagated, and only the difference between the optimal real supply temperature and the optimal forecasted supply temperature should be taken into consideration.

Table 5.4: MAE and MAPE forecasting errors for demand

Season	**Heating**		**Cooling**	
	MAE	**MAPE**	**MAE**	**MAPE**
Winter	153.20	4.98%	26.56	1.16%
Spring	81.17	2.64%	6.58	0.29%
Summer	72.78	2.36%	132.95	5.80%
Autumn	51.41	1.67%	74.92	3.27%
AVERAGE	89.64	2.91%	60.25	2.63%

5.2.3.2 Results

Figure 4.26 depicts how demand forecast is accurate. The optimisation results are only significantly affected on those days when the forecast differs significantly from the real demand. One example is the first day (Monday) of the autumn week for cooling: the demand forecast values are lower than in reality, and the forecasted optimised temperature is higher than the real optimised temperature. Figure 5.13 depicts the ideal results of optimised temperatures using real and forecasted results. Table 5.5 depicts the MAE and MAPE errors for the 4 weeks that represent the seasons.

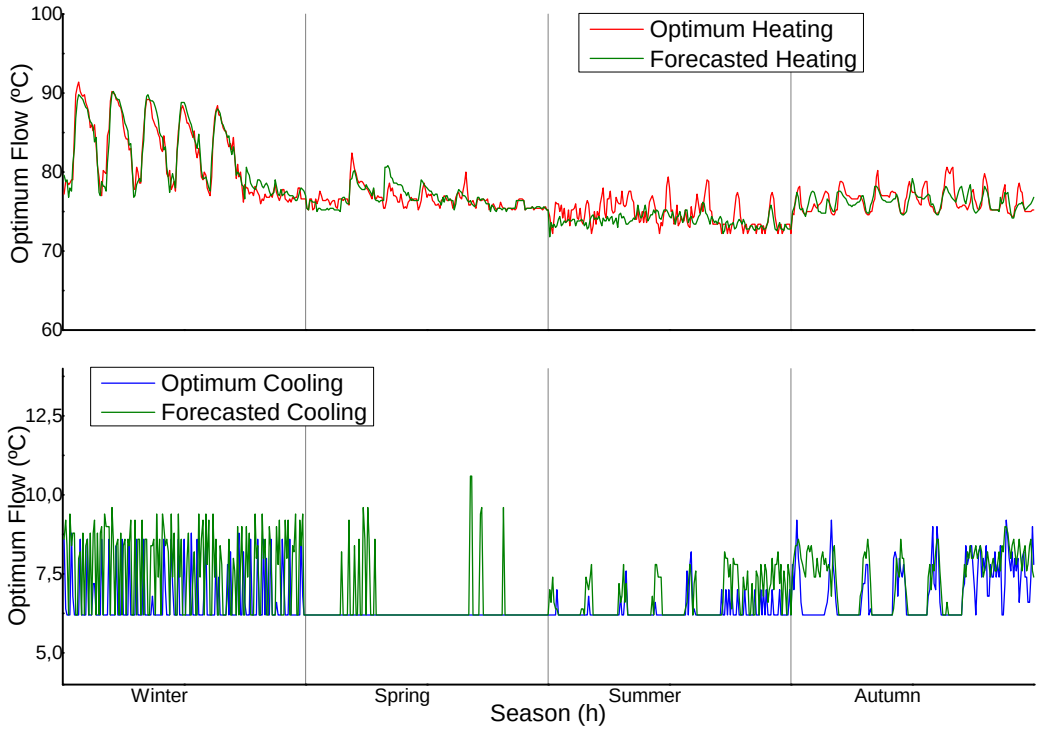

Figure 5.13: Supply temperatures for heating and cooling in the DHC

Table 5.5: Demand forecast error

Season	**MAE**		**MAPE**	
	Heating	**Cooling**	**Heating**	**Cooling**
Winter	0.97°C	1.40°C	3.1%	23.3%
Spring	0.70°C	0.25°C	2.2%	4.2%
Summer	1.31°C	0.40°C	4.2%	6.7%
Autumn	0.99°C	0.57°C	3.2%	9.5%
AVERAGE	0.99°C	0.66°C	3.2%	11.0%

5.2.3.3 Conclusions

To optimise the supply temperature, the thermal demand has been forecasted using the explanatory variable presented in Section 5.1.1.4. The demand prediction is used to optimise the supply temperature to minimise distribution

costs. These results indicate low errors in terms of MAPE: 2.91% for heating and 2.63% for cooling demand forecasting. The higher errors can be found in low-demand season, which means winter for cooling and summer for heating. The error for cooling in winter is particularly high as the ΔT for cooling energy is usually 6°C. Such errors are propagated to the optimal supply temperature, which achieved a much higher error rate: 3.2% for heating and 11.0% for cooling. Besides the increase in MAPE due to error propagation, the average MAE for temperature was as low as 0.99°C and 0.66°C for heating and cooling. This error is so low that it can be neglected, because the temperature regulation is not always as sharp as observable from Figure 4.23. Therefore, the method and demand forecast can be used for supply temperature optimisation.

Chapter 6

Conclusions

6.1 Conclusions

In this thesis, parts of the EMS optimisation tool XEMS13 for hybrid power plant generators were developed and used. The tool has proven to be suitable for planning, studying modifications, and managing power plants [62, 105, 122]. The optimisation uses a steady-state power flow approach by dividing the time horizon into time steps where the boundary conditions are fixed and invariable. The results provided by the EMS are the generators' schedules on hourly bases, where the load is matched with a mix of energy generators without the help of energy storage.

The EMS can work with different power plant configurations and with different hybrid systems that provide heating, cooling, and electricity to the customers.

The EMS has been used to find solutions to real problems in generation and to seek improvement of day-to-day operations. As depicted in Section 4.3.1 and in [61], a real-life situation of cooling generation was optimised considering condensing boundaries. Condensing restrictions can be minimised with the use of EMS and weather information. The selection of a proper generation strategy can avoid cooling shortages in the face of extreme climatic conditions. An application of the EMS to improve power plant efficiency is presented in Section 4.3.2 and in [117]. The improvement comes from controlling supply temperature to decrease heat loss and harness thermal mass. The decrease of heat loss implies lower energy requirements for power plant generation. Thus, there is an excess of energy to be stored in the energy

storage system and in the network's thermal mass to avoid auxiliary generation. The EMS is also used for day-to-day scheduling of the power plant that uses thermal demand and energy prices to provide generation and supply strategies.

To implement these improvements in the power plant, some modifications were carried out on the plant during this researches.

- Dataloggers were installed to establish communication between thermal substations and the power plant's SCADA; this enables the acquisition of thermal demand information in real time.
- Installation of two three-way valves that mix generation and DH return water to obtain the desired heating supply temperature.
- Include an hourly table to fix the supply temperature set point in the power plant's SCADA. This set point is sought for the three-way valve.

This thesis and the improvements to the power plant have assisted SAMPOL to gain maturity and awareness in O&M, thereby achieving the aims presented in Section 1.3. This thesis is the beginning of energy supply optimisation research for the company and has provided knowledge on heat loss and smart thermal distribution. Similarly, SAMPOL has gained important knowledge about storage, DHC networks, and improvements in energy storage usage [26]. In the future, it will be necessary to use the EMS to schedule the CHP's operation demand forecasts and energy price forecasts.

Demand forecasts do not have a significant influence on plant scheduling optimisation because demand does not vary significantly over weeks. Moreover, this information can only influence the CHP load. The CHP is never scheduled in partial load for practical reasons and also because at partial load, the efficiency of the CHP decreases compared to the nominal regimen. Nevertheless, if the demand is higher than the CHP's thermal generation, the auxiliary boilers match the demand. This means than whenever the demand is higher than the CHP generation, the demand forecast error does not influence the final power plant schedule. Thus, the thermal demand forecast does not have a significant impact on CHP scheduling or power plant scheduling. As Section 4.3.4 notes, an average heating error of 2.91% and an average cooling error of 2.63% has an impact of 0.48% on the optimisation.

On the other hand, thermal forecast gains importance in terms of temperature supply optimisation. The demand forecast influences the difference

between the mass flow and temperature , which are optimised with the EMS. Section 5.2.3 and [21] indicate that the same forecasting error has an impact on the optimisation of 3.2% for heating and 11.0% for cooling. Despite the increase in error for optimisation, the actual supply temperature error is below 1°C, which is admissible.

Energy price forecasts play a more important role in energy optimisation than thermal forecasts. Price Forecaster had a very important role during 2013, when the prices were subjected to great variability and when it made a difference to the CHP schedule due to low prices [141]. Practically speaking, energy price forecasts are important when the market price is close to the break-even point of the CHP. In real operations, energy price forecasts are used to modify (if required) the weekly pre-scheduled generation in case there are operators available. As noted in Section 4.3.4, energy price forecasts have a greater impact on optimisation than its error; an average error of 2.75% has an average impact of 4.74% on the optimisation. This demonstrates that the real goal of forecasting in this thesis is not accuracy but forecasting's impact on power plant optimisation.

Renewable energy forecasts were needed to obtain energy price forecasts. As observed in Section 5.2.2 and [98, 60], although the errors achieved in the forecasting of RES power were not very low, they were insignificant when used for the purpose of generating the explanatory variable. Although the RES forecast is useful, the transport system operator currently provides a longer horizon and more accurate solar and wind forecasts. This was the main reason to abandon this line of research within this thesis and use transport system operator RES forecasts to forecast energy prices.

Energy price forecasting that uses a transport system operator forecast would likely be the most accurate method for practical 1-day ahead forecasting. This method is used when the energy prices are close to the cost of starting the CHP engines, and it is possible to modify the operator's shift. In reality, this situation does not happen often.

This thesis was proposed as an optimisation for a solar DHC. Thus, a solar generation forecaster was developed in expectation of a future scenario where a solar collector field becomes a viable option. One practical outcome of this thesis is that a hypothesis and some theoretical results are enough to change old-fashioned strategies. It would be interesting to calculate the starting point to evaluate the degree of improvement of the new strategy, but it is not always easy to compare with a baseline.

6.2 Future Research

The work and tasks developed in this thesis have been carried out as part of an industrial PhD research. Therefore, they are naturally applicable to real-life problems. This work has enabled the company to gain knowledge and know-how in the field of power plant optimisation and the operational implications of heat losses, thermal inertia harnessing, and cooling generation. This knowledge was gained from the different studies performed with the proposed EMS, which is based on Matlab.

This line of research remains open to further development and improvement. For technical reasons and to increase usability, the next step is to upload an EMS to a web platform which all the power plant operators can easily access. Other potential areas for research include close-real time simulations and predictive modelling. The idea of a 'digital twin' can also be pursued in the near future. This digital twin can simulate real-life situations and learn from the real power plant.

With regard to forecasting, this thesis has developed a useful forecaster of energy prices that can forecast up to 7 days ahead. These forecasts are useful for weekly scheduling of energy sales to the grid. One possible future research line is to forecast market tendencies to understand when would be more profitable to run the CHP over the year. On the other hand, the renewable energy forecast research line is unlikely to be continued in SAMPOL due the nonexistence of renewable energy installations.

6.3 Dissemination

The work carried out in this thesis has been disseminated in five journal publications, presented in seven international conferences and it has obtained three different awards.

6.3.1 Journal Publications

Optimal management of a complex DHC plant, authored by **N. Perez-Mora**, P. Lazzeroni, V. Martinez-Moll, M. Repetto, and published in Energy Conversion and Management 145 (2017) 386-397. doi:10.1016/j.enconman.2017.05.002.

Solar district heating and cooling: A review, authored by **N. Perez-Mora**, F. Bava, M. Andersen, C. Bales, G. Lennermo, C. Nielsen, S. Furbo, V. Martinez-Moll, and published in International Journal of Energy Research 42 (4) (2018). 1419-1441. doi:10.1002/er.3888.

Optimal DHC energy supply harnessing its thermal mass, authored by **N. Perez-Mora**, P. Lazzeroni, V. Martinez-Moll, M. Repetto, and published in Applied Thermal Engineering 133 (October 2017) (2018) 520-531. doi:10.1016 /j.applthermaleng.2018.01.072.

Spanish Energy Market. Overview towards price forecast, authored by **N. Perez-Mora**, V. Martinez-Moll, and published in International Journal of Energy Economics and Policy 8 (3)(2018) 1-7. ISSN: 2146-4553.

DHC Supply and Generation Optimization towards 4^{th} *Generation*, authored by **N. Perez-Mora**, P. Lazzeroni, V. Martinez-Moll, M. Repetto, and published in International EuroHeat&Power Magazine (issue IV/2018) p.17-20. ISSN 1613-0200-22698.

6.3.2 Congress Proceedings

Short-Term Spanish Aggregated Solar Energy Forecast, authored by **N. Perez-Mora**, V. Canals, V. Martinez-Moll, presented in 13th International Work-Conference on Artificial Neural Networks, IWANN 2015, and published on proceedings no. 07122, Springer Verlag, Palma de Mallorca (Spain), 2015, pp. 307-319. doi:10.1007/978-3-319-19222-226.

Spanish Renewable Energy Generation Short-Term Forecast, authored by **N. Perez-Mora**, V. Martinez-Moll, V. Canals, presented in ISES Solar World Congress 2015, and published on proceedings International Solar Energy Society, Freiburg, Germany, 2016, pp. 1-12. doi:10.18086/swc.2015.07.10.

DHC Load Management Using Demand Forecast, authored by **N. Perez-Mora**, V. Martinez-Moll, V. Canals, presented in SHC 2015 International Conference on Solar Heating and Cooling for Buildings and Industry, and published on proceedings Energy Procedia 91 (C) (2016) 557-566. doi:10.1016 /j.egypro.2016.06.198.

Optimal Solar District Cooling Harvesting Scenarios, authored by **N. Perez-Mora**, P. Lazzeroni, M. Repetto, V. Canals, V. Martinez-Moll, presented in EuroSun2016, and published on proceedings International Solar Energy Society, Freiburg, Germany, 2016, pp. 1-11. doi:10.18086/eurosun.2016.05.07.

XEMS13: An hybrid-Energy generation Management System, authored by **N. Perez-Mora**, P. Lazzeroni, M. Repetto, presented in 2016 IEEE International Conference on Smart Grid Communications (SmartGridComm), and published on proceedings IEEE SmartGridComm, IEEE, 2016, pp. 20-25. doi:10.1109/SmartGridComm. 2016.7778732.

Spanish Energy Market. Overview towards price forecast, authored by **N. Perez-Mora**, V. Martinez-Moll, presented in 3rd International Conference New Energy and Future Energy Systems, NEFES 2017, in Kunming, China, and published on the conference proceedings.

Optimization of District Heating and Cooling Power Plant: the case of Parc Bit, authored by **N. Perez-Mora**, V. Martinez-Moll, presented in 12th Conference on Sustainable Develpment of Energy, Water and Environment Systems, SDEWES 2017, in Dubrovnik, Croatia, and published on the conference proceedings.

6.3.3 Awards

Best Oral Presentation awarded at the 3rd International Conference New Energy and Future Energy Systems, NEFES 2017, in Kunming, China on 24th September 2017.

2nd place winner at ***6th International DHC+ student award*** awarded by DHC+ & International Energy Agency at the Global District Energy Days in Helsinki, Finland on 26th September 2018.

Runner-up of the prize Best Energy Management for Large Enterprises ***VI Premios eficiencia energética A3e - El Instalador*** awarded by Asociación de Empresas de Eficiencia Energética at the IV Foro Nacional de Eficiencia Energética (FOROGEn) in Madrid, Spain on 22nd November 2018.

Bibliography

[1] SHINE.
URL https://www.uni-kassel.de/projekte/solnet-shine/home.html

[2] Gartner, Planning Guide for Data and Analytics, Tech. rep., Gartner (2017).
URL https://www.gartner.com/binaries/content/assets/events/keywords/catalyst/catus8/2017_planning_guide_for_data_analytics.pdf

[3] M. S. Jamel, A. Abd Rahman, A. H. Shamsuddin, Advances in the integration of solar thermal energy with conventional and non-conventional power plants, Renewable and Sustainable Energy Reviews 20 (2013) 71–81. doi:10.1016/j.rser.2012.10.027.
URL http://dx.doi.org/10.1016/j.rser.2012.10.027

[4] O. Ibrahim, F. Fardoun, R. Younes, H. Louahlia-Gualous, Review of water-heating systems: General selection approach based on energy and environmental aspects, Building and Environment 72 (2014) 259–286. doi:10.1016/j.buildenv.2013.09.006.

[5] M. Sivak, Potential energy demand for cooling in the 50 largest metropolitan areas of the world: Implications for developing countries, Energy Policy 37 (4) (2009) 1382–1384. doi:10.1016/j.enpol.2008.11.031.

[6] European Commission Directorate-General for Energy, Energy climate policy framework EU 2020-2030, Tech. Rep. 2013, European Commission, Brussels (2014).

[7] D. F. Dominković, B. Ćosić, Z. Bačelić Medić, N. Duić, A hybrid optimization model of biomass trigeneration system combined with

pit thermal energy storage, Energy Conversion and Management 104 (2015) 90–99. doi:10.1016/j.enconman.2015.03.056.

[8] H. Al Moussawi, F. Fardoun, H. Louahlia-Gualous, Review of trigeneration technologies: Design evaluation, optimization, decision-making, and selection approach, Energy Conversion and Management 120 (2016) 157–196. doi:10.1016/j.enconman.2016.04.085.
URL http://dx.doi.org/10.1016/j.enconman.2016.04.085

[9] F. A. Al-Sulaiman, F. Hamdullahpur, I. Dincer, Trigeneration: A comprehensive review based on prime movers, International Journal of Energy Research 35 (3) (2011) 233–258. doi:10.1002/er.1687.
URL http://doi.wiley.com/10.1002/er.1687

[10] D. Connolly, H. Lund, B. V. Mathiesen, M. Leahy, A review of computer tools for analysing the integration of renewable energy into various energy systems, Applied Energy 87 (4) (2010) 1059–1082. doi:10.1016/j.apenergy.2009.09.026.
URL http://dx.doi.org/10.1016/j.apenergy.2009.09.026

[11] G. Chicco, P. Mancarella, Distributed multi-generation: A comprehensive view, Renewable and Sustainable Energy Reviews 13 (3) (2009) 535–551. doi:10.1016/j.rser.2007.11.014.

[12] G. Chicco, P. Mancarella, From cogeneration to trigeneration: Profitable alternatives in a competitive market, IEEE Transactions on Energy Conversion 21 (1) (2006) 265–272. doi:10.1109/TEC.2005.858089.

[13] Y. Wang, Y. Huang, E. Chiremba, A. P. Roskilly, N. Hewitt, Y. Ding, D. Wu, H. Yu, X. Chen, Y. Li, J. Huang, R. Wang, J. Wu, Z. Xia, C. Tan, An investigation of a household size trigeneration running with hydrogen, Applied Energy 88 (6) (2011) 2176–2182. doi:10.1016/j.apenergy.2011.01.004.
URL http://dx.doi.org/10.1016/j.apenergy.2011.01.004

[14] P. J. Mago, L. M. Chamra, Analysis and optimization of CCHP systems based on energy, economical, and environmental considerations, Energy and Buildings 41 (10) (2009) 1099–1106. doi:10.1016/j.enbuild.2009.05.014.

[15] J. Wang, Z. J. Zhai, Y. Jing, C. Zhang, Particle swarm optimization for redundant building cooling heating and power system, Applied Energy 87 (12) (2010) 3668–3679. doi:10.1016/j.apenergy.2010.06.021.
URL http://dx.doi.org/10.1016/j.apenergy.2010.06.021

[16] H. Ghaebi, M. H. Saidi, P. Ahmadi, Exergoeconomic optimization of a trigeneration system for heating, cooling and power production purpose based on TRR method and using evolutionary algorithm, Applied Thermal Engineering 36 (1) (2012) 113–125. doi:10.1016/j.applthermaleng.2011.11.069.
URL http://dx.doi.org/10.1016/j.applthermaleng.2011.11.069

[17] H. Cho, P. J. Mago, R. Luck, L. M. Chamra, Evaluation of CCHP systems performance based on operational cost, primary energy consumption, and carbon dioxide emission by utilizing an optimal operation scheme, Applied Energy 86 (12) (2009) 2540–2549. doi:10.1016/j.apenergy.2009.04.012.
URL http://dx.doi.org/10.1016/j.apenergy.2009.04.012

[18] T. A. Williams, M. Bohn, H. W. Price, Solar Thermal Hybridization Issues, Tech. Rep. October 1994, National Renewable Energy Laboratory (1995).

[19] M. Isaac, D. P. van Vuuren, Modeling global residential sector energy demand for heating and air conditioning in the context of climate change, Energy Policy 37 (2) (2009) 507–521. doi:10.1016/j.enpol.2008.09.051.

[20] A. Poredos, A. Kitanovski, District heating and cooling for efficient energy supply, 2011 International Conference on Electrical and Control Engineering (2011) 5238–5241doi:10.1109/ICECENG.2011.6058201.

[21] N. Perez-Mora, V. Martinez-Moll, V. Canals, DHC Load Management Using Demand Forecast, Energy Procedia 91 (C) (2016) 557–566. doi:10.1016/j.egypro.2016.06.198.

[22] J. L. Fannou, C. Rousseau, L. Lamarche, K. Stanislaw, Experimental analysis of a direct expansion geothermal heat pump in heating mode, Energy and Buildings 75 (2014) 290–300.

doi:10.1016/j.enbuild.2014.02.026.
URL http://dx.doi.org/10.1016/j.enbuild.2014.02.026

[23] B. Rezaie, M. a. Rosen, District heating and cooling: Review of technology and potential enhancements, Applied Energy 93 (2012) 2–10. doi:10.1016/j.apenergy.2011.04.020.
URL http://dx.doi.org/10.1016/j.apenergy.2011.04.020

[24] W. Gang, S. Wang, F. Xiao, D. C. Gao, District cooling systems: Technology integration, system optimization, challenges and opportunities for applications, Renewable and Sustainable Energy Reviews 53 (2016) 253–264. doi:10.1016/j.rser.2015.08.051.
URL http://dx.doi.org/10.1016/j.rser.2015.08.051

[25] H. Lund, S. Werner, R. Wiltshire, S. Svendsen, J. E. Thorsen, F. Hvelplund, B. V. Mathiesen, 4th Generation District Heating (4GDH). Integrating smart thermal grids into future sustainable energy systems., Energy 68 (2014) 1–11. doi:10.1016/j.energy.2014.02.089.
URL http://dx.doi.org/10.1016/j.energy.2014.02.089

[26] N. Perez-Mora, F. Bava, M. Andersen, C. Bales, G. Lennermo, C. Nielsen, S. Furbo, V. Martínez-Moll, Solar district heating and cooling: A review, International Journal of Energy Research 42 (4) (2018) 1419–1441. doi:10.1002/er.3888.
URL http://doi.wiley.com/10.1002/er.3888

[27] Y. Li, Y. Rezgui, H. Zhu, District heating and cooling optimization and enhancement – Towards integration of renewables, storage and smart grid, Renewable and Sustainable Energy Reviews 72 (2017) 281–294. doi:10.1016/j.rser.2017.01.061.

[28] D. Olsthoorn, F. Haghighat, P. A. Mirzaei, Integration of storage and renewable energy into district heating systems: A review of modelling and optimization, Solar Energy 136 (2016) 49–64. doi:10.1016/j.solener.2016.06.054.

[29] J. Söderman, Optimisation of structure and operation of district cooling networks in urban regions, Applied Thermal Engineering 27 (16 SPEC. ISS.) (2007) 2665–2676. doi:10.1016/j.applthermaleng.2007.05.004.

[30] H. Tol, S. Svendsen, Improving the dimensioning of piping networks and network layouts in low-energy district heating systems connected to low-energy buildings: A case study in Roskilde, Denmark, Energy 38 (1) (2012) 276–290. doi:10.1016/j.energy.2011.12.002.

[31] B. Bøhm, H. Kristjansson, Single, twin and triple buried heating pipes: On potential savings in heat losses and costs, International Journal of Energy Research 29 (14) (2005) 1301–1312. doi:10.1002/er.1118.

[32] Y. Başoğul, A. Keçebaş, Economic and environmental impacts of insulation in district heating pipelines, Energy 36 (10) (2011) 6156–6164. doi:10.1016/j.energy.2011.07.049.

[33] M. Pirouti, A. Bagdanavicius, J. Ekanayake, J. Wu, N. Jenkins, Energy consumption and economic analyses of a district heating network, Energy 57 (2013) 149–159. doi:10.1016/j.energy.2013.01.065.
URL http://dx.doi.org/10.1016/j.energy.2013.01.065

[34] J. Danielewicz, B. Sniechowska, M. A. Sayegh, N. Fidorow, H. Jouhara, B. Gniechowska, M. A. Sayegh, N. Fidorow, H. Jouhara, Three-dimensional numerical model of heat losses from district heating network pre-insulated pipes buried in the ground, Energy 108 (2016) 172–184. doi:10.1016/j.energy.2015.07.012.

[35] M. Perpar, Z. Rek, S. Bajric, I. Zun, Soil thermal conductivity prediction for district heating pre-insulated pipeline in operation, Integration and Energy System Engineering, European Symposium on Computer-Aided Process Engineering 2011 44 (1) (2012) 197–210. doi:10.1016/j.energy.2012.06.037.

[36] D. Hillel, Introduction to Soil Physics, Elsevier, Amhersty, MA, 1982. doi:10.1016/C2009-0-03052-9.
URL http://linkinghub.elsevier.com/retrieve/pii/C20090030529

[37] G. a. Florides, S. a. Kalogirou, Annual ground temperature measurements at various depths, Proceedings of CLIMA 2005 (2005) ?doi:Proceedings of CLIMA 2005, Lausanne, Switzerland.

[38] H. Tol, S. Nielsen, S. Svendsen, Case studies in low[HYPHEN]energy district heating systems : Determination of dimensioning methods for

planning the future heating infrastructure, in: IFME World Congress of Municipal Engineering, 2012, p. 1.

[39] A. Dalla Rosa, H. Li, S. Svendsen, Method for optimal design of pipes for low-energy district heating, with focus on heat losses, Energy 36 (5) (2011) 2407–2418. doi:10.1016/j.energy.2011.01.024.

[40] A. Dalla Rosa, J. Christensen, Low-energy district heating in energy-efficient building areas, Energy 36 (12) (2011) 6890–6899. doi:10.1016/j.energy.2011.10.001.

[41] Y. Li, L. Fu, S. Zhang, X. Zhao, A new type of district heating system based on distributed absorption heat pumps, Energy 36 (7) (2011) 4570–4576. doi:10.1016/j.energy.2011.03.019.
URL http://dx.doi.org/10.1016/j.energy.2011.03.019

[42] C. Bordin, A. Gordini, D. Vigo, An optimization approach for district heating strategic network design, European Journal of Operational Research 252 (1) (2014) 296–307. doi:10.1016/j.ejor.2015.12.049.
URL http://dx.doi.org/10.1016/j.ejor.2015.12.049

[43] M. Noussan, M. Jarre, A. Poggio, Real operation data analysis on district heating load patterns, Energy 129 (2017) 70–78. doi:10.1016/j.energy.2017.04.079.

[44] M. Kuosa, K. Kontu, T. Mäkilä, M. Lampinen, R. Lahdelma, Static study of traditional and ring networks and the use of mass flow control in district heating applications, Applied Thermal Engineering 54 (2) (2013) 450–459. doi:10.1016/j.applthermaleng.2013.02.018.
URL http://dx.doi.org/10.1016/j.applthermaleng.2013.02.018

[45] M. Vesterlund, J. Dahl, A method for the simulation and optimization of district heating systems with meshed networks, Energy Conversion and Management 89 (2015) 555–567. doi:10.1016/j.enconman.2014.10.002.
URL http://dx.doi.org/10.1016/j.enconman.2014.10.002

[46] K. Sartor, P. Dewalef, Experimental validation of heat transport modelling in district heating networks, Energy- doi:10.1016/j.energy.2017.02.161.

[47] K. Sartor, D. Thomas, P. Dewallef, A comparative study for simulating heat transport in large district heating networks., Proceedings of Ecos 2015 - the 28Th International Conference on Efficiency, Cost, Optimization, Simulation and Environmental Impact of Energy Systems.

[48] Z. Li, W. Wu, M. Shahidehpour, J. Wang, B. Zhang, Combined heat and power dispatch considering pipeline energy storage of district heating network, IEEE Transactions on Sustainable Energy 7 (1) (2016) 12–22. doi:10.1109/TSTE.2015.2467383.

[49] W. Gu, J. Wang, S. Lu, Z. Luo, C. Wu, Optimal operation for integrated energy system considering thermal inertia of district heating network and buildings, Applied Energy 199 (2017) 234–246. doi:10.1016/j.apenergy.2017.05.004.
URL http://dx.doi.org/10.1016/j.apenergy.2017.05.004

[50] J. Zheng, Z. Zhou, J. Zhao, J. Wang, Integrated heat and power dispatch truly utilizing thermal inertia of district heating network for wind power integration, Applied Energy 211 (November 2017) (2018) 865–874. doi:10.1016/j.apenergy.2017.11.080.

[51] P. Li, H. Wang, Q. Lv, W. Li, Combined Heat and Power Dispatch Considering Heat Storage of Both Buildings and Pipelines in District Heating System for Wind Power Integration, Energies 10 (7) (2017) 893. doi:10.3390/en10070893.
URL http://www.mdpi.com/1996-1073/10/7/893

[52] K. Difs, M. Danestig, L. Trygg, Increased use of district heating in industrial processes. Impacts on heat load duration, Applied Energy 86 (11) (2009) 2327–2334. doi:10.1016/j.apenergy.2009.03.011.

[53] C. Monteiro, T. Santos, L. A. Fernandez-Jimenez, I. J. Ramirez-Rosado, M. S. Terreros-Olarte, Short-term power forecasting model for photovoltaic plants based on historical similarity, Energies 6 (2013) 2624–2643. doi:10.3390/en6052624.

[54] O. D. Rubin, B. a. Babcock, The impact of expansion of wind power capacity and pricing methods on the efficiency of deregulated electricity markets, Energy 59 (2013) 676–688. doi:10.1016/j.energy.2013.07.020.

[55] O. Operator, Daily and intraday electricity market operating rules, Tech. Rep. July, OMEL, Madrid, Spain (2013).

[56] REE, El Sistema Eléctrico Español, Tech. rep., Red Eléctrica de España, Madrid, Spain (2016).

[57] S. Flake, W. Mueller, An ASM Definition of the Dynamic OCL 2.0 Semantics, in: International Conference on Renewable Energies and Power Quality (ICREPQ'14), no. 12, Springer Verlag, Cordoba (Spain), 2004, pp. 226–240. doi:10.1007/978-3-540-30187-5-17.

[58] C. Chen, S. Duan, T. Cai, B. Liu, Online 24-h solar power forecasting based on weather type classification using artificial neural network, Solar Energy 85 (11) (2011) 2856–2870. doi:10.1016/j.solener.2011.08.027.
URL http://dx.doi.org/10.1016/j.solener.2011.08.027

[59] F. Cassola, M. Burlando, Wind speed and wind energy forecast through Kalman filtering of Numerical Weather Prediction model output, Applied Energy 99 (2012) 154–166. doi:10.1016/j.apenergy.2012.03.054.
URL http://dx.doi.org/10.1016/j.apenergy.2012.03.054

[60] N. Perez-Mora, V. Martinez-Moll, V. Canals, Spanish Renewable Energy Generation Short-Term Forecast, in: Proceedings of the ISES Solar World Congress 2015, no. November, International Solar Energy Society, Freiburg, Germany, 2016, pp. 1–12. doi:10.18086/swc.2015.07.10.
URL http://proceedings.ises.org/citation?doi=swc.2015.07.10

[61] N. Perez-Mora, P. Lazzeroni, V. V. Martínez-Moll, M. Repetto, Optimal management of a complex DHC plant, Energy Conversion and Management 145 (2017) 386–397. doi:10.1016/j.enconman.2017.05.002.
URL http://linkinghub.elsevier.com/retrieve/pii/S0196890417304260

[62] N. Perez-Mora, P. Lazzeroni, M. Repetto, XEMS13: An hybrid-Energy generation Management System, in: 2016 IEEE International Conference on Smart Grid Communications (SmartGridComm), no. IEEE International Conference on Smart Grid Communications, IEEE, 2016, pp. 20–25. doi:10.1109/SmartGridComm.2016.7778732.
URL http://ieeexplore.ieee.org/document/7778732/

[63] J. Zhang, B. Ge, H. Xu, An equivalent marginal cost-pricing model for the district heating market, Energy Policy 63 (2013) 1224–1232. doi:10.1016/j.enpol.2013.09.017.
URL http://dx.doi.org/10.1016/j.enpol.2013.09.017

[64] Euroheat & Power, Combined Heat and Power and District Heating in the EU Emissions Trading Scheme, Tech. Rep. July, Euroheat & Power (2007).
URL www.ecoheatcool.org

[65] H. Li, Q. Sun, Q. Zhang, F. Wallin, A review of the pricing mechanisms for district heating systems, Renewable and Sustainable Energy Reviews 42 (2015) 56–65. doi:10.1016/j.rser.2014.10.003.
URL http://dx.doi.org/10.1016/j.rser.2014.10.003

[66] S. Werner, N. Constantinescu, EcoHeatCool WP1: The European heat market, Work package deliverable of Ecohaetcool EU project (2006) 58–62.

[67] European Technology Platform on Renewable Heating and Cooling, Common Implementation Roadmap for Renewable Heating and Cooling Technologies, Tech. rep., European Technology Platform on Renewable Heating and Cooling (2014).
URL www.rhc-platform.org

[68] F. Freschi, L. Giaccone, P. Lazzeroni, M. Repetto, Economic and environmental analysis of a trigeneration system for food-industry: A case study, Applied Energy 107 (2013) 157–172. doi:10.1016/j.apenergy.2013.02.037.

[69] P. Mancarella, Distributed multi-generation options to increase environmental efficiency in smart cities, in: 2012 IEEE Power and Energy Society General Meeting, IEEE, 2012, pp. 1–8. doi:10.1109/PESGM.2012.6345129.

[70] E. Carpaneto, P. Lazzeroni, M. Repetto, Optimal integration of solar energy in a district heating network, Renewable Energy 75 (0) (2015) 714–721. doi:10.1016/j.renene.2014.10.055.

[71] Directive 2012/27/EU of the European Parliment and of the Council on energy efficiency.

[72] Y. Riffonneau, S. Bacha, F. Barruel, S. Ploix, Optimal Power Flow Management for Grid Connected PV Systems With Batteries, IEEE Transactions on Sustainable Energy 2 (3) (2011) 309–320. doi:10.1109/TSTE.2011.2114901.

[73] K. M. Powell, W. J. Cole, U. F. Ekarika, T. F. Edgar, Optimal chiller loading in a district cooling system with thermal energy storage, Energy 50 (2013) 445–453. doi:10.1016/j.energy.2012.10.058.
URL http://dx.doi.org/10.1016/j.energy.2012.10.058

[74] Z. W. Geem, Solution quality improvement in chiller loading optimization, Applied Thermal Engineering 31 (10) (2011) 1848–1851. doi:10.1016/j.applthermaleng.2011.02.030.
URL http://dx.doi.org/10.1016/j.applthermaleng.2011.02.030

[75] M. Sameti, F. Haghighat, Optimization approaches in district heating and cooling thermal network, Energy and Buildings 140 (2017) 121–130. doi:10.1016/j.enbuild.2017.01.062.
URL http://dx.doi.org/10.1016/j.enbuild.2017.01.062

[76] F. J. Nogales, a. J. Conejo, Electricity price forecasting through transfer function models, Journal of the Operational Research Society 57 (2006) 350–356. doi:10.1057/palgrave.jors.2601995.

[77] H. K. Alfares, M. Nazeeruddin, Electric load forecasting: Literature survey and classification of methods, International Journal of Systems Science 33 (October 2014) (2002) 23–34. doi:10.1080/00207720110067421.

[78] L. Suganthi, A. a. Samuel, Energy models for demand forecasting - A review, Renewable and Sustainable Energy Reviews 16 (2) (2012) 1223–1240. doi:10.1016/j.rser.2011.08.014.
URL http://dx.doi.org/10.1016/j.rser.2011.08.014

[79] N. Sehgal, K. K. Pandey, Artificial intelligence methods for oil price forecasting: a review and evaluation, Energy Systems 6 (4) (2015) 479–506. doi:10.1007/s12667-015-0151-y.

[80] J. M. Douglas, Conceptual design of chemical processes, McGraw-Hill, New York, New York, USA, 1988. doi:10.1002/jctb.280460308.

URL http://doi.wiley.com/10.1002/jctb.280460308 http://link.springer.com/10.1007/s11269-006-9039-x

[81] R. S. Pindyck, The Long-Run Evolutions of Energy Prices, The Energy Journal 20 (2). doi:10.5547/ISSN0195-6574-EJ-Vol20-No2-1.
URL http://www.iaee.org/en/publications/ejarticle.aspx?id=1308

[82] E. Schwartz, J. E. Smith, Short-Term Variations and Long-Term Dynamics in Commodity Prices, Management Science 46 (7) (2000) 893–911. doi:10.1287/mnsc.46.7.893.12034.

[83] N. Krichene, Crude Oil Prices: Trends and Forecast, IMF Working Papers 08 (133) (2008) 1. doi:10.5089/9781451869927.001.

[84] M. Mazraati, S. T. Jazayeri, Oil price movements and production agreements, OPEC Review 28 (3) (2004) 207–226. doi:10.1111/j.0277-0180.2004.00134.x.
URL http://doi.wiley.com/10.1111/j.0277-0180.2004.00134.x

[85] V. G. Azevedo, L. M. Campos, Combination of forecasts for the price of crude oil on the spot market, International Journal of Production Research 54 (17) (2016) 5219–5235. doi:10.1080/00207543.2016.1162340.

[86] A. J. Conejo, J. Contreras, R. Espínola, M. A. Plazas, Forecasting electricity prices for a day-ahead pool-based electric energy market, International Journal of Forecasting 21 (3) (2005) 435–462. doi:10.1016/j.ijforecast.2004.12.005.
URL http://linkinghub.elsevier.com/retrieve/pii/S0169207004001311

[87] J. Contreras, R. Espinola, F. J. F. F. J. F. Nogales, A. J. Conejo, R. Espínola, S. Member, F. J. F. F. J. F. Nogales, ARIMA models to predict next-day electricity prices, IEEE Transactions on Power Systems 18 (3) (2003) 1014–1020. doi:10.1109/TPWRS.2002.804943.
URL http://ieeexplore.ieee.org/document/1216141/

[88] H. Mohammadi, L. Su, International evidence on crude oil price dynamics: Applications of ARIMA-GARCH models, Energy Economics 32 (5) (2010) 1001–1008. doi:10.1016/j.eneco.2010.04.009.
URL http://linkinghub.elsevier.com/retrieve/pii/S0140988310000654

[89] M. Khashei, M. Bijari, An artificial neural network (p, d, q) model for timeseries forecasting, Expert Systems with Applications 37 (1) (2010) 479–489. doi:10.1016/j.eswa.2009.05.044.
URL http://dx.doi.org/10.1016/j.eswa.2009.05.044

[90] X. Yao, Evolving artificial neural networks, Proceedings of the IEEE 87 (1999) 1423–1447. arXiv:1108.1530, doi:10.1109/5.784219.

[91] S. I. Sulaiman, T. A. K. A. Rahman, I. Musirin, Partial Evolutionary ANN for Output Prediction of a Grid-Connected Photovoltaic System, International Journal of Computer and Electrical Engineering 1 (1) (2009) 40–45. doi:10.7763/IJCEE.2009.V1.7.
URL http://www.ijcee.org/show-7-14-1.html

[92] A. Andalib, F. Atry, Multi-step ahead forecasts for electricity prices using NARX: A new approach, a critical analysis of one-step ahead forecasts, Energy Conversion and Management 50 (3) (2009) 739–747. doi:10.1016/j.enconman.2008.09.040.

[93] N. Amjady, Day-Ahead Price Forecasting of Electricity Markets by a New Fuzzy Neural Network, IEEE Transactions on Power Systems 21 (2) (2006) 887–896. doi:10.1109/TPWRS.2006.873409.
URL http://ieeexplore.ieee.org/document/1626395/

[94] M. L. Alomar, V. Canals, N. Perez-Mora, V. Martínez-Moll, J. L. Rosselló, FPGA-Based Stochastic Echo State Networks for Time-Series Forecasting, Computational Intelligence and Neuroscience 2016 (ND) (2016) 1–14. doi:10.1155/2016/3917892.

[95] G. Reikard, Predicting solar radiation at high resolutions: A comparison of time series forecasts, Solar Energy 83 (3) (2009) 342–349. doi:10.1016/j.solener.2008.08.007.

[96] R. Huang, T. Huang, R. Gadh, N. Li, Solar generation prediction using the ARMA model in a laboratory-level micro-grid, in: 2012 IEEE 3rd International Conference on Smart Grid Communications, SmartGridComm 2012, 2012, pp. 528–533. doi:10.1109/SmartGridComm.2012.6486039.

[97] C. Paoli, C. Voyant, M. Muselli, M.-L. Nivet, Forecasting of preprocessed daily solar radiation time series using neural networks, Solar

Energy 84 (12) (2010) 2146–2160. doi:10.1016/j.solener.2010.08.011.
URL http://dx.doi.org/10.1016/j.solener.2010.08.011

[98] N. Perez-Mora, V. Canals, V. Martinez-Moll, Short-Term Spanish Aggregated Solar Energy Forecast, in: 13th International Work-Conference on Artificial Neural Networks, IWANN 2015, no. 07122, Springer Verlag, Palma de Mallorca (Spain), 2015, pp. 307–319. doi:10.1007/978-3-319-19222-2-26.
URL http://link.springer.com/10.1007/978-3-319-19222-2-26

[99] S. N. Chandramowli, F. A. Felder, Impact of climate change on electricity systems and markets - A review of models and forecasts, Sustainable Energy Technologies and Assessments 5 (2014) 62–74. arXiv:arXiv:1011.1669v3, doi:10.1016/j.seta.2013.11.003.
URL http://dx.doi.org/10.1016/j.seta.2013.11.003

[100] E. Erdem, J. Shi, ARMA based approaches for forecasting the tuple of wind speed and direction, Applied Energy 88 (4) (2011) 1405–1414. doi:10.1016/j.apenergy.2010.10.031.
URL http://dx.doi.org/10.1016/j.apenergy.2010.10.031

[101] M. Paulescu, V. Badescu, M. Brabec, Tools for PV (photovoltaic) plant operators: Nowcasting of passing clouds, Energy 54 (2013) 104–112. doi:10.1016/j.energy.2013.03.005.
URL http://dx.doi.org/10.1016/j.energy.2013.03.005

[102] G. Li, J. Shi, On comparing three artificial neural networks for wind speed forecasting, Applied Energy 87 (7) (2010) 2313–2320. doi:10.1016/j.apenergy.2009.12.013.
URL http://dx.doi.org/10.1016/j.apenergy.2009.12.013

[103] A. Qazi, H. Fayaz, A. Wadi, R. G. Raj, N. Rahim, The artificial neural network for solar radiation prediction and designing solar systems: a systematic literature review, Journal of Cleaner Production 104 (2015) 1–12. doi:10.1016/j.jclepro.2015.04.041.

[104] F. D'Urso, A. Giarratana, P. Lazzeroni, E. Pons, M. Repetto, L. Spairani, L. Vandoni, G. Zamboni, F. D 'urso, A. Giarratana, P. Lazzeroni, E. Pons, M. Repetto, L. Spairani, L. Vandoni, G. Zamboni, An optimization and management tool for

complex multi-generation systems, EEEIC 2016 - International Conference on Environment and Electrical Engineering (2016) 0–5doi:10.1109/EEEIC.2016.7555543.

[105] N. Perez-Mora, P. Lazzeroni, M. Repetto, V. Canals, V. Martinez-Moll, Optimal Solar District Cooling Harvesting Scenarios, in: Proceedings of EuroSun2016, International Solar Energy Society, Freiburg, Germany, 2016, pp. 1–11. doi:10.18086/eurosun.2016.05.07.
URL http://proceedings.ises.org/citation?doi=eurosun.2016.05.07

[106] P. Lazzeroni, M. Repetto, Integration of different energy vectors in polygeneration systems, in: 2016 IEEE Smart Energy Grid Engineering (SEGE), IEEE, 2016, pp. 181–185. doi:10.1109/SEGE.2016.7589522.
URL http://ieeexplore.ieee.org/document/7589522/

[107] SCIP.
URL http://scip.zib.de

[108] GUROBI.
URL www.gurobi.com

[109] MATLAB.
URL https://es.mathworks.com/products/matlab.html

[110] B. G. E. P, J. G. M., Time series analysis: forecasting and control, San Francisco, CA: Holden-Day 1976 (1) (1970) 575.

[111] Gobierno de España, T. y. C. Ministerio de Industria, Instituto para la Diversificación y Ahorro de Energía IDAE, Guía técnica para la medida y determinación del calor útil, de la electricidad y del ahorro de energía primaria de cogeneración de alta eficiencia. (Technical guide to measure and determine useful heat, electricity and primary energy savings on high effic, Tech. rep., Gobierno de España. Ministerio de Industria, Turismo y Comercio (2008).

[112] F. Yu, K. Chan, Part load performance of air-cooled centrifugal chillers with variable speed condenser fan control, Building and Environment 42 (11) (2007) 3816–3829. doi:10.1016/j.buildenv.2006.11.029.

[113] D. Didion, R. Radermacher, Part-load performance characteristics of residential absorption chillers and heat pump, International Journal of Refrigerationdoi:10.1016/0140-7007(84)90011-2.

[114] A. P. W. Li, Kam;Priddy, Power plant system design, Wiley, 1985.

[115] E. Rubio-Castro, M. Serna-Gonzalez, J. M. Ponce-Ortega, M. A. Morales-Cabrera, Optimization of mechanical draft counter flow wet-cooling towers using a rigorous model, Applied Thermal Engineering 31 (16) (2011) 3615–3628. doi:10.1016/j.applthermaleng.2011.07.029.
URL http://dx.doi.org/10.1016/j.applthermaleng.2011.07.029

[116] F. P. Incropera, D. P. DeWitt, T. L. Bergman, A. S. Lavine, Fundamentals of Heat and Mass Transfer, John Wiley & Sons, Inc., 2007. arXiv:1105-, doi:10.1073/pnas.0703993104.

[117] N. Perez-Mora, P. Lazzeroni, V. V. Martínez-Moll, M. Repetto, Optimal DHC energy supply harnessing its thermal mass, Applied Thermal Engineering 133 (October 2017) (2018) 520–531. doi:10.1016/j.applthermaleng.2018.01.072.
URL https://doi.org/10.1016/j.applthermaleng.2018.01.072

[118] B. Bohm, Heat losses from buried district heating pipes, International Journal of Energy Research 1 (January) (1999) 1311–1334.

[119] European Committee for Standardization, EN 13941. Design and installation of preinsulated bonded pipe systems for district heating, Tech. rep., European Committee for Standardization, Brussels (2010).

[120] G. Mihalakakou, M. Santamouris, J. Lewis, D. Asimakopoulos, On the application of the energy balance equation to predict ground temperature profiles, Solar Energy 60 (3-4) (1997) 181–190. doi:10.1016/S0038-092X(97)00012-1.

[121] J. Wu, D. L. Nofziger, Incorporating Temperature Effects on Pesticide Degradation into a Management Model, Journal of Environment Quality 28 (1) (1999) 92. doi:10.2134/jeq1999.00472425002800010010x.

[122] N. Perez-Mora, V. Martínez-Moll, Optimization of District Heating and Cooling Power Plant : the case of Parc Bit, in: SDEWES, Dubrovnik, 2017, pp. 1–10.

[123] J. G. Da Silva Fonseca, T. Oozeki, T. Takashima, G. Koshimizu, Y. Uchida, K. Ogimoto, Use of support vector regression and numerically predicted cloudiness to forecast power output of a photovoltaic power plant in Kitakyushu, Japan, Progress in Photovoltaics: Research and Applications 20 (July 2011) (2012) 874–882. doi:10.1002/pip.1152.
URL http://dx.doi.org/10.1002/pip.1160

[124] G. d. E. Ministerio Industria Energía y Turismo, Ministerio Industria Energía y Turismo, Gobierno de España.
URL http://www.minetur.gob.es

[125] J. Davies, D. McKay, Evaluation of selected models for estimating solar radiation on horizontal surfaces (1989). doi:10.1016/0038-092X(89)90027-3.

[126] A. Biga, R. Rosa, Estimating solar irradiation sums from sunshine and cloudiness observations (1980). doi:10.1016/0038-092X(80)90334-5.

[127] E. Lorenz, J. Hurka, D. Heinemann, H. G. Beyer, Irradiance forecasting for the power prediction of grid-connected photovoltaic systems, IEEE Journal of Selected Topics in Applied Earth Observations and Remote Sensing 2 (1) (2009) 2–10. doi:10.1109/JSTARS.2009.2020300.

[128] R. H. Inman, H. T. C. Pedro, C. F. M. Coimbra, Solar Forecasting Methods for Renewable Energy Integration, Progress in Energy and Combustion Science 39 (6) (2013) 535–576. doi:10.1016/j.pecs.2013.06.002.

[129] J. a. Duffie, W. a. Beckman, Solar Engineering of Thermal Processes, John Wiley & Sons, Inc., Hoboken, NJ, USA, 2013. doi:10.1002/9781118671603.
URL http://doi.wiley.com/10.1002/9781118671603

[130] N. Sharma, P. Sharma, D. Irwin, P. Shenoy, Predicting solar generation from weather forecasts using machine learning, in: 2011 IEEE International Conference on Smart Grid Communications, SmartGridComm 2011, 2011, pp. 528–533. doi:10.1109/SmartGridComm.2011.6102379.

[131] H. Long, Z. Zhang, Y. Su, Analysis of daily solar power prediction with data-driven approaches, Applied Energy 126 (2014) 29–37.

doi:10.1016/j.apenergy.2014.03.084.
URL http://dx.doi.org/10.1016/j.apenergy.2014.03.084

[132] S. Astariz, C. Perez-Collazo, J. Abanades, G. Iglesias, Towards the optimal design of a co-located wind-wave farm, Energy 84 (2015) 15–24. doi:10.1016/j.energy.2015.01.114.

[133] P. Sørensen, A. D. Hansen, P. A. C. Rosas, Wind models for simulation of power fluctuations from wind farms, Journal of Wind Engineering and Industrial Aerodynamics 90 (12-15) (2002) 1381–1402. doi:10.1016/S0167-6105(02)00260-X.

[134] E. Dotzauer, Simple model for prediction of loads in district-heating systems, Applied Energy 73 (3-4) (2002) 277–284. doi:10.1016/S0306-2619(02)00078-8.

[135] T. C. Park, U. S. Kim, L. H. Kim, W. H. Kim, Y. K. Yeo, Optimization of district heating systems based on the demand forecast in the capital region, Korean journal of chemical engineering 26 (6) (2009) 1484–1496. doi:10.2478/s11814-009-0282-8.

[136] P. Potočnik, E. Strmčnik, E. Govekar, Linear and Neural Network-based Models for Short-Term Heat Load Forecasting, Strojniški vestnik – Journal of Mechanical Engineering 61 (9) (2015) 543–550. doi:10.5545/sv-jme.2015.2548.

[137] Red Eléctrica España, Generation and Demand data base (2018).
URL https://demanda.ree.es

[138] AccuWeather, No Title.
URL https://www.accuweather.com/en/es/spain-weather

[139] Y. Zhang, S. Wistar, J. A. Piedra-Fernandez, J. Li, M. A. Steinberg, J. Z. Wang, Locating visual storm signatures from satellite images, in: 2014 IEEE International Conference on Big Data (Big Data), 2014, pp. 711–720. doi:10.1109/BigData.2014.7004295.

[140] M. Benghanem, Optimization of tilt angle for solar panel: Case study for Madinah, Saudi Arabia, Applied Energy 88 (4) (2011) 1427–1433. doi:10.1016/j.apenergy.2010.10.001.
URL http://dx.doi.org/10.1016/j.apenergy.2010.10.001

[141] N. Perez-Mora, V. Martinez-Moll, Spanish Energy Market. Overview towards price forecast, International Journal of Energy Economics and Policy 8 (3) (2018) 1–7.

[142] A. Mellit, A. M. Pavan, A 24-h forecast of solar irradiance using artificial neural network: Application for performance prediction of a grid-connected PV plant at Trieste, Italy, Solar Energy 84 (5) (2010) 807–821. doi:10.1016/j.solener.2010.02.006.

Appendices

Appendix A

Heat Loss Formulae

The following formulation is extracted from [119] Annex D.

A.1 Calculation of heat loss per pipe pair

The heat loss for supply pipe ϕ_s and for return pipe ϕ_r are calculated from:

$$\begin{aligned} \phi_s &= U_1(t_s - t_{soil}) - U_2(t_r - t_{soil}) \\ \phi_r &= U_1(t_r - t_{soil}) - U_2(t_s - t_{soil}) \end{aligned} \tag{A.1}$$

The overall heat loss will be:

$$\phi_s + \phi_r = 2U\left(\frac{t_s + t_r}{2} - t_{soil}\right) \tag{A.2}$$

where
U_1 and U_2 are the coefficients of heat loss;
t_s and t_r are the supply and return temperatures;
t_{soil} is the undisturbed soil temperature at depth Z.

For symmetric pipe structures the heat loss coefficients can be calculated from:

$$U_1 = \frac{R_s + R_i}{(R_s + R_i)^2 - R_h^2} \tag{A.3}$$

$$U_2 = \frac{R_h}{(R_s + R_i)^2 - R_h^2} \tag{A.4}$$

where
R_s is the thermal insulance of the soil;
R_i is the thermal insulance of the insulating material;
R_h is the thermal insulance of the heat exchange between flow and return pipe.

The thermal insulance is the specific insulation resistance.
The overall heat loss coefficient is:

$$U = U_1 - U_2 = \frac{1}{R_s + R_i + R_h} \tag{A.5}$$

A.2 Thermal insulance of the soil

$$R_s = \frac{1}{2\pi\lambda_s} \ln \frac{4Z_c}{D_c} \tag{A.6}$$

where
Z_c is a corrected value of depth z, so that the surface transition insulance R_o at the soil surface is included: $Z_c = Z + R_o\lambda_s$;
Z is the distance from the surface to the middle of the pipe;
λ_s can usually be valuated at 1.5 - 2W/mK for wet soil; For dry sand λ_s $\approx$1.0W/mK
R_o can usually be valuated at 0.0685m^{2}K/W.

A.3 Thermal insulance of insulation material

$$R_i = \frac{1}{2\pi\lambda_i} \ln \frac{D_{PUR}}{d_0} \tag{A.7}$$

where
D_{PUR} is the diameter of the insulation material;
d_0 is the outer diameter of the service pipe;
λ_i is the coefficient of thermal conductivity for the PUR insulation; The limit for λ_i in EN 253 is $\lambda_i = 0.033$W/mK. For practical calculations $\lambda_i = 0.030$W/mK

or according to the producer specification. The coefficient of thermal conductivity is increasing during the course of time. In heat loss calculation the average value of λ throughout the service life of the pipe system should be used.

A.4 Thermal insulance of the heat exchange between supply and return pipe

$$R_h = \frac{1}{4\pi\lambda_s} \ln\left(1 + \left(\frac{2Z_c}{C}\right)^2\right) \tag{A.8}$$

where
C is the distance between the centre lines of the two pipes.